COMPUTATION OF ACOUSTIC BACKSCATTER AND ATTENUATION COEFFICIENTS IN MUSCLE TISSUE UTILIZING A REFERENCE PHANTOM

BY

ROGER LEE SCHEER

B.S., University of Illinois, 1989

THESIS

Submitted in partial fulfillment of the requirements
for the degree of Master of Science in Electrical Engineering
in the Graduate College of the
University of Illinois at Urbana-Champaign, 1994

Urbana, Illinois

UNIVERSITY OF ILLINOIS AT URBANA-CHAMPAIGN

THE GRADUATE COLLEGE

JUNE 1994

WE HEREBY RECOMMEND THAT THE THESIS BY

ROGER LEE SCHEER

ENTITLED__COMPUTATION OF ACOUSTIC BACKSCATTER AND ATTENUATION

COEFFICIENTS IN MUSCLE TISSUE UTILIZING A REFERENCE PHANTOM

BE ACCEPTED IN PARTIAL FULFILLMENT OF THE REQUIREMENTS FOR

THE DEGREE OF_____MASTER OF SCIENCE

_____
Director of Thesis Research

_____
Head of Department

Committee on Final Examination†

_____
Chairperson

_____

_____

_____

_____

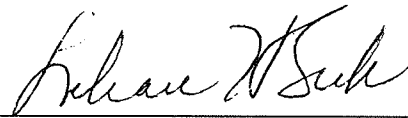† Required for doctor's degree but not for master's.

O-517

UNIVERSITY OF ILLINOIS AT URBANA-CHAMPAIGN

GRADUATE COLLEGE DEPARTMENTAL FORMAT APPROVAL

THIS IS TO CERTIFY THAT THE FORMAT AND QUALITY OF PRESENTATION OF THE

THESIS SUBMITTED BY ROGER LEE SCHEER   AS ONE OF THE REQUIREMENTS FOR

THE DEGREE OF MASTER OF SCIENCE   ARE ACCEPTABLE TO THE DEPARTMENT

OF ELECTRICAL AND COMPUTER ENGINEERING.

JUNE 23, 1994
Date of Approval

Departmental Representative

DEDICATION

This thesis is dedicated to my wife, Jodie, and to my children, Chad and Carly.

I will never be able to put into words how much I appreciate you three! Thanks for your patience, sacrifice, encouragement, help, and love. Thanks for believing in me!

ACKNOWLEDGMENTS

all of your encouragement, help, and tolerance. Thanks to you, I can now say longissimus dorsi muscle.

Thanks to Bob Cicone for cheerfully fixing my countless problems with the cyber-world! Thanks also to Billy McNeil, Kay Carnes, and Wanda Elliott for all their help and encouragement.

Finally, I wish to express my appreciation to the National Livestock and Meat Board, which supported the research project, and the State of Illinois for its help in financing my education.

TABLE OF CONTENTS

CHAPTER 1

INTRODUCTION

Current beef grade determination in the United States is made by a human observer who often has as little as 6 sec per animal to assign a retail quality grade to the meat. This system is extremely vulnerable to interobserver variability. An accurate and precise automated grading system is needed and desired by the industry. Ultrasound offers considerable promise in fulfilling this need [1].

Ultrasound has long been utilized for its imaging and diagnostic capabilities in the medical sciences. A great deal of research has been done on both the tissue characterization capabilities of ultrasound and its safety. Medical ultrasound devices utilize the backscatter information from acoustic signals to produce an image based on the relative intensities of reflections from within the irradiated tissue. It has long been suggested that a more quantitative analysis of this backscatter information, such as determining the backscatter coefficient, would provide for a more complete tissue characterization of the medium being probed [2]. Determination of the backscatter coefficient has traditionally required time-consuming measurements and complex calculations [3].

Attenuation is one of the acoustic properties originally targeted for evaluation in a current study at the University of Illinois to determine the feasibility of using ultrasound to grade beef [1]. Attenuation is a measure of the amount of acoustic signal loss that occurs as a signal propagates within the medium. It is reasonable

to expect that attenuation measurements from beef muscle tissue would vary with changes in muscle texture and marbling and with varying thicknesses of external fat layers. Traditionally, acoustic attenuation has been measured using through-transmission techniques in which the signal is transmitted through the tissue and collected on the opposite side to be measured for signal loss [4]. This type of acoustic measurement would not be feasible, however, in a slaughterhouse environment.

The Reference Phantom Method was developed at the University of Wisconsin [5] to measure the backscatter and attenuation coefficients of *in vivo* tissue using backscatter measurements and minimal computational requirements. This method utilizes a reference measurement of a well-characterized phantom, in addition to the tissue measurement, to eliminate the instrumentation dependent factors affecting the computation of these two acoustic quantities. The Reference Phantom Method was developed for and has been successfully demonstrated on acoustically smooth tissues such as liver [6].

There is considerable contrast between the characterization of acoustic signals in liver and muscle tissues. The multiple boundaries and high density of scatterers in muscle tissue cause the received ultrasonic echo signal to be inherently more random and coarse in nature.

The focus of this thesis is the adaptation of the Reference Phantom Method for use on muscle tissue and its utilization on beef muscle tissue for comparison of tissue property variance between animals. Chapter 2 restates the origin theoretical derivation of the Reference Phantom Method [7]. Chapter 3 describes the application of the method to the problem of characterizing the backscatter and attenuation properties of muscle tissue. Chapter 4 is a description of the software developed for the implementation of the method. Chapter 5 details the data collection equipment and methodology utilized in obtaining the data used to

examine the applicability of the Reference Phantom Method to the task of characterizing beef muscle tissue. Chapter 6 examines the results obtained from these data and makes a comparison of the results with those obtained from through-transmission attenuation measurements and from dissection measurements of the same animal tissue. Finally, Chapter 7 draws conclusions from these results and makes suggestions for future work on this topic.

CHAPTER 2

REFERENCE PHANTOM METHOD

Ultrasound imaging systems generate gray scale images based on the relative backscatter levels in the tissue being scanned. The resolution of ultrasound images is dependent on the transmission path, instrumentation factors, and acoustic properties of the tissue. Extraction of quantitative information from the backscatter ultrasound data would provide additional and useful information from the RF data [8]. In medical ultrasound for example, a precise way to quantify the backscatter coefficient of *in vivo* tissue could assist in early detection of diseases that alter the scattering characteristics of tissue [7].

Accurate determination of the backscatter coefficient must account for all path and instrument-dependent factors affecting the echo signal. This has traditionally required detailed knowledge of the transducer's beam pattern and a priori knowledge of the acoustic properties of the tissue under test [3].

The Reference Phantom Method, developed by L. Yao et al. at the University of Wisconsin in Madison [5], provides a means to determine the acoustic backscatter and attenuation coefficients from ultrasound data without extensive beam pattern calculations or prior knowledge of the exact acoustic properties of the tissue. Instrument-dependent factors affecting the scattered signal are accounted for by comparison of the echo signals from the medium under test and those of a well-characterized reference phantom. The data from both measurements must be

collected using the same equipment with the same settings at the same frequencies and acquired over the same depths. The instrument and path-related factors of the measurements can then be canceled by dividing the measurements from the tissue by the measurement from the phantom.

The acoustic backscatter coefficient, η, which is defined as the differential scattering cross section per unit volume measured at a 180 degree scattering angle [7], is directly proportional to the amount of energy reflected directly back towards the transducer. Reflection of ultrasonic energy within a body occurs from boundaries between tissue layers or from small obstructions or particles (scatterers) within the tissue and varies with frequency. Therefore, η is dependent on the frequency of the ultrasound wave and the acoustic properties of the tissue under test.

The attenuation coefficient, α, is a number chosen such that the exponential, $\exp(-\alpha z)$, where z represents the distance traveled, describes the attenuation of the propagating acoustic wave per unit length traveled in a given medium. The attenuation of an echo signal at the transducer from a scatterer is described as $\exp(-2\alpha z)$, where z is the distance from the transducer to the scatterer. Therefore, $\eta \cdot \exp(-2\alpha z)$ is proportional to the amount of acoustic energy that is received by the transducer from the scatterer.

2.1 Theory

In the following discussion of the Reference Phantom Method, scatterers are assumed to be spatially randomly distributed and the scattered wave fronts are assumed to be spherical in the region of the transducer. The transducer is also assumed to be operated in pulse echo mode.

The echo signal voltage received at the transducer as a function of time can then be written as [3]

$$V(t) = \int_0^\infty d\omega\, T(\omega)\, A_{00}(\omega)\, e^{-i\omega t}\, \Phi(\omega) \iiint_\Omega dr N(r) [A_0(r,\omega)]^2 \qquad (1)$$

where $T(\omega)$ is the complex valued transfer function describing the effect of the transducer's geometry on the received echo signal. $N(r)$ is the number density of scatterers in a neighborhood about the point r and the triple integral is over Ω, the volume containing scatterers in the field. $I(\omega)$ is the value of the angle distribution factor for the scattered wave at 180 degree scattering angle. The factor, $A_{00}(\omega)$, is the complex superposition coefficient for an acoustic pulse at a point r relative to the transducer. The exponential, $e^{-i\omega t}$, denotes that the propagating field is time harmonic [9], and $A_0(r,\omega)$ is the Rayleigh integral [7]:

$$A_0(r,\omega) = \iint_s d\bar{s}\, \frac{e^{[ik-\alpha(\omega)]|r-\bar{r}|}}{|r-\bar{r}|} \qquad (2)$$

Here the integration is across the active surface of the transducer, and the integration variable, $\bar{r}$, is the distance from the transducer element to the point r in the field. The variable k is the wave number. Uniform attenuation is assumed throughout the entire depth of the measurement in Equation (2). The more general case of nonuniform attenuation will be discussed below.

To evaluate Equation (1) at a narrow band of frequencies centered on a frequency of interest, ω_1, the echo voltage signal is filtered with a band-pass filter, $P(\omega - \omega_1)$, having center frequency ω_1.

Equation (1) becomes

$$V(\omega_1,t) = \int_0^\infty d\omega\, T(\omega)\, A_{00}(\omega)\, e^{-i\omega t}\, P(\omega - \omega_1)\, \Phi(\omega) \iiint_\Omega dr N(r) \left[A_0(r,\omega) \right]^2 \quad (3)$$

Assuming the medium is pulse interrogated and the discrete scatterers in the medium under test can be considered to be randomly distributed with a small scatter number density, the coherent element of the scattering is negligible and only the incoherent scattering is important [10]. Under these conditions it can be shown [3] that the ensemble average squared of Equation (3) is

$$\overline{V^*(t)V(t)} = N(r) \iiint_\Omega d\bar{r} \int_0^\infty d\omega\, T^*(\omega)\, A_{00}^*(\omega) e^{i\omega t}\, \Phi^*(\omega) \left[A_0^*(\bar{r},\omega) \right]^2$$
$$\times \int_0^\infty d\bar{\omega}\, T(\bar{\omega})\, A_{00}(\bar{\omega}) e^{i\bar{\omega}t} \Phi(\bar{\omega}) \left[A_0(\bar{r},\bar{\omega}) \right]^2 \quad (4)$$

The attenuation component of Equation (2) can be separated from the two-dimensional integral with negligible effect provided the distance from the transducer to the field point is greater than the diameter of the transducer [7]. Equation (2) then becomes

$$A_0(r,\omega) \approx \left[e^{-\alpha(\omega)z} \iint_s d\bar{s}\, \frac{e^{ik|r-\bar{r}|}}{|r-\bar{r}|} \right] = e^{-\alpha(\omega)z} A(r,\omega) \quad (5)$$

If the bandwidth of the filter, $P(\omega - \omega_1)$, is sufficiently narrow, the values of the scattering and attenuation functions at the center frequency, ω_1, can be considered constants with respect to the integration and can be removed from the

The instrument and path-dependent terms are now separate. The instrument-dependent terms remain inside the volume integral while the path-dependent terms now appear outside of the integral.

The attenuation coefficient in the exponential is multiplied by 4 in Equation (6). The path length, z, is first doubled to account for the forward and return paths. The exponential is then squared in Equation (4) for the ensemble average of the amplitude squared voltage calculation.

Allowing $I_{ph}(\omega_1, t)$ to represent the amplitude squared voltage for the echo voltage signal collected from the reference phantom, the phantom equation analogous to Equation (9) is then

$$I_{ph}(\omega_1, t) = BSC_{ph}(\omega_1) \, e^{-4\alpha_{ph}(\omega_1)z} \iiint_{\Omega} d\vec{r} \; G^*(\vec{r}, \omega_1, t) G(\vec{r}, \omega_1, t) \qquad (10)$$

Noting that both signals contain identical instrument-dependent factors, the ratio of Equation (9) to Equation (10) is

$$\frac{I(\omega_1, t)}{I_{ph}(\omega_1, t)} = \frac{BSC(\omega_1) e^{-4\alpha(\omega_1)z}}{BSC_{ph}(\omega_1) e^{-4\alpha_{ph}(\omega_1)z}} = \frac{I(\omega_1, z)}{I_{ph}(\omega_1, z)} \qquad (11)$$

where c is the speed of sound in the given medium and $z = (ct/2)$. It is assumed in Equation (11) that the speed of sound is the same in both the unknown tissue and the phantom. Different speeds of sound between mediums and within a medium can be corrected, by computing the thickness of each medium and using these individual distances with the speeds of each medium to calculate the time of flight

through that area of the tissue. The total time is then twice the distance traveled divided by the speed of sound in that medium.

For convenience let

$$\mathrm{RI}(\omega_1) = \frac{I(\omega_1, z)}{I_{ph}(\omega_1, z)} \qquad (12)$$

$$\Delta\alpha(\omega_1) = \alpha(\omega_1) - \alpha_{ph}(\omega_1) \qquad (13)$$

$$\mathrm{RB}(\omega_1) = \frac{BSC(\omega_1, z)}{BSC_{ph}(\omega_1, z)} \qquad (14)$$

Equation (11) now simplifies to

$$\mathrm{RI}(\omega_1, z) = RB(\omega_1)e^{-4\Delta\alpha(\omega_1)z} \qquad (15)$$

where $\mathrm{RI}(\omega_1, z)$ is calculated from the measured echo voltage signal. It is obtained by processing and comparing the data acquired from the unknown tissue and the reference phantom. The backscatter coefficient and the attenuation can be calculated from Equation (15).

2.2   Attenuation

As stated above, uniform attenuation is assumed in Equations (2) through (15). These equations are easily expanded to a more general form that accounts for a region of nonuniform acoustic properties.

Rewriting Equation (15) using Equation (11)

$$\text{RI}(\omega_1, z) = \text{RB}(\omega_1)\frac{ATTN\ (unknown)}{ATTN\ (phantom)} \qquad (16)$$

where *ATTN* (*unknown*) and *ATTN* (*phantom*) are the nonuniform attenuations encountered in the propagation paths for the unknown tissue (medium under test) and the reference phantom, respectively. Each is equal to the integral over the path of the point by point attenuation encountered.

$$ATTN\ (unknown) = \exp\left[-4\int_0^z a(w_1, \bar{z})d\bar{z}\right] \qquad (17)$$

$$ATTN\ (phantom) = \exp\left[-4\int_0^z a_{ph}(w_1, \hat{z})d\hat{z}\right] \qquad (18)$$

Substituting Equations (17) and (18) into Equation (16) yields

$$\text{RI}(\omega_1, z) = \text{RB}(\omega_1)\exp\left[-4\int_0^z a\ (w_1, \bar{z})d\bar{z}\right]\exp\left[4\int_0^z a_{ph}\ (w_1, \hat{z})d\hat{z}\right] \qquad (19)$$

The propagation path of the unknown and phantom measurements can be divided according to tissue regions within the media. The region of interest (ROI) is defined as the section of the tissue or phantom from which the data to be processed will be collected. The ROI must be a region with uniform acoustic properties for calculation of the backscatter and attenuation coefficients in this region. The integrated attenuations for each measurement can be separated into

two parts - the attenuation of the propagation path from the transducer to the ROI and the attenuation that occurs within the ROI.

Let *ATTN* 1 and *ATTN* 0 be the attenuation of the propagation path from the transducer to the boundary of the ROI at z_1 for the unknown sample under test and the reference phantom, respectively.

Equation (19) can be rewritten as

$$RI(\omega_1, z) = RB(\omega_1)\frac{ATTN\,1}{ATTN\,0}\left\{\exp\left[-4\int_{z_1}^{z_2} a\,(\omega_1,\bar{z})d\bar{z}\right]\exp\left[4\int_{z_1}^{z_2} a_{ph}\,(\omega_1,\hat{z})d\hat{z}\right]\right\} \tag{20}$$

$$RI(\omega_1, z) = RB(\omega_1)\left[\frac{ATTN\,1}{ATTN\,0}\right]\left\{\exp\left[-4\int_{z_1}^{z_2}\Delta a(\omega_1,\bar{z})d\bar{z}\right]\right\} \tag{21}$$

Equation (21) assumes a priori knowledge of the attenuation values for the propagation path of the sample under test as well as the phantom. This could realistically be accomplished by applying the Reference Phantom Method to each successive layer in sequence or by constructing a reasonable estimate from prior knowledge of the path.

Because the acoustic properties of the ROIs of both the phantom and tissue are uniform, Equation (21) reduces to

$$RI(\omega_1, z) = RB(\omega_1)\left[\frac{ATTN\,1}{ATTN\,0}\right]\exp\left(-4\Delta a\,(\omega_1)[z_2 - z_1]\right) \tag{22}$$

Taking the natural logarithm of both sides of Equation (22) results in

$$\ln[\text{RI}] = \left\{ \ln[\text{RB}] + \ln\left[\frac{ATTN\,1}{ATTN\,0}\right] \right\} - 4\Delta\,a\,(\omega_1)[z - z_1] \tag{23}$$

Note that Equation (23) is in point slope form: $Y = B + mz$. Therefore, a plot of the natural logarithm of the amplitude squared signal, $\ln(RI)$, over the ROI, will have a slope equal to $[-4\Delta\alpha\,(\omega_1)]$. The attenuation coefficient of the ROI can then be obtained from $\Delta\alpha\,(\omega_1)$ and Equation (13).

2.3 Computation of Backscatter Coefficient

After solving for $\Delta\alpha\,(\omega_1)$, the ratio of the backscatter coefficients can be calculated at each depth of interest from Equation (15):

$$RB(\omega_1) = RI(\omega_1, z)e^{4\,\Delta\alpha(\omega_1)z} \tag{24}$$

Assuming the backscatter coefficient of the phantom is known, the backscatter coefficient of the tissue under test can then be calculated.

$$BSC(\omega_1, z) = RB(\omega_1, z)BSC_{ph}(\omega_1, z) \tag{25}$$

CHAPTER 3

APPLICATION OF THE REFERENCE PHANTOM
METHOD TO MUSCLE TISSUE

The Reference Phantom Method was originally developed for use with an
acoustically smooth medium such as liver tissue [6]. The object of this research is
to apply the Reference Phantom Method to less smooth muscle tissue for the
purpose of obtaining more precise and repeatable grading criterion for beef.
Where compatible, the original method as developed by Yao [7] was used.
Because of the differences in objectives and application between Yao's original
development and this project, adaptations were necessary to apply this method to
muscle tissue.

The major difficulties in adapting the Reference Phantom Method to muscle
tissue come from the fact that echo returns from muscle tissue are more randomly
spaced and more varied in amplitude than in softer tissues such as liver. Multiple
tissue boundaries within the muscle structure often cause spiked returns that can
easily be misinterpreted by software in calculating the attenuation.

3.1 Calculation of the Filtered Amplitude Squared Voltage Ratio

The amplitude squared voltage, $I(\omega_1, t)$, from Equation (6), is proportional to the
point by point intensity of the entire data set at ω_1. $I(\omega_1, t)$ is the quantity from
which the attenuation coefficient and backscatter coefficient ratio are computed.

A flow chart of the general methodology of processing the echo voltage signal into the amplitude squared voltage signal is shown in Figure 1.

The echo signal voltage, defined in Equation (1), is fed into dual multipliers where the signal is multiplied by a cosine or a sine wave at the analysis frequency. This separates the real and imaginary parts of Equation (1) for quadrature processing and translates the analysis frequency to ω_1.

The multiplier and the low-pass filter effectively form a band-pass filter centered at ω_1. This reduces the wide band input signal to a narrow band signal for analysis. The output from each low-pass filter into the squarer is

$$V_u(\omega_1, t) = \int_0^\infty V(\bar{t}) p(t - \bar{t}) \cos(\omega_1 \bar{t}) d\bar{t} \tag{26}$$

$$V_l(\omega_1, t) = \int_0^\infty V(\bar{t}) p(t - \bar{t}) \sin(\omega_1 \bar{t}) d\bar{t} \tag{27}$$

Here Equation (26) represents the output of the low-pass filter for the upper or real signal branch of Figure 1, and Equation (27) is the output for the low-pass filter of the lower or imaginary signal branch. Equations (26) and (27) can be further expanded to show the quadrature terms at the input of the filters.

$$V_u(\omega_1, t) = \tfrac{1}{2} \int_0^\infty V(\bar{t}) p(t - \bar{t}) e^{i\omega_1 \bar{t}} d\bar{t} + \tfrac{1}{2} \int_0^\infty V(\bar{t}) p(t - \bar{t}) e^{-i\omega_1 \bar{t}} d\bar{t} \tag{28}$$

$$V_l(\omega_1, t) = \tfrac{1}{2i} \int_0^\infty V(\bar{t}) p(t - \bar{t}) e^{i\omega_1 \bar{t}} d\bar{t} - \tfrac{1}{2i} \int_0^\infty V(\bar{t}) p(t - \bar{t}) e^{-i\omega_1 \bar{t}} d\bar{t} \tag{29}$$
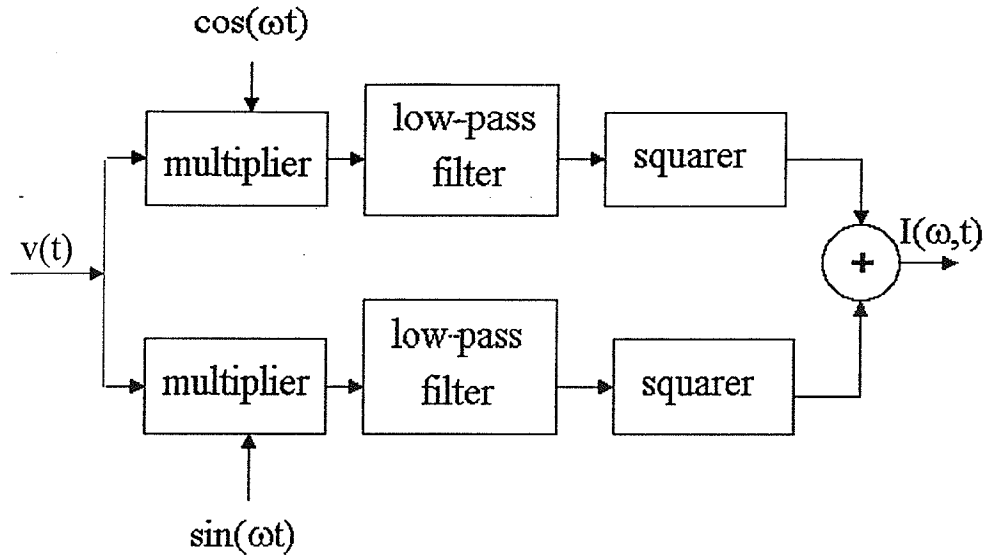
Figure 1: Flow chart for processing of the amplitude squared voltage [7].

Squaring Equations (28) and (29) individually and adding them together eliminate the imaginary terms. The output of the adder is

$$I(\omega_1, t) = \frac{1}{2}\left[\int_0^\infty V(\bar{t})p(t-\bar{t})d\bar{t}\right]^2 \qquad (30)$$

The low-pass filter implemented in the signal processing, $p(t)$, is a three-term Blackman-Harris window [7] expressed as

$$p(t) = a_0 - a_1\cos\left[\left(\frac{2\pi}{\tau}\right)t\right] + a_2\cos\left[2\left(\frac{2\pi}{\tau}\right)t\right] \qquad (31)$$

In Equation (31), $a_0 = 0.42323$, $a_1 = 0.49755$, and $a_2 = 0.07922$ and $\tau = 4\,\mu\sec$ is the time duration used for the window. This is the same filter used by Yao in his original application of the method. His optimization of the time duration and analysis of the window are well-documented [7]. Window duration values were rechecked using amplitude squared ratios from muscle and phantom data. The amplitude response leveled off at $\tau = 4\,\mu\sec$ and above in a similar fashion to Yao's results. The minimum time value was chosen to optimize the frequency response versus spectrum shift.

The amplitude squared voltage, $I(\omega_1, t)$, is first calculated for the phantom. The ratio of the amplitude squared voltages, $RI(\omega_1, t)$, is calculated for each A-line of the animal scan, at each depth and frequency. The $RI(\omega_1, t)$ values for each individual A-line are then averaged to calculate the $RI(\omega_1, t)$ value for the particular depth and frequency.

3.2 Calculation of the Attenuation Coefficient

With the attenuation of the phantom known and the $RI(\omega_1, t)$ value computed, the attenuation of the muscle tissue can be computed using Equation (23). The values for $RI(\omega_1, t)$ within the region of interest (ROI) can be plotted against the depth. A curve-fitting technique is then used to achieve the best linear fit for the plotted data as shown in Figure 2. The slope of this linear fit is the negative of four times the difference in attenuation between the muscle tissue and the reference phantom. Using Equations (13) and (23)

$$\Delta\alpha(\omega_1) = -\tfrac{1}{4}\,m \tag{32}$$

$$\alpha(\omega_1) = \Delta\alpha(\omega_1) + \alpha_{ph}(\omega_1) \tag{33}$$

Due to the roughness of the echo returns from the muscle data, the depth range for calculating attenuation is 3 cm wide. This is a depth twice that used to calculate the backscatter ratio. The increased number of sampling points in the ROI was needed to smooth out the spikes in the returns caused by tissue boundary reflections and made the resulting attenuation values more consistent. Increasing the depth range beyond 3 cm would decrease the number of usable A-lines substantially due to the shape of the longissimus dorsi muscle and the need to ensure that the entire depth range has the same acoustic properties.

PLOT OF AMPLITUDE SQUARED VOLTAGE RATIOS

(simulated data)
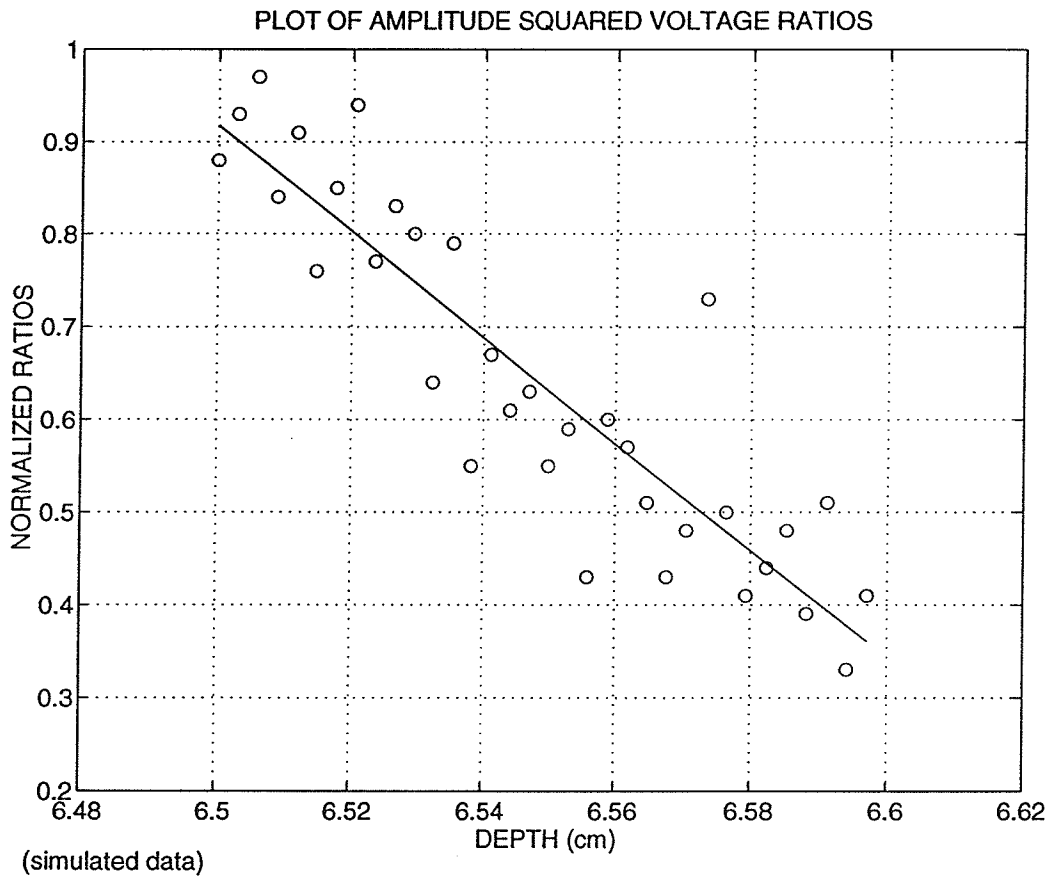
Figure 2: Plot of $RI(\omega_1, z)$. $\Delta\alpha(\omega_1)$ from the slope of the least squares fit.

3.3 Computation of the Backscatter Coefficient Ratio

Once $RI(\omega_1, t)$ and $\Delta\alpha(\omega_1)$ are known, the backscatter coefficient ratio can be calculated using Equation (24) . Since all animal data in this study are referenced to the same phantom, it was not necessary to convert the backscatter information from a ratio into a backscatter coefficient. Therefore, the backscatter values were left in ratio form for analysis.

3.4 Data Analysis

Because the object of this research is to compare the attenuation and backscatter properties of the muscle tissue of each animal to that of the others, correlation will be used as the primary analysis tool. Correlation is a mathematical tool to determine the degree to which one data set is similar to another data set (simple correlation) or to determine the degree to which one data set is similar to two or more other data sets (multiple correlation). A linear correlation between two data sets means that the relationship between the data can be described by a linear equation. A positive linear or direct correlation between two data sets, (P,Q), implies that the Q increases with a increase in P. A negative linear or inverse correlation between P and Q implies that Q decreases with an increase in P.

The correlation coefficient, r, ranges from -1 to 1. A correlation coefficient equal to 1 implies complete positive correlation, and $r = -1$ would imply that the data sets are completely inversely related. An r value of zero signifies that the two data sets are completely uncorrelated [11].

For the analysis of the data in this research, version 4.0 of the spreadsheet program, Excel, by the Microsoft Corporation, Redmond, Washington, will be used.

Excel calculates the correlation of two sequences using [12]

$$r = \frac{\frac{1}{n}\sum_{i=1}^{n}(x_i - \bar{x})(y_i - \bar{y})}{\sigma_x \sigma_y}$$
(34)

where $\sigma_x = \sqrt{\frac{x_i^2}{n}}$ is the standard deviation of x and $\bar{x}$ is the mean value of x.

CHAPTER 4

SOFTWARE IMPLEMENTATION OF
THE REFERENCE PHANTOM METHOD

All processing was implemented with software to make developmental changes easier to accomplish. However, the majority of the signal processing implemented for this research could be accomplished using hardware components.

The software consists of two types of files. All data processing software was written as Matlab m-files and interpreted by the UNIX version of Matlab, a commercial software package sold by The MathWorks, Natick, MA [13]. In addition to the Matlab files, a C program was used to convert raw data files into Matlab data files. Copies of the software files are in the appendices.

4.1 Preprocessing

The input data are in the form of digitized files of the raw RF echo signals. The animal data were collected in acoustic lines (A-lines) of 5000 bytes each representing 15 cm in depth. Six to seven A-lines, each at a different gain setting, were collected at each location during a scan. The animal scan files containing A-lines at gain settings of 36 dB were selected for analysis of all three scans This represents the maximum gain setting that did not characteristically saturate the echo signal in the depth range of interest.

The animal tissue data used in this study were collected from the longissimus dorsi muscles of cattle along a line perpendicular to the spine at the twelfth rib. Due to the documented bilateral symmetry of the longissimus dorsi on either side of the spine [14], A-lines were used from both sides of the animal to increase the number of samples.

The reference phantom data were collected in acoustic lines of 8192 bytes, each representing 24 cm in depth. The 72 dB gain RF files were used from the phantom scans. The higher gain setting was necessary to increase the signal to noise ratio of the phantom data for processing. The differences in gain settings between the muscle and phantom data files were compensated for by multiplying the amplitude of the tissue data by a constant before processing.

The RF input files were converted to Matlab input files using the programs in Appendix B. They are modified from a program, originally written by Richard Qian of the Bioacoustics Research Laboratory at the University of Illinois, that utilizes the standardized savemat format [13]. The input files are then loaded in the manner described in Appendix A.

4.2 Program Execution

The master program file, *animal.m*, initiates the processing sequence. All Matlab m-files, the six animal data files, and the phantom data file must be in the directory in which the active Matlab program is resident for execution of the processing software. The main purposes of *animal.m* are to initiate the *bacscat.m* subprogram for each scan in sequence and to output the processed data files at the end of the processing.

A vector containing three fat thickness measurements corresponding to the measured the fat thickness of the animal at 5, 10, and 15 centimeters from the spine must be provided to *animal.m*, along with the animal number, when it is

initiated. Fat thickness measurements are input in inches and converted to meters within the program.

The Matlab file *bacscat.m* is the main execution file for each individual scan. After setting up the speed and attenuation values for fat [4], muscle [4], hide [15], and the phantom [15], *bacscat.m* loads the desired animal and phantom data through the *getdata.m* subprogram. In addition to loading in data from external files, *getdata.m* selects the A-lines from each side of the animal that are most directly over the longissimus dorsi muscles. *getdata.m* also reduces the file length of the phantom data to 5000 bytes per A-line and combines the selected right-side and left-side files of the animal data.

The subprogram *fatprog.m* converts the fat thickness data from inches to meters and then uses the Matlab functions polyfit and polyval [16] to create a second-degree polynomial fit to the data. This second-degree polynomial is then used to interpolate that fat thickness value at the location of each A-line.

The attenuation coefficient for each media is calculated as [9]

$$\left| \alpha \; (Np \, / \, m) \right| \; = \; \left(\frac{1}{8.68} \right) \left| attn \, (dB \, / \, m) \right| \tag{35}$$

4.2.1 Processing the reference phantom data

The amplitude squared voltage, $I_{ph}(\omega_1, z)$, for the entire extended depth range of interest in the phantom is calculated first. $I_{ph}(\omega_1, z)$ is calculated in 0.5 cm steps for each depth from 6 to 9 cm at each analysis frequency. The data are then stored for comparison to the amplitude squared voltages of the muscle tissue in the attenuation and backscatter calculations.

$I_{ph}(\omega_1, z)$ is calculated by first range gating the RF signal at the incremented depth, Z. The Matlab file *gate.m* is called, and the entire phantom data matrix is

passed to it. *gate.m* range gates a 1 mm section of the RF signal, centered around Z, for each A-line (row) in the phantom data matrix. The gated phantom matrix is then passed to the Matlab file *phprocess.m*.

The Matlab file, *phprocess.m*, calculates $I_{ph}(\omega_1, z_0)$ for each analysis frequency from a gated matrix centered at each Z_0. A point by point estimate of the amplitude squared voltage is calculated for each individual column of each row of the range gated section in the gated matrix. Each column's value is multiplied by a sine and cosine wave at the analysis frequency and at a time calibrated to the depth of that individual data point. This separates the real and imaginary components of the echo signal. Both components are then convolved with the Blackman-Harris filter described in Chapter 3 and multiplied by their respective complex conjugates. The squared real and imaginary components are added together to form the ensemble average squared voltage described in Equation (12). The estimates of the amplitude squared voltage are averaged across each gated section of the A-line and then across all rows of the matrix for depth Z_0 and frequency ω_1 to calculate $I_{ph}(\omega_1, z_0)$. The output of this section of the program is an [m x n] matrix of amplitude squared voltage values for the phantom. The index m is the number of depths analyzed between 6 and 9 cm, and n is the number of analysis frequencies.

4.2.2 Computation of the attenuation coefficient

From the *bacscat.m* subprogram file, the next step passes the data matrix and the variable, longdepth, to the Matlab file *longgate.m*. Longdepth is a vector of depths spaced every half millimeter from 6 to 9 cm. The purpose of the *longgate.m* subprogram is to return a single range gate from the animal data matrix that extends for the entire width of the vector, longdepth.

As mention in Chapter 3, the attenuation is calculated over the full 3 cm depth section of the muscle tissue at each of the analysis frequencies. The first attempt at computing the attenuation of the muscle tissue was to calculate it for each individual range cell in the same manner as that described for the calculation of the estimates of amplitude squared voltages for the phantom. The range cells were then averaged across all of the available A-lines. This produced widely varying values for the attenuation coefficient due to the coarse nature of the muscle data. Calculating the attenuation across the entire original 1.5 cm range cell smoothed the data and greatly increased the consistency of the results. Using a 3 cm range cell improved the results further. Increasing the depth range further would decrease the number of usable A-lines substantially, due to the shape of the longissimus dorsi muscle and the need to ensure that the entire ROI has constant acoustic properties.

The 3 cm gated RF signal is then passed to the Matlab file *roiattn.m*. The purpose of *roiattn.m* is to return the attenuation coefficient of the muscle tissue and the difference in the attenuation coefficients of the muscle tissue and phantom.

A matrix of estimated amplitude squared voltage values for each column and of each row of the longer gated matrix is returned to *roiattn.m* by the Matlab file *attnprocess.m*. These estimated values are calculated using processing identical to that described for the phantom with the exception that the estimates are not averaged within the *attnprocess.m* subprogram.

After receiving the estimate matrix from *attnprocess.m*, the next step in the *roiattn.m* subprogram is to divide the estimate matrix by the average value of the amplitude squared voltage from the phantom. This creates an estimated matrix of amplitude squared voltage ratio values, $ri(\omega_1, z_0)$.

The attenuation for each A-line's range gated section is then calculated from the natural logarithm of $ri(\omega_1, z_0)$ using Equation (23). A one-degree polynomial is fit to the data from each section of each A-line using the Matlab function, polyfit [16]. Polyfit forms a Vandermonde matrix and solves the least squares problem for a polynomial of the desired order. The polynomial is then evaluated at the first and last elements of longdepth and divided by the distance between these two elements to calculate the slope. The difference in the attenuation between the muscle tissue and the phantom, $\Delta\alpha(\omega_1)$, is calculated for each A-line using Equation (32) and then averaged across all of the A-lines to obtain a value for the desired analysis frequency. The attenuation of the muscle tissue, $\alpha(\omega_1)$, is calculated in a similar manner using Equation (33).

4.2.3 Computation of the amplitude squared voltage ratio

The computation of the amplitude squared voltage for the muscle tissue, $I(\omega_1, z)$, is nearly identical to that of the phantom. The Matlab file *gate.m* is the same subprogram that is used in the phantom processing. The single exception here is that *gate.m* is operated over a depth range of only 1.5 cm. The Matlab file *process.m* is identical to *phprocess.m* with two exceptions. The non-homogeneous nature of the animal carcass is taken into consideration, and the ratio of the amplitude voltage of the muscle to that of the phantom, $RI(\omega_1, z)$, is computed in addition to $I(\omega_1, z)$.

The nonhomogeneous nature of the animal carcass is dealt with when converting the depth to the time-of-flight. The speed of sound in fat and in the hide are compensated for. The thickness of the fat (fz) is selected for each individual A-line from the vector fathick, generated by the Matlab file *fatprog.m* described above. An average value for the thickness of the animal's hide is used during the

processing of the hide-on scan data. The variable hz is set to zero for the hide-off and cold scan data processing.

Hide thickness measurements were not taken for the majority of the animals scanned. The average thickness and speed of sound values are from an analysis of animals 77 through 128 accomplished in the Bioacoustics Research Laboratory.

4.2.4 Computation of the backscatter coefficient ratio

The final subprogram accessed from *bacscat.m* is the Matlab file *bscoef.m*. The purpose of *bscoef.m* is to convert the ratio of amplitude squared voltages into a ratio of the backscatter coefficients using Equation (24). The attenuation of the propagation path is separated into that which occurs before the region of interest (attnknown) and that which occurs within the region of interest (attnROI). This involves keeping track of the attenuation and the thickness of each tissue region. The subprogram then calculates an estimate of the backscatter ratio (rb) for each data point within the gated RF signal by multiplying the total path attenuation by the ratio of the amplitude squared voltages for each data point. The average of the rb estimates is then computed and returned to *bacscat.m*.

The average backscatter ratio for each depth is then averaged for each analysis frequency. One value of $RB(\omega_i)$ and one value for the attenuation in dB/cm are returned to *animal.m* for each analysis frequency after each scan. This concludes the processing for an individual scan. *animal.m* then stores the returned information and executes *bacscat.m* again for the next scan until all three have been accomplished.

4.2.5 Output

After executing and receiving results for the hide-on, hide-off, and cold scans, *animal.m* writes two ASCII files to the directory in which the active Matlab

application is resident. It creates one file for the backscatter information *(bsc.asc)* and one file for the attenuation values *(attn.asc)*. Both files are nineteen-element column vectors. The first element contains the animal number, the next six contain the values from the hide-on at each analysis frequency, the elements 8 through 13 contain the values for the hide-off scan, and elements 14 through 19 contain the values for the cold scan. Each set of values is arranged from the lowest frequency to the highest.

CHAPTER 5

DATA COLLECTION

All data processed for this research project were collected using the Beef Ultrasound Grading System (BUGS) equipment. BUGS is an experimental data collection system built for the purpose of attaining a data base for the development of an ultrasound grading system for beef [1]. BUGS is a joint research project between the Bioacoustics Research Laboratory and the Meat Sciences Laboratory at the University of Illinois.

5.1 Equipment

BUGS consists of a scanning table superstructure (Figure 3) and an equipment rack (Figure 4). The scanning table superstructure consists of a removable carcass mounting structure and the main superstructure assembly. The carcass mounting structure secures the main superstructure to the beef carcass and can be removed for cleaning. The main superstructure assemble houses seven electric motors and positioning actuators and two 1.0 MHz Panametrics transducers with focal distances of 101 mm (Figure 5). The positioning system is fully automated and allows for three-dimensional positioning of the transducers within 85 mm up and down and 200 mm right or left from the center of the scan. The system also allows for a rotation of the angle of contact between the transducers and the carcass of up to 25 degrees.
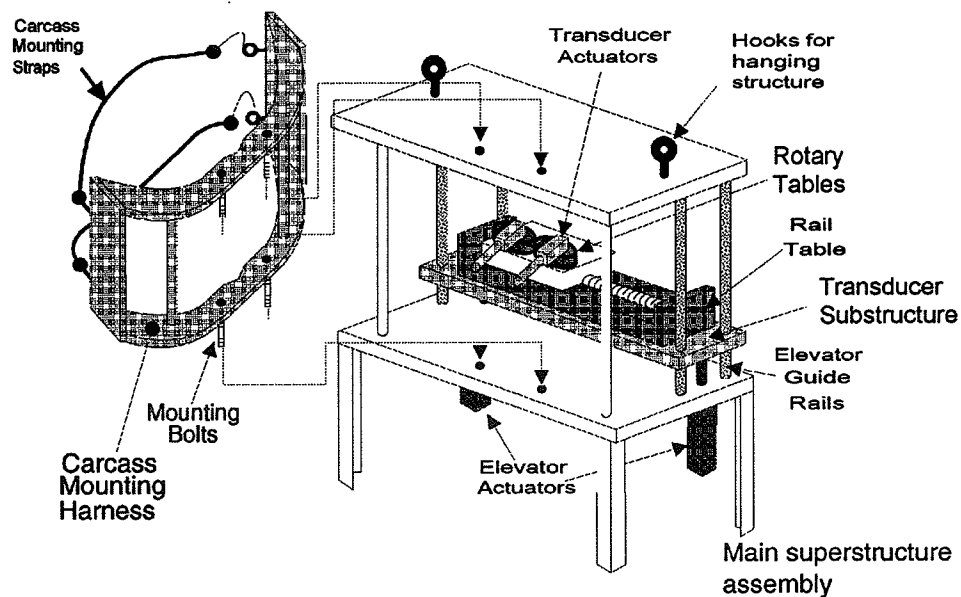
Figure 3: BUGS scanning table superstructure [1].
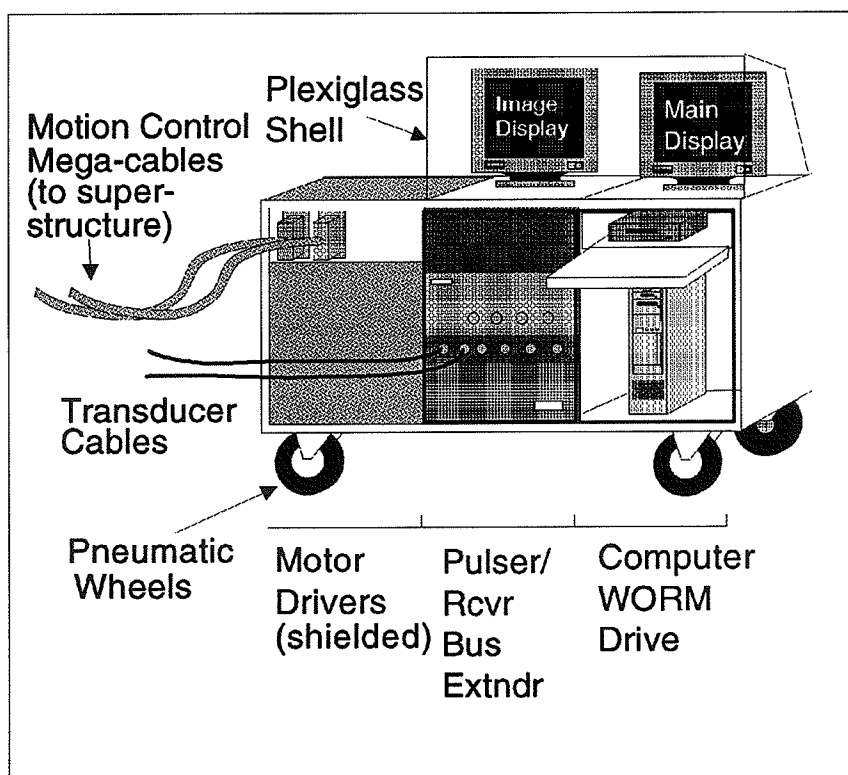
Figure 4: BUGS equipment rack [1].

The transducers are driven by a RITEC RAM 10000 pulser/receiver housed on the accompanying equipment rack. The equipment rack also houses seven Compumotor S57-83-E motor driver units, a 486/33 MHz PC with a 550 MB hard drive, and a Panasonic LF5010 WORM drive for permanent data storage. The electronics on the scanning table structure are connected to the motor controllers on the equipment rack by two large Mega-cables. Each transducer is connected to the pulser/receiver by a coaxial cable and a multiplexor. The received echo voltage is digitized at 50 MHz with a Gage CS250 A/D card. The digitized data are then stored on the hard drive until they can be transferred to the WORM drive for backup and to the laboratories Sun Sparc2 workstation via ETHERNET.
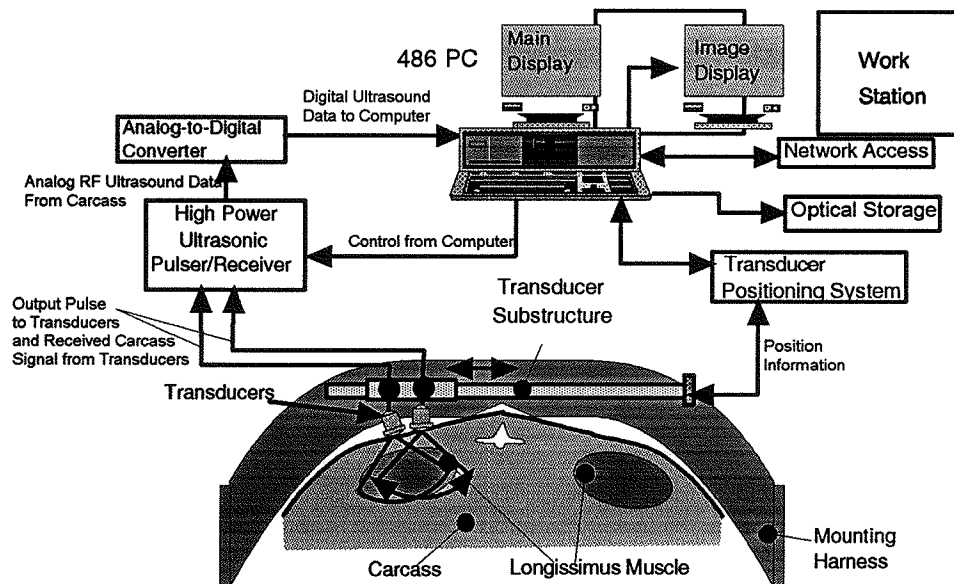
Figure 5: Scanning table attached to carcass with data acquisition and storage paths [1].

5.2 Horizontal Scan Protocol

The data used for backscatter analysis are collected using the horizontal scan protocol. This protocol is centered by placing the left or "a" transducer directly over the animal's spine at the twelfth rib. During the full horizontal scan protocol, the machine makes a lower, a center, and an upper scan over the longissimus dorsi muscle in the animal's back (Figure 6). The center scan protocol starts at 200 mm to the animal's right side and scans to the animal's spine and then from 200 mm on the animal's left side to the spine. The lower and upper scan protocols of the full horizontal scan start at 200 mm to the animal's right side and scan to the animal's spine. Both are positioned 70 mm from the twelfth rib. Data are collected by both transducers at 1 mm intervals along these horizontal scanning lines. At each data collection point, multiple A-lines are collected, each at different gain settings.

Due to the immense amount of data collected, only data collected from the "a" transducer were selected for use in the backscatter calculations.
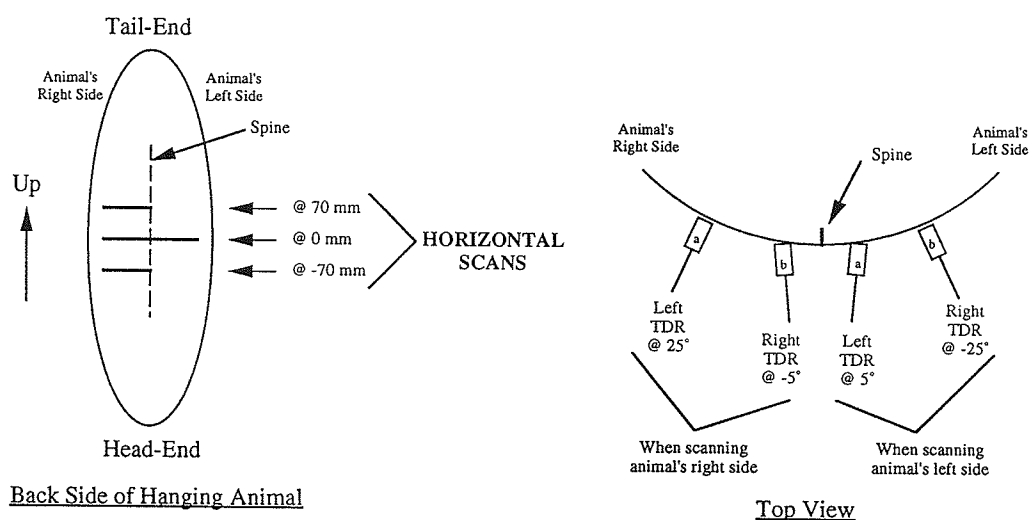
Figure 6: Horizontal scan protocol.

5.3 Scan Types

Three types of scans were accomplished on each animal: a hide-on, a hide-off, and a cold. In addition to the animal scans, a reference phantom scan was done with each animal. The reference phantom was designed and manufactured by ATS Laboratories (Bridgeport, CT) specifically to mimic the tissue of the longissimus dorsi muscle and to attach to the main superstructure of the BUGS scanning table. The material of the reference phantom was characterized in the Bioacoustics Research Laboratory and found to have an attenuation value of 1.0 dB/cm MHz and a speed of sound of 1600 m/s. The scan protocol used for the phantom is similar to the animal's right-side portion of the center horizontal scan protocol with 85 A-line locations spaced 1 mm apart. Six A-lines were collected at each location with gain values of 36, 42, 48, 54, 60, and 72 dB. Eighty of the 85 A-lines with gain values of 72 dB were used from each phantom scan with 5 A-lines being omitted due to their proximity to the center support structure of the phantom. The 72 dB gain value was selected to provide a good signal to noise ratio at the analysis depth range. The file nomenclature of the phantom file used for backscatter analysis is *pra72m00.dat*.

The hide-on scan was started within 20 min after the animal had been killed and was accomplished with the animal's hide still on the carcass. Muscle and fat temperatures were approximately 37 degrees Celsius. For this scan, the animal's hair was removed leaving bare hide in the area to be scanned. The hide-on horizontal scan protocol consisted of only the center portion of the full horizontal scan protocol with 120 A-line locations on each side of the spine.

Seven A-lines were collected at each location with gain values of 12, 18, 24, 30, 36, 42, and 48 dB. The nomenclatures of the hide-on files used for backscatter analysis are *nra36m00.dat* and *nla36m01.dat*.

The hide-off scan was accomplished immediately after the animal had been skinned and disemboweled. Muscle and fat temperatures were approximately 37 degrees Celsius. On the animal, the hide-off scan employed the full horizontal scan protocol with 120 A-line locations per animal side. To remain consistent with the phantom and hide-on scans, only data from the center portion of the horizontal scan protocol were used for backscatter analysis. Six A-lines were collected at each location with gain values of 18, 24, 30, 36, 42, and 48 dB. The nomenclatures of the hide-off files used for backscatter analysis are *fra36m01.dat* and *fla36m02.dat*.

The cold scan was accomplished after the carcass had been refrigerated for a minimum of 12 h. Normal muscle and fat temperatures for the cold scan were approximately 10 degrees Celsius. The cold scan also employed the full horizontal scan protocol with 120 A-line locations per animal side and, to remain consistent, only data from the center portion of the horizontal scan protocol were used for backscatter analysis. Six A-lines were collected at each location with gain values of 18, 24, 30, 36, 42, and 48 dB. The nomenclatures of the cold files used for backscatter analysis are *cra36m01.dat* and *cla36m02.dat*.

On all three animal scans, sixty-eight of the A-lines with gain values of 36 dB from the animal's right side and sixty from the animal's left side were selected. The 36 dB gain value was selected because it is the highest gain value for which the echo signal does not characteristically saturate in the region of interest. The elimination of some of the A-lines was required to ensure that scan areas were directly over the region of interest. Hide-on and hide-off scans on a single animal were accomplished the same day. Cold scans were accomplished within 36 h of the time that the animal was killed.

CHAPTER 6

RESULTS AND ANALYSIS

6.1 Description of Data

Data were collected from hide-on, hide-off, and cold scans for each of 108 animals, numbered 21 through 128, with the exception of animal 70. The hide-on scan for animal 70 was not accomplished due to a technical problem that occurred after the scan was started. The hide-off and cold scans were accomplished on animal 70 and are included in the data tables in Appendices D and E.

The processing software for the hide-on scan must account for the hide as a transmission medium. The hide is extremely attenuating (9.33 dB/cm at 1.0 MHz) [15] compared to fat at the same temperature [4]. This can be seen by comparing the plot of a hide-on A-line in Figure 7 with the plot of a hide-off A-line in Figure 8. Both plots are from the same location of the same animal during the respective scans and are from data collected at a gain setting of 36 dB. The first centimeter on both plots is occupied by the thickness of the standoff. The standoff is a boot-like protective cover for the transducer that couples the ultrasound energy to the carcass.

To estimate the location of the fat/muscle boundary, the average hide thickness of 0.7 cm can be used along with the average fat thickness which is 2.21 cm for animal 61. Added to the 1 cm standoff thickness, this estimates the muscle
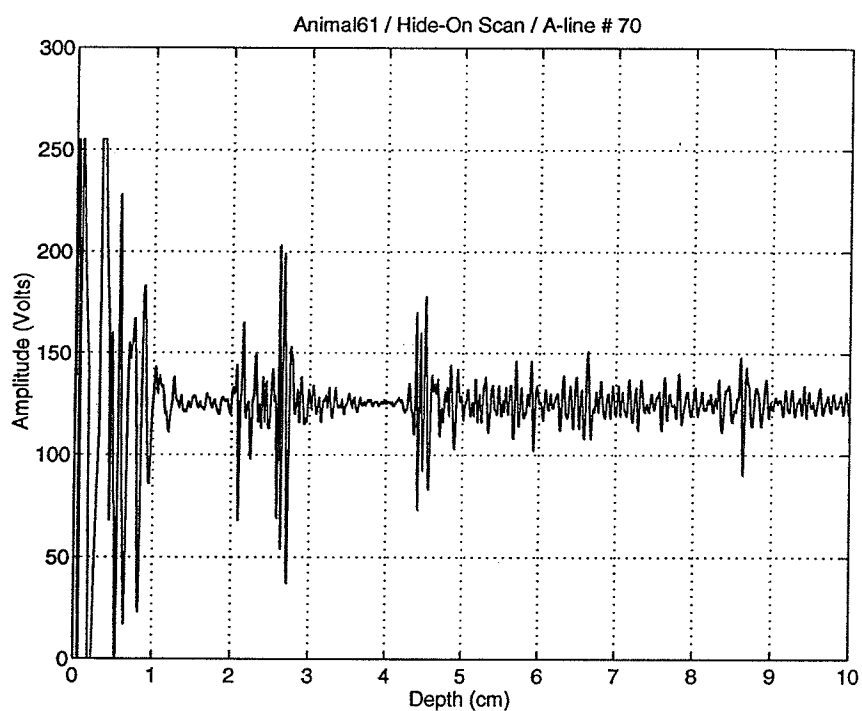
Figure 7: Plot of A-line number 70 from the hide-on scan of animal number 61.
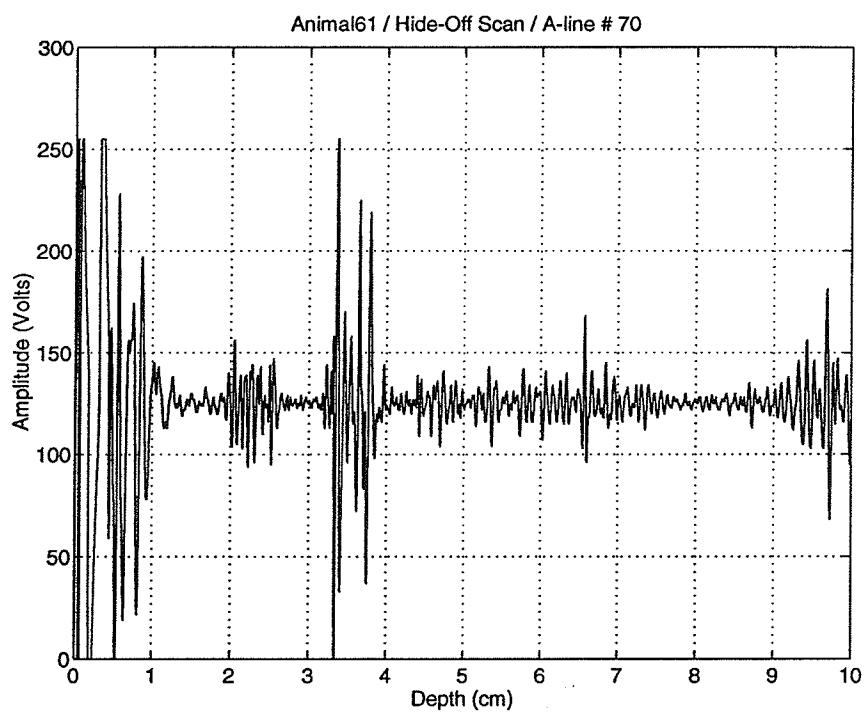
Figure 8: Plot of A-line number 70 from the hide-off scan of animal number 61.

boundary at about 3.9 cm for the hide-on scan and at about 3.2 cm for the hide-off scan.

Looking first at the hide-off plot in Figure 8, it appears that the fat thickness estimate of 2.21 cm is very close to being correct. The spike located at 3.2 to 3.3 cm in Figure 7 is a reflection from the fat/muscle boundary. Comparison of this boundary with that in Figure 7 indicates that the fat/muscle boundary for the hide-on scan occurs at about 4.2 to 4.3 cm. This indicates a hide thickness of about 1 cm and is in agreement with the spike at about 2 cm where the hide/fat boundary appears to be located. Both plots demonstrate the erratic amplitude characteristics of an echo signal from muscle tissue and contain large spikes indicative of tissue boundaries.

The cold-scan A-line plotted in Figure 9 is also from the same animal and location as the A-lines in Figures 7 and 8 and is also from data collected at a gain setting of 36 dB. The attenuation value of fat at 10 degrees Celsius (6.0 dB/cm at 1.0 MHz) is three times that of fat at 23 degrees Celsius [4]. This increase in attenuation of the signal is noticeable in Figure 9. The amplitude of the spiked returns at the fat/muscle boundary of the cold scan plot is more than 50 Volts less than the amplitude at the same point on the hide-off plot due to this increase in attenuation.

The distance that the ultrasound signal travels in the standoff material is ignored in the signal processing. Because the same standoffs were used for the animal and phantom scans, the inclusion of the standoff attenuation and speed values in the calculations would fall out of the computation in Equation (21). The standoff thickness of 1 cm would have to be deducted from the analysis depth, along with the fat and hide thickness, for calculating the distance within the muscle tissue to each data point. The minimum analysis depth of 6 cm was chosen to ensure that the analysis depths will always be within the muscle tissue.
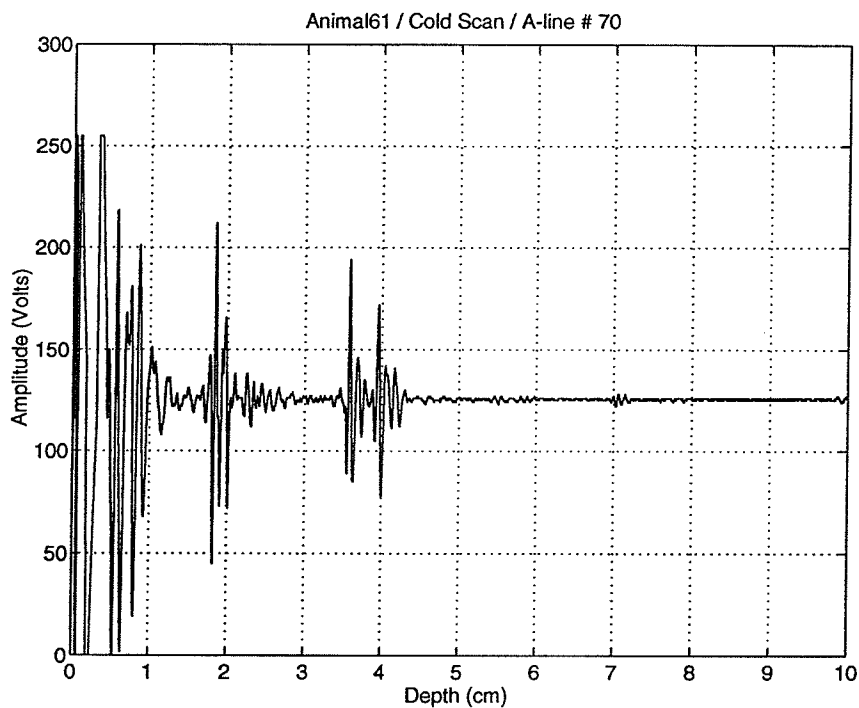
Figure 9: Plot of A-line number 70 from the cold scan of animal number 61.
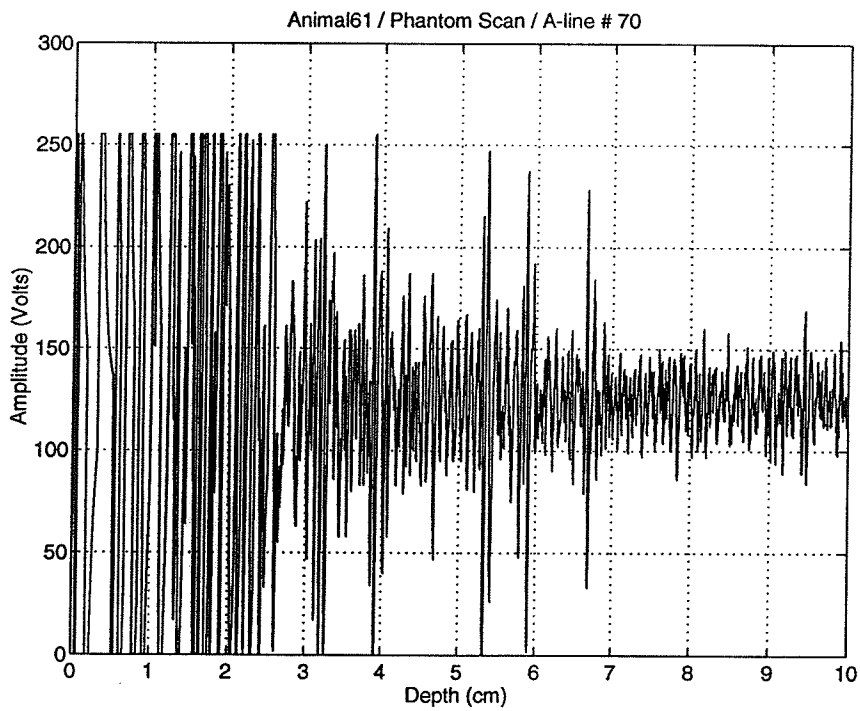
Figure 10: Plot of A-line number 70 from the phantom scan of animal number 61.

Figure 10 is a plot of A-line number 70 from the reference phantom and is plotted from data collected at a gain setting of 72 dB. This phantom data were collected concurrently with the animal scans of animal number 61. As Figure 10 shows, the 72 dB gain setting causes saturation below the 4 cm depth but allows for better evaluation of the signal in the 6 to 9 cm range.

The A-lines plotted in Figures 7, 8, 9, and 10 are representative of typical data analyzed for the 108 animals used in this project.

6.2 Phantom on Phantom Results

To validate the software and determine its accuracy and repeatability, the phantom data were run using the same phantom data file as the unknown tissue data and as the reference phantom. The depth range used for this analysis was 6 to 9 cm and the analysis frequencies were 0.7 to 1.2 MHz in 0.1 MHz steps. The fat and hide thicknesses were set to zero and all speeds were set to the speed of sound in the phantom (1600 m/s). Theoretically, the attenuation output by the program would be the attenuation of the phantom (1 dB/cm MHz). Using Equation (24), the difference in attenuation, $\Delta\alpha\left(\omega_1\right)$, would then be zero and the ratio of the backscatter coefficients would ideally be unity.

Attenuation and backscatter ratios for phantom-on-phantom scans from a cross section of the total 108 phantom scans were computed. Table 1 shows the attenuation results of the phantom-on-phantom scans and Table 2 lists the backscatter coefficient ratios. All tables in this chapter were input and calculated using Microsoft Excel, version 4.0.

The average attenuation value at 1 MHz for all phantoms computed was 2.1 dB/cm which is about 1.0 dB/cm, higher than the known value of the phantom. There are also significant changes in the attenuation values and attenuation slope values between phantom scans. A probable source of this variance is the

changing environment on the kill floor where the phantom scans were accomplished.

Table 1: Attenuation results for phantom on phantom scans of 11 phantoms.

Phantom	27	37	50	61	65	69	81	96	107	118	133
.7 MHz	2.347	1.807	1.712	2.177	1.819	1.925	1.594	1.297	1.265	1.445	1.399
.8 MHz	2.569	2.108	1.818	2.059	2.082	1.983	1.560	1.374	1.556	1.647	1.736
.9 MHz	2.558	1.985	2.065	2.426	2.232	2.036	1.723	1.577	1.643	1.817	1.966
1.0 MHz	2.609	2.051	2.322	2.220	2.027	2.049	1.818	1.706	1.990	2.125	2.181
1.1 MHz	2.361	1.944	1.985	2.362	2.120	1.929	1.909	1.741	1.994	2.096	2.138
1.2 MHz	2.675	2.100	2.266	2.631	2.123	2.187	1.878	1.992	1.937	2.117	2.322
Ave	2.520	1.999	2.028	2.313	2.067	2.018	1.747	1.615	1.731	1.875	1.957
Std Dev dB/cm	.1349	.1139	.2409	.2039	.1389	.0980	.1470	.2557	.2950	.2860	.3395
Slope dB/cm MHz	.3049	.2969	1.008	.8494	.4083	.3320	.7320	1.344	1.435	1.433	1.725

Table 2: Backscatter ratio data for phantom on phantom scans of 11 phantoms.

Phantom	27	37	50	61	65	69	81	96	107	118	133
.7 MHz	176.9	32.06	23.78	103.1	33.28	46.55	16.39	6.444	5.827	10.25	8.875
.8 MHz	261.3	60.49	24.19	51.85	55.72	40.66	10.74	5.989	10.62	14.11	18.70
.9 MHz	183.4	29.89	38.49	120.7	65.30	35.10	13.11	8.288	10.19	17.63	28.19
1.0 MHz	157.0	26.88	63.13	45.71	24.89	26.68	12.91	9.062	22.14	33.90	40.47
1.1 MHz	52.07	13.98	15.90	52.30	24.35	13.37	12.54	7.390	16.40	22.58	25.77
1.2 MHz	102.7	16.70	28.19	89.36	17.93	21.97	8.314	11.88	9.983	17.63	33.61
Ave	155.6	30.00	32.28	77.17	36.91	30.72	12.33	8.175	12.53	19.35	25.94
Std Dev	71.99	16.60	16.81	31.51	19.16	12.35	2.688	2.141	5.792	8.228	11.12
Slope	-292.9	-62.67	6.236	-40.67	-60.37	-60.93	-10.05	9.186	14.30	22.46	44.89

The experiments involving animal numbers 27 and 37 were accomplished during the summer on a warm kill floor while the animals numbered above 80 where scanned during the winter on an unheated kill floor. To help evaluate the possibility that the temperature of the phantom material could be causing fluctuations in the measurements, phantom scan number 133 was accomplished immediately after storing the phantom inside a cooler at 10 degrees Celsius for

more than 12 h. The possible effect of temperature on the attenuation values can be seen in the slope values of Table 1. There is an increase in the slope of the attenuation values (dB/cm MHz) with a decrease in the temperature of the phantom. The highest slope value corresponds to phantom scan number 133, which was undoubtedly the coldest scan, and the two lowest slope values correspond to the scans accomplished on the hot kill floor during the summer months. The fact that the three scans accomplished between phantom numbers 60 and 70 agree relatively closely also supports the concept of temperature dependence in the slope values. Phantoms 61, 65, and 69 were all scanned within a three-week period during the autumn.

Another thing that could be a contributing factor to the fluctuations in the attenuation and backscatter ratio values is the fact that the phantom material is designed to mimic muscle tissue. Figure 10 demonstrates the coarseness of the phantom echo signal. This could cause fluctuations in both attenuation and backscatter, but would tend to increase the backscatter ratio values to a greater extent due to point-by-point changes in the amplitude squared voltage values. Backscatter values are affected directly by any factors affecting the measurements and then indirectly by these same factors again through their effect on the attenuation values. This doubling affect is due to the fact that the backscatter ratio is computed by multiplying the amplitude squared voltage ratio by the attenuation value, and the attenuation value is obtained by averaging the logarithm of this same amplitude squared voltage ratio value over the 3 cm range gate. Therefore, any factor affecting the amplitude squared voltage will have multiple effects on the backscatter coefficient ratio.

It should be noted, however, that the average slope value for all 11 phantom scans analyzed (0.897 dB/cm MHz) is within 10.5 percent of the 1.0 dB/cm MHz phantom attenuation value.

6.3 Comparison with Through-Transmission Attenuation Measurements

Through-transmission attenuation measurements of samples from the longissimus dorsi muscle of 40 of the animals scanned by the BUGS system were made by Nadine Smith and Thida Lwin of the Bioacoustics Research Laboratory at the University of Illinois [4]. These measurements were made on excised samples of the muscle tissue that were approximately 16 cm square and between 4 and 7 cm thick at temperatures of 37, 20, and 4 degrees Celsius after storage in a minus 70 degree freezer. Measurements were recorded in 1 MHz steps from 1.0 to 7.0 MHz. Both parallel and perpendicular orientations of the muscle were measured for most samples and temperatures [15]. Correlation coefficients comparing the hide-on (HON), hide-off (HOF), and cold scans to the through-transmission measurements (TTM) at the respective temperatures were calculated for each animal for which through-transmission measurements were available and are listed in Tables 3 and 4. Table 3 contains correlation coefficients of the attenuation values for 1 MHz using both parallel and perpendicular orientations when available.

Table 3: Correlation of 1.0 MHz backscatter and TTM attenuation values.

	Temp	Orient	HON	HOF	COLD
TTM	37	perp	-0.0830	-0.1580	
TTM	37	parallel	-0.1087	-0.1122	
TTM	20	perp		0.1470	
TTM	20	parallel		0.1327	
TTM	4	perp			-0.1290
TTM	4	parallel			-0.0660

Because the hide-off scans were accomplished after the animal had been skinned and disemboweled, it is possible that the muscle temperature during this scan did

not remain at a constant 37 degree body temperature for the entire scan. For this reason the HOF attenuation values were correlated with both the 20 and 37 degree TTM measurements. It should be noted, however, that the backscatter attenuation data used in this analysis are from the center horizontal scan which is accomplished first in the hide-off scan protocol before much cooling, if any, could occur.

Table 4 is a listing of the correlation coefficient values from a comparison of the dB/cm MHz slope values of the two attenuation measurement methods. A complete listing of the measured TTM values and the backscatter attenuation values correlated with them is in Appendix F [15].

Table 4: Correlation of backscatter to through transmission slope values.

	Temp	Orient	HON	HOF	COLD
TTM	37	perp	0.0960	0.2896	
TTM	37	parallel	-0.1557	0.2624	
TTM	20	perp		0.0389	
TTM	20	parallel		0.0797	
TTM	4	perp			0.1108
TTM	4	parallel			-0.0140

The magnitude of the correlation coefficients between the two attenuation measurements is not high. This is not surprising after consideration of some of the differences between the samples that were measured by each method and the equipment used. The TTM measurements were made on samples that were small relative to the size of the sample available for backscatter measurements. Additionally, the TTM samples were not fresh samples and were measured in a temperature-controlled water bath. Temperatures within the muscle tissue on the

carcass inherently vary at least somewhat during data collection due to the nature of the environment in which the experiment is conducted.

The analysis frequencies used in the two methods only coincide at 1.0 MHz. The TTM data were collected at 1.0, 2.0, 3.0, 4.0, 5.0, 6.0, and 7.0 MHz while the backscatter data were collected at .7, .8, .9, 1.0, 1.1, and 1.2 MHz.   The 1.0 MHz value represents a value near the center frequency of the BUGS system's ultrasound spectrum but is at the edge of the spectrum for the TTM measurements.

The correlation information in Tables 3 and 4 underscore the effect that the animal's hide has on the attenuation measurements. Correlation between the perpendicular orientation and the hide-on scan values is extremely low for both the attenuation and the slope values. The analogous values for the hide-off scans correlate the best of all the correlations done between the two methods. The relatively high values for the correlation between the hide-off scan and the TTM values at 37 degrees also reinforce the assumption that the attenuation values from the hide-off scan are the most accurate of the three scans.

The correlation information also strengthens the assumption that the muscle tissue used for backscatter data collection from the hide-off scan has not cooled off by the time the center horizontal scan is accomplished. The correlation coefficients of the hide-off scan with the 37 degree measurement are substantially better than those with the 20 degree TTM measurements. The information also seems to indicate a strong preference of the cold scan for the perpendicular orientation.

6.4   Correlation Between Animal Scans

To look at the similarities between the three different types of animal scans, all values of each of the respective attenuation and backscatter ratios at each frequency were correlated with the analogous values of the other two scans. The

slopes of the attenuation and backscatter ratios of each type of scan were also correlated against the slopes of the other two. Tables 5 and 6 list the results of these correlations. A complete listing of the data is in Appendices D and E.

Table 5: Correlation coefficients of animal scan attenuation values and slopes.

	.7 MHz	.8 MHz	.9 MHz	1.0 MHz	1.1 MHz	1.2 MHz	Slope
HOF/HON	-0.0898	0.0099	0.037	-0.0008	-0.0159	-0.0578	-0.5287
HOF/COLD	0.0401	0.0334	0.0261	0.0151	0.009	0.0528	0.1426
HON/COLD	0.0349	0.0595	0.0287	0.0113	-0.006	-0.0056	-0.1786

Table 6: Correlation coefficients of animal backscatter coefficient ratios and slopes.

	.7 MHz	.8 MHz	.9 MHz	1.0 MHz	1.1 MHz	1.2 MHz	Slope
HOF/HON	-0.0429	-0.0318	-0.0156	-0.0147	-0.0047	-0.0137	-0.0460
HOF/COLD	-0.0232	-0.0192	-0.0168	-0.0144	-0.0188	-0.0189	-0.0227
HON/COLD	-0.0135	-0.0079	-0.0074	-0.0061	-0.0110	-0.0132	-0.0129

Correlation between scans is poor. This is especially true of the backscatter coefficient ratios and is not surprising given that all of the other indicators showing differences between values from one type scan to the next.

Table 5 does indicate that the slope of the attenuation values correlates relatively well compared to the individual attenuation values within the scan types. This is a very positive aspect. The slope is a better indicator of changes within the muscle structure because it is averaged over the range of attenuation values.

6.5 Correlation with Carcass Measurements

To facilitate the evaluation of the acoustic measures extracted from the ultrasonic data collected as described in Chapter 5, each of the 108 animals

scanned was dissected by the staff of the Meat Science Laboratory at the University of Illinois. Fat thicknesses, degree of marbling, muscle thicknesses, muscle color, and muscle weight were among the physical measures recorded during dissection. Muscle composition and tenderness testing were also done on each of the animals [17].

All physical measures and carcass composition data were correlated with the backscatter coefficient ratio and attenuation results for all three scans of all 108 animals in the data base. Values for each analysis frequency and the respective slopes of these values for each animal and scan were correlated with the dissection data [17].

Some very promising correlations were obtained from the hide-off backscatter attenuation values. As shown in Table 7, correlation coefficients for correlations between the attenuation slopes and the last rib fat thickness values at 5, 10, and 15 cm distances from the animal's spine (LR5FT, LR10FT, and LR15FT) over the longissimus dorsi muscle were very high. All three coefficient values were highly significant (P < .0001) and individual attenuation values for specific analysis frequencies also correlated extremely well.

Table 7: Correlation coefficients for carcass measures and backscatter attenuation values.

	.7 MHz	.8 MHz	.9 MHz	1.0 MHz	1.1 MHz	1.2 MHz	Slope
LR5FT	0.3434	0.4775	0.5801	0.6604	0.6882	0.7145	0.6369
LR10FT	0.2498	0.3925	0.5151	0.6081	0.6508	0.6938	0.7248
LR15FT	0.2542	0.4053	0.5268	0.6082	0.6531	0.6897	0.7087
LDEE	0.1886	0.2743	0.3569	0.4252	0.4535	0.4718	0.4797
LDH2O	-0.1536	-0.2411	-0.3208	-0.3906	-0.4186	-0.4407	-0.4746

Shown also in Table 7 are correlations of hide-off attenuation values with the longissimus muscle either extract (LDEE) and water content (LDH2O). These

measures also correlated well. All correlation coefficient values in Table 7 were significant (P < .05) except for the (LDH2O / 0.7 MHz) value. All of the correlation coefficients for the slope values were highly significant (P < .0001).

The backscatter coefficient ratio value did not correlate nearly as well for the same set of data comparisons. The slope correlation coefficients for the backscatter coefficients from the hide-off scans are listed in Table 8. The individual correlation coefficients for each frequency were clustered fairly tightly around the absolute value of the slope coefficient but were all positive except for the LDH2O values. Correlation coefficient values were significant.

Table 8: Slope correlation coefficients for hide-off backscatter ratio values.

LR5FT	LR10FT	LR15FT	LDEE	LDH2O
-0.2961	-0.2903	-0.2382	-0.2058	0.1652

Hide-on scan correlation values for attenuation were extremely poor. None of the attenuation correlation coefficients of the hide-on scan values were significant (P < .05). The backscatter correlation coefficients for the hide-on fat thickness measures were very close to those obtained for the hide-off scan:

LR5FT = -.2938, LR10FT = -.2871, and LR15FT = -.2036.

The cold scan attenuation values were also very poor with no significant correlation coefficient values to report. However, the cold-scan backscatter values for the fat thickness correlations were the best obtained for backscatter coefficient ratios and are highly significant (P < .0001).

Table 9: Correlation coefficients for cold scan backscatter coefficient ratio slope values.

LR5FT	LR10FT	LR15FT	LDEE	LDH2O
-0.4591	-0.3927	-0.3963	-0.2183	0.2474

CHAPTER 7

CONCLUSIONS

Comparison of the backscatter attenuation data with the carcass dissection data indicates that this method has good potential as an indicator of some types of beef tissue properties at least for warm carcass hide-off scans. The high correlation of the attenuation values to the fat thickness seems to indicate that there is a uniform and repeatable effect on the signal by the thickness of fat that it propagates through to get to the muscle tissue.

The reasonably strong correlation of the hide-off attenuation values and the fat and water contents of the muscle (LDEE and LDH2O) should not be overlooked. Both correlation coefficients were highly significant. The fact that these two correlation coefficients are nearly equal in amplitude and opposite in sign warrants investigation. This could be more than coincidence due to the fact that water and protein tend to have an inverse relationship with the fat content within muscle tissue.

The poor performance of the method with the hide-on scan is not surprising. The hide is a relatively thin layer of highly attenuating tissue in close proximity to the transducer. The outgoing acoustical wave sees a large discontinuity at the outer hide boundary, propagates in the highly attenuating medium for a short time, and then sees another large discontinuity at the inner boundary of the hide. The

acoustical wave will experience large reflections at each boundary of the hide, both entering the carcass and exiting it. These reflections will not only disperse the signal but are likely to cause at least some degree of distortion in the transmitted wave as well. This analysis is supported by the relatively low correlation of the hide-on scan to the through transmission measurements and the carcass data. It can not be discounted, however, that the slope of the hide-on attenuation data correlated the closest to the hide-off data in Table 5.

The cold-scan data has a very low correlation with the hide-off scan and the through-transmission measurement data. An examination of Figure 9 indicates that one possible cause of this could be that the signal to noise ratio is too low in the region of interest. The fact that the backscatter coefficient ratio correlated reasonably well with the carcass data on the cold scan would tend to indicate, though, that the signal is of a high enough level to be useful. Additional processing runs of the cold scan data using the backscatter program would be helpful in deciding the usefulness of this scan.

The analysis accomplished in this research seems to indicate that there is a temperature dependence in the attenuation of the phantom material. More investigation is needed to establish if there definitely is a temperature dependency and to characterize it. Ensuring that the phantom is at the same temperature each time that it is scanned would also solve any temperature-dependent errors in the calculations.

Although this method shows considerable promise as an indicator of tissue properties in beef, it does not show promise as an indicator of absolute attenuation or backscatter coefficients. It was able to indicate some trends in the data and correlated with fair agreement to the through-transmission measurements when comparing the hide-off scan data, but this method was not able to determine the attenuation value of the phantom to any degree of accuracy.

APPENDIX A

BACKSCATTER ATTENUATION PROGRAM OPERATING MANUAL

Appendix A is an instructional manual on how to run the backscatter program.

* Backscatter Attenuation Program Operating Manual   *

*   *

* Roger L. Scheer   *

* Bioacoustics Research Laboratory   *

* Department of Electrical and Computer Engineering   *

* University of Illinois   *

* June 10, 1994   *

*   *

A.1 Introduction

This is the first version of this file, a guide to the software used

in conjunction with MATLAB in the automatic estimation of

the acoustic attenuation of muscle tissue in the Beef Ultrasound

Grading System (BUGS) project, ongoing at the University of Illinois.

The software described in this document has all been developed for the specific

purpose of facilitating the estimation of acoustic backscatter

and attenuation utilizing an adaptation of the Reference Phantom Method developed by Yao [7].

The software consists of two types of files:

i) A program written in C that converts raw data files into Matlab data files.

ii) Matlab m-files which are interpreted by Matlab, a commercial software package sold by The Math Works, Natick, MA.

A.2 Input/Output

A.2.1 Preprocessing

The BUGS system collects a large amount of data from each carcass.

Each scan is done with two transducers (A & B), each of which collects data at each of the various gain settings [1]. The programs described here currently utilize only the A transducer at the 36 dB gain setting (72 dB for phantom data) and operate directly on the raw RF data preprocessed into Matlab readable files. The preprocessing is done via the C program, *rf_to_ml*, located in *ecstasy/bugs/scheer/rf_to_ml* for all but the phantom files. The phantom files are processed using *phrf_to_mat*. These programs utilize the standard *savemat* type format recommended by the Math Works.

A.2.2 RF Files

The raw data (RF) files selected from the backup data files stored on optical disk or tape are

\data\anml_xxx\hide_on\nra36m00.dat

\data\anml_xxx\hide_on\nla36m01.dat

\data\anml_xxx\hide_off\fra36m01.dat

\data\anml_xxx\hide_off\fla36m02.dat

\data\anml_xxx\cold\cra36m01.dat

\data\anml_xxx\cold\cla36m02.dat

\data\anml_xxx\phantom\pra72m00.dat

The converted Matlab input files are stored on ECSTASY in

/bugs/scheer/data/anml_xxx/nra36m00.mat

/bugs/scheer/data/anml_xxx/nla36m01.mat

/bugs/scheer/data/anml_xxx/fra36m01.mat

/bugs/scheer/data/anml_xxx/fla36m02.mat

/bugs/scheer/data/anml_xxx/cra36m01.mat

/bugs/scheer/data/anml_xxx/cla36m02.mat

/bugs/scheer/data/anml_xxx/pra72m00.mat

A.2.3 Output files

The Matlab routine produces two ASCII output files per animal. One file
(*bsc.asc*) contains the backscatter ratios of the tissue with respect to the reference
phantom and one file (*attn.asc*) contains attenuation values, in decibels, of the
muscle tissue at each analysis frequency. Both ASCII files are 19-element column
vectors. The first element is the animal number. Elements 2 thru 7 are the
attenuation or backscatter ratio values for the hide-on scan with element number 2
being the value at the lowest evaluation frequency and element number 7 being the
value for the highest of the 6 evaluation frequencies. Elements 8 thru 13 are the
frequency-dependent values for the hide-off scan in the same manner and elements
14 thru 19 are the values for the cold scan.

The output files are created in the directory that Matlab is run from and
are transferred manually to */bugs/scheer/Results/anml_xxx* .

A.3 Program Files

A.3.1 C files

The following are the executable C files used to convert the binary raw data
files (*X.dat*) into a Matlab file (*X.mat*):

> *rf_to_ml*

> *phrf_to_mat*   (phantom files only)

The source code for these programs can be found in files:

> */bugs/scheer/Data/C*   and   */bugs/scheer/Data/Cph*

The UNIX file *easy* can be used as a script to convert all seven files.

> Type, " chmod +x easy " , and then type, " easy " .

> All files from *C* and *Cph* must be in the same directory for *easy* to run.

A.3.2 M-files

The processing of the converted RF Matlab files is accomplished by

(i)   transferring the required input files to the */bugs/scheer/program* directory

(ii) starting up Matlab

(iii) executing the Matlab file, *animal.m*, following the directions in the

> help *animal.m* file

> animal.m utilizes the following Matlab m-files as subprograms:

>> *bacscat.m, getdata.m, fatprog.m, gate.m, phprocess.m,*

>> *longgate.m, roiattn.m, attnprocess.m, process.m,*

>> *voltsq.m, bscoef.m*

(iv) the input *X.mat* files and resulting *X.asc* output files are then transferred

> back into the */bugs/scheer/Data/anml_xxx* and */bugs/scheer/Results/anml_xxx*

> directories for storage.

A.4 Processing Mechanics

This section is devoted to describing the mechanics of the data
processing in a step by step fashion. Processing is essentially the
same for hide-on, hide-off, and cold scans. The only difference being
the additional consideration of the hide's attenuation for the hide-on scan.

A.4.1 Complete processing instructions

(i)   transfer the above listed X.dat input files to their respective animal's
         directories in */bugs/scheer/anml_xxx*

(ii)   convert the binary X.dat files to Matlab readable X.mat files using
         the *phrf_to_mat* program for the *pra72m00.dat* file and the *rf_to_ml*
         program for the remaining 6 *X.dat* files. (Can be done using *easy*)

(iii)   transfer the seven applicable *X.mat* files from a single animal into the
         /bugs/scheer/Program directory

(iv)   start Matlab from within the *Program* directory

(v)   execute *animal.m* from within Matlab by typing "help animal" from
         within the program and following the instructions

(vi)   upon completion, move the Matlab data files and the output (*X.asc*)
         files into the respective animal directory in */bugs/scheer/Data/anml_xxx*

APPENDIX B

DATA CONVERSION PROGRAMS

The C programs in Appendix B are for the purpose of translating the raw RF data into Matlab data files that can be read and manipulated by Matlab.

```
/*  UNIX script to execute C conversion programs for binary to Matlab    */
/*  program name is:   " easy"                                           */
/*  To execute type:   ' chmod +x easy'    < Return >                    */
/*  Then type:  ' easy '                                                 */
```

```
phrf_to_mat pra72m00.dat pra72m00.mat
rf_to_ml nra36m00.dat nra36m00.mat
rf_to_ml nla36m01.dat nla36m01.mat
rf_to_ml fra36m01.dat fra36m01.mat
rf_to_ml fla36m02.dat fla36m02.mat
rf_to_ml cra36m01.dat cra36m01.mat
rf_to_ml cla36m02.dat cla36m02.mat
```

```c
/*  phrf_to_mat.c                                                    */

/*  C program to convert the phantom binary data files to Matlab format   */

/*  I.   C include files                                              */


#include <math.h>
#include <stdio.h>

/* II.  Default Parameters */

#define LENGTH_HEADER           1024
#define MAX_NUMBER_A_LINE     85
#define MAX_LENGTH_A_LINE    8192

/* invoke by
rf_to_ml infile.dat output.mat
*/
extern void savemat();
main(argc, argv)
int argc;
char *argv[];
        {
        FILE            *infile, *outfile;
        unsigned char
        buff[LENGTH_HEADER+MAX_NUMBER_A_LINE*MAX_LENGTH_
A_LINE];
        double          dbuff[MAX_LENGTH_A_LINE],
rfsignal[MAX_NUMBER_A_LINE*MAX_LENGTH_A_LINE];
        int             header_len, length_a_line, number_a_line;
        int             n, m, x, y;

        infile = fopen(argv[1], "r");
        fread(buff, sizeof(char), LENGTH_HEADER, infile);
        fclose(infile);
        header_len = LENGTH_HEADER;
     length_a_line = buff[210]*256+buff[209];
     number_a_line = buff[212]*256+buff[211];
     printf("%d %d\n",length_a_line,number_a_line);

/* read in data */
        infile = fopen(argv[1], "r");
```

```
        fread(buff, sizeof(char),
LENGTH_HEADER+number_a_line*length_a_line, infile);
        fclose(infile);
        for (n = 0; n < number_a_line; n++)
                for (m = 0; m < length_a_line; m++)
                        rfsignal[m*number_a_line+n] =
(double)buff[header_len+n*length_a_line+m];

        outfile = fopen(argv[2], "w");
        savemat(outfile, 1000, "im", number_a_line,length_a_line, 0, rfsignal,
(double *) 0);
        fclose(outfile);
        } /* End of main */
```

```c
/*   rf_to_ml.c                                                    */

/*   C program to convert the animal binary data files to Matlab format   */

/*   I.   C include files */


#include <math.h>
#include <stdio.h>

/* II.   Default Parameters */
#define LENGTH_HEADER            1024
#define MAX_NUMBER_A_LINE        150
#define MAX_LENGTH_A_LINE        5000

/* invoke by
rf_to_ml infile.dat output.mat
*/

extern void savemat();

main(argc, argv)
int argc;
char *argv[];
        {
        FILE            *infile, *outfile;
        unsigned char
        buff[LENGTH_HEADER+MAX_NUMBER_A_LINE*MAX_LENGTH_
A_LINE];
        double          dbuff[MAX_LENGTH_A_LINE],
rfsignal[MAX_NUMBER_A_LINE*MAX_LENGTH_A_LINE];
        int             header_len, length_a_line, number_a_line;
        int             n, m, x, y;

        infile = fopen(argv[1], "r");
        fread(buff, sizeof(char), LENGTH_HEADER, infile);
        fclose(infile);
        header_len = LENGTH_HEADER;
    length_a_line = buff[210]*256+buff[209];
    number_a_line = buff[212]*256+buff[211];

/* read in data */
        infile = fopen(argv[1], "r");
```

```
        fread(buff, sizeof(char),
LENGTH_HEADER+number_a_line*length_a_line, infile);
        fclose(infile);
        for (n = 0; n < number_a_line; n++)
                for (m = 0; m < length_a_line; m++)
                        rfsignal[m*number_a_line+n] =
(double)buff[header_len+n*5000+m];
        outfile = fopen(argv[2], "w");
        savemat(outfile, 1000, "im", number_a_line, length_a_line, 0, rfsignal,
(double *) 0);
        fclose(outfile);

} /* End of main */
```

```
/*

* savemat - C language routine to save a matrix in a MAT-file.
*
* We recommend that you use this routine, and its companion loadmat.c,
* for all writing and reading of MAT-files.  These routines implement
* "access methods" for MAT-files.  By using these routines, instead
* of writing your own code to directly access the MAT-file format,
* you will be unaffected by any changes that may be made to the MAT-file
* structure at a future date.
*
* Here is an example that uses 'savemat' to save two matrices to disk,
* the second of which is complex:
*
*       FILE *fp;
*       double xyz[1000], ar[1000], ai[1000];
*       fp = fopen("foo.mat","wb");
*       savemat(fp, 2000, "xyz", 2, 3, 0, xyz, (double *)0);
*       savemat(fp, 2000, "a", 5, 5, 1, ar, ai);
*    fclose(fp);
*
* Author J.N. Little 11-3-86
* Revised 7-23-91 to support ANSI-C
*/

#include <stdio.h>

typedef struct {
    long type;   /* type */
    long mrows;  /* row dimension */
    long ncols;  /* column dimension */
    long imagf;  /* flag indicating imag part */
    long namlen; /* name length (including NULL) */
} Fmatrix;

#ifdef __STDC__
void savemat(FILE *fp, int type, char *pname, int mrows, int ncols,
        int imagf, double *preal, double *pimag)
#else
void savemat(fp, type, pname, mrows, ncols, imagf, preal, pimag)
FILE *fp;      /* File pointer */
int type;      /* Type flag: Normally 0 for PC, 1000 for Sun, Mac, */
               /* Apollo, and other Motorola format, */
```

```
                /* 2000 for VAX D-float, 3000 for VAX G-float, and */
                /* 4000 for CRAY */
                /* Add 1 for text variables, 2 for sparse matrices */
                /* See LOAD in reference section of guide for more info.*/
char *pname;    /* pointer to matrix name */
int mrows;      /* row dimension */
int ncols;      /* column dimension */
int imagf;      /* imaginary flag */
double *preal;  /* pointer to real data */
double *pimag;  /* pointer to imag data */
#endif
{
        Fmatrix x;
        int mn;

        x.type = type;
        x.mrows = mrows;
        x.ncols = ncols;
        x.imagf = imagf;
        x.namlen = strlen(pname) + 1;
        mn = x.mrows * x.ncols;

        fwrite(&x, sizeof(Fmatrix), 1, fp);
        fwrite(pname, sizeof(char), (int)x.namlen, fp);
        fwrite(preal, sizeof(double), mn, fp);
        if (imagf) {
            fwrite(pimag, sizeof(double), mn, fp);
        }
}
```

APPENDIX C

SIGNAL PROCESSING PROGRAMS

The programs in Appendix C are Matlab m-files called from the master program file, *animal.m*, to process the input data into attenuation and backscatter coefficient ratio values.


```
%
% ANIMAL.M                              (master program)
% function[count1,count2,elapsed_time] =
%                        animal(fatthickness_values,animal_number)
% count# is the number of elements stored in each file of that scan number.
% elapsed_time is the number of seconds that it took to run the program.
% fatthickness is a [1X3] vector of the fat  measurements (in inches) at 5 cm,
% 10 cm, & 15 cm (respectively) from the animals spine.
% animal_number is the sequence number of the animal being processed.
% animal.m writes two ASCII files as output.  attn.asc for the attenuation data
% and bsc.asc for the backscatter ratio data.  Each file is a 19 element column
% vector.  The first element is the animal number followed by the 6 hide-on
% values, then 6 hide-off values and finally 6 cold-scan values.

function[count1,count2,time] = animal(fat,anml_num)

depth = .06:.0005:.075;      % depth = 6 to 7.5 cm in .5 mm steps
longdepth = .06:.0005:.09;   % use longer (3cm) depth for attenuation
freq = [.7 .8 .9 1.0 1.1 1.2]*1e6;        % analysis freqs
attn(1) = anml_num;      % first row in ASCII data files
bsc(1) = anml_num;       %      is the animal number

tic;
```

```
scan = 2;                  % Hide_On scan
[bscratios,dbattn] = bacscat(depth,longdepth,freq,scan,fat);
  attn(2:7) = dbattn(:);
  bsc(2:7) = bscratios(:);

scan = 3;                  % Hide_Off scan
[bscratios,dbattn] = bacscat(depth,longdepth,freq,scan,fat);
  attn(8:13) = dbattn(:);
  bsc(8:13) = bscratios(:);

scan = 4;                  % cold scan
[bscratios,dbattn] = bacscat(depth,longdepth,freq,scan,fat);
  attn(14:19) = dbattn(:);
  bsc(14:19) = bscratios(:);

bfid = fopen('bsc.asc','w');              %  ascii output file of
count1 = fprintf(bfid,'%8.5e/n',bsc);     %     backscatter data
status = fclose(bfid);

afid = fopen('attn.asc','w');             %  ascii output file of
count2 = fprintf(afid,'%8.4g/n',attn);    %     attenuation data
status = fclose(afid);
time = toc;
end                        % end program
```

```
% BACSCAT.M
% function[resultbsc,resultattn] =
%              bacscat(depth,longdepth,freq,scantypenumber,fatthickness)
% depth is a row vector of the depths at which the A-lines in the datamatrix
% are to be evaluated for the backscatter processing.  longdepth is a row
% vector containing an extended depth range for attenuation evaluation.
% freq is a row vector containing the desired evaluation freq's
% scantypenumber is:  1 = phantom;  2 = hide_on;  3 = hide_off;  4 = cold.
% fatthickness is a [1X3] vector of the fat  measurements (in inches) at 5 cm,
%  10 cm, & 15 cm (respectively) from the animals spine.
% resultbsc and resultattn are matrices containing the average values of
% the backscatter coef ratio and attenuation coef (dB) at each frequency.


function[ratiobsc,resat] = bacscat(depth,longdepth,freq,scan,fat)


global Z CNTRFREQ SPEED1 SPEED2;
hz = 0;                    % hz is the ave hide thickness
max_z = .15;               % max depth for the scan (in meters).
max_phz = .15;             % max depth of the phantom (meters).
dbhideattn = 9.33;         % ave attn from hide at 1 MHz (per cm)
phspeed = 1600;            % speed of sound in phantom (m/sec).


    if scan == 2           % Hide_On scan
      dbfatattn = 2.1;       % db per cm
      SPEED1 = 1597;       % speed1 = speed in muscle tissue (m/sec)
      SPEED2 = 1430;       % speed2 = speed in fat (m/sec)
      hz = .007;           % ave hide thickness (meters)
    elseif scan == 3       % Hide_Off scan
      dbfatattn = 2.1;       % db per cm
      SPEED1 = 1597;       % speed1 = speed in muscle tissue (m/sec)
      SPEED2 = 1430;       % speed2 = speed in fat (m/sec)
    elseif scan == 4       % Cold scan
      dbfatattn = 6.0;       % db per cm
      SPEED1 = 1575;       % speed1 = speed in muscle tissue (m/sec)
      SPEED2 = 1581;       % speed2 = speed in fat (m/sec)
     elseif scan == 1      % Phantom on Phantom
      dbfatattn = 1.0;       % db per cm / attn of phantom material
      SPEED1 = 1600;       % speed1 = speed in phantom (m/sec)
      SPEED2 = 1430;
      fat = [0 0 0];       %  set fat thickness vector to zeros
    end                    % end if loop
```

```
phantdata = getdata(1);      %  gets data for # of scan
data = getdata(scan);
datamatx = 63.1 * data;      % compensates for 36 dB higher gain on
                             %     the phantom.
fathick = fatprog(fat);      % fatprog fits a polynomial to the
                             %     the 3 measured thicknesses in fat
hidealpha = abs((dbhideattn*100)/8.686);      % Nepers/meter
fatalpha = abs((dbfatattn*100)/8.686);        % Nepers/meter
        % calculated from:  dbfatattn=20*log(exp(-4*fatalpha*z);


for k = 1:size(longdepth,2)
   Z = longdepth(k);
   [gatedphantom,increm] = gate(phantdata,max_phz);

   for j = 1:size(freq,2)
      CNTRFREQ = freq(1,j);
      phantampsq(k,j) = phprocess(gatedphantom,phspeed,increm);
   end
end
[longate,inc] = longgate(datamatx,longdepth);    % longer gate for attn
 for q = 1:size(freq,2)
   CNTRFREQ = freq(q);
% Phantom attenuation is 1dB/cm/MHz.
   phattn = (1.0)*100*(CNTRFREQ/1.0e6);
% attn per meter per MHz
   phalpha(1,q) = abs(phattn/8.686);     % dBphant=20*log(exp(-4*alpha*z))

   [al,delal] = roiattn(phantampsq,longate,longdepth,fathick,inc,hz,phalpha(q),q);
        % roiattn calculates the attenuation in the unknown tissue.
   alpha(1,q) = al;
   deltalpha(1,q) = delal;
 end                           % end q for loop


resat = (abs(alpha)/100)*8.686;               % attn in dB/cm
 for k = 1:size(depth,2)
   Z = depth(1,k);
   [gatedmatrix,inc] = gate(datamatx,max_z);

   for j = 1:size(freq,2),
      CNTRFREQ = freq(1,j);
   [ampsqRatio] = process(gatedmatrix,inc,fathick,hz,phantampsq(k,j));
   bscoef(deltalpha(1,j),ampsqRatio,phalpha(1,j),fatalpha,fathick,hidealpha,hz);
```

```
  resbsc(k,j) = bsc;
 end                        % end k "for" loop.
end                        % end j "for" loop.

for u = 1:size(freq,2)          % averages bsc ratio values across depths
  sum = 0;                      %              at each frequency
   for v = 1:size(depth,2)
      sum = sum + resbsc(v,u);
   end;
  ratiobsc(u) = sum/size(depth,2);
end

end                        % end program.
```

```
% GETDATA.M
% function data = getdata(scan_type_number);
% scan _type_number is the number corresponding to the desired scan.
%  1 = phantom,   2 = hide_on,    3 = hide_off,    4 = cold.
% data is the returned data matrix.

function data = getdata(scan)
if scan == 1
    load pra72m00.mat;
    data = im(1:80,1:5000);          % shortens length to 15cm and selects A-lines
elseif scan == 2                      % hide on
    load nra36m00.mat;
    data1 = im;
    load nla36m01.mat;
    data = [data1(51:118,:);im(1:60,:)];        % selects A-lines
 elseif scan == 3                     % hide off
    load fra36m01.mat;
    data1 = im;
    load fla36m02.mat;
    data = [data1(51:118,:);im(1:60,:)];        % selects A-lines
elseif scan == 4                      % cold
    load cra36m01.mat;
    data1 = im;
    load cla36m02.mat;
    data = [data1(51:118,:);im(1:60,:)];        % selects A-lines
end              % end if
end                    % end program
```

```
% FATPROG.M
% function fatthickness = fatprog(fatmeasurements)
% fatthickness is a row vector whos elements are the fat thickness value (m)
% for the corresponding row of the datamatrix (corresponding A-line).
% fatmeasurements is a three element row vector containing the fat depth
% values (in inches) at 5 cm, 10 cm, and 15 cm from the spine, respectively.

function fthick = fatprog(fat)

x = [.05 .10 .15];          % fat thickness measurement distances from spine cm
correctedfat = fat*(2.56/100);     % 2.56 cm per inch X (1m / 100 cm)
p = polyfit(x,correctedfat,2);     % quadratic fit to data points

for r = 1:128               % 128 a-lines

  if r < 69                            % A-lines from animal's left side
    distance = (151 - r)/1000;         % distance from the spine in meters
    if distance >= .05 & distance <= .15
      fthick(r) = polyval(p,distance);
    elseif distance < .05              % if less that 5 cm mark use
      fthick(r) = correctedfat(1);     %    level approximation
    end              % end if
  end                % end if

  if r > 68                            % A-lines from animal's left side
    distance = (96-r)/1000;
    if distance >= .05 & distance <= .15
      fthick(r) = polyval(p,distance);
    elseif distance < .05
      fthick(r) = correctedfat(1);
    end              % end if
  end                % end if

end                  % end for loop
end                  % end program
```

```
% GATE.M
% function[gatedmatrix,increment]  =  gate(datamatrix,max_z)
% gatedmatrix is a matrix of the returned range gated section of the echo data
% Each row of gatedmatrix is from operating on the same row of datamatrix
% Each column contains the gated depth data for the corresponding column of the
% datamatrix at the depth z.          increment is the # of columns per meter.
% datamatrix is a matrix of raw echo data
% max_z is the maximum recorded depth of the scan.


function[gatedmatrix,increment] = gate(datamatrix,max_z)


global Z
columns = size(datamatrix,2);
increment = columns/max_z;
% sets up data pts per meter in the scanvector.
% increment = array elements per meter
  zi = round(increment*Z);
  zli = zi - round(.0005*increment);        % RANGE CELL 1mm WIDE
  zri = zi + round(.0005*increment);
% zi is the index of the column at mean depth.
% ROI is 1.0 mm wide centered at the data pt corresponding to z


  t = (zri - zli) + 1;
  i = size(datamatrix,1);
  gatedmatrix = zeros(i,t);



for j = 1:i
  gatedmatrix(j,:) = datamatrix(j,zli:zri);
end                % end j "for" loop.
% On each row of gatedmatrix (jth row) t-1 columns are available for
% storage of the gated signal.  The first column of each row contains the
% variable described above.

gatedmatrix = gatedmatrix - 128;
% This removes the dc bias and sets the center voltage value to zero.


end                % end program.
```

```
% PHPROCESS.M
% function Ampsqvolt  =  phprocess(gatedmatrix,speed1,increment)
% Ampsqvolt is the ave of the amp squared voltage signal from the range
% gated input voltage (gatedmatrix) signal. Ampsqvolt is an
% ave value of the amplitude sq values for depth Z .
% gatedmatrix is the range gated data matrix where the first column of
% each row is the medium depth for the gated data.
% speed1 is the speed of sound in the phantom
% increment is the # of columns per meter


function Ampsqvolt = phprocess(gatedmatx,speed,increm)

global Z CNTRFREQ;
% Fixed variables for this calculation:
tau = 4e-6;              % tau = duration of the window
b = 2*pi/tau;
zl = (Z - .0005);           % zl is the lower (left side) limit of the ROI
        % ROI is 1.0 mm wide centered at the data pt corresponding to Z
[m,deltzi] = size(gatedmatx);
xx = zeros(1,deltzi);
Ampsq = zeros(1,m);

for r = 1:m,
 vreal = xx;
 vimag = xx;
 BH = xx;
 imfiltvolt = xx;
 refiltvolt = xx;
 imagsq = xx;
 realsq = xx;

  for k = 1:deltzi,
    d = zl + (1/increm)*(k-1);
    t = 2*(d/speed);
    vreal(k) = gatedmatx(r,k).*cos(2*pi*CNTRFREQ*t);
    vimag(k) = gatedmatx(r,k).*sin(2*pi*CNTRFREQ*t);
    BH(k) = 0.42323 - 0.49755*cos(b*t) + 0.07922*cos(2*b*t);
  end                     % end k "for" loop.
  imfiltvolt = conv(vimag,BH);
  refiltvolt = conv(vreal,BH);
  imagsq = imfiltvolt .* conj(imfiltvolt);
  realsq = refiltvolt .* conj(refiltvolt);
```

```
Estimators(r,:) = imagsq + realsq;
estcol = size(Estimators,2);
 Add = 0;
  for j = 1:estcol
    Add = Add + Estimators(r,j);
  end                       % end j "for" loop.
  Ampsq(1,r) =  Add/estcol;
end                         % end row "for" loop.
  Ampsum = 0;
for q = 1:m, Ampsum = Ampsum + Ampsq(1,q);, end
Ampsqvolt = Ampsum/m;
end                         % end program
```

```
% LONGGATE.M
% function[gatedmatrix,increment] = longgate(datamatrix,depth)
% gatedmatrix is a matrix of the returned range gated section of the echo
% data. z is the depth of interest (mean depth). columns is the # of columns in the
% datamatrix, datamatrix is a matrix of raw echo data. Each row of gatedmatrix is
% from operating on the same row of datamatrix. Each column contains the gated
% depth data for the corresponding column of the datamatrix at the depth z.
% increment is the # columns per meter.
% max_z is the maximum recorded depth of the scan.
% depth is a row vector of analysis depths.

function[gatedmatrix,increment] = longgate(datamatrix,longdepth)

max_z = .15;
sz = size(datamatrix);
columns = sz(2);
increment = columns/max_z;
% sets up data pts per meter in the scanvector.
% increment = array elements per meter
  zl = longdepth(1);                    % start of ROI
  zr = longdepth(size(longdepth,2));    % depth of ROI
  zli = round(zl*increment);                   % element index
  zri = round(zr*increment);
% Region of Interest is 3.0 cm wide
i = sz(1);


for j = 1:i; gatedmatrix(j,:) = datamatrix(j,zli:zri); end;
  % for loop chops section of datamatrix out
  gatedmatrix = gatedmatrix - 128;
    % This removes the dc bias and sets the center voltage value to zero.
end                    % end program.
```

```
% ROIATTN.M
% function[phalpha,alpha,deltalpha] =
%              phattn(phantampsq,longate,longdepth,fathick,inc,hz,)
% phalpha, alpha, & deltalpha are the phantom, unknown, & difference
% attenuation coef values (Np/m)
% phantmpsq is the ave of the amp squared voltage from the phantom
% longgate is a modified gate program that range gates the entire range
% specified in longdepth in one single gate.
% longdepth is a row vector containing an ext'd depth range for attn evaluation.
% fathick is a row vector containing the fat thickness  value for each a-line.
% inc is the number of columns per meter.      hz is the hide thickness value.

function[alpha,deltalpha] =
              roiattn(phantampsq,longate,longdepth,fathick,inc,hz,phalpha,index)

global CNTRFREQ Z SPEED1 SPEED2;
[row,col] = size(phantampsq);
sum = 0;
for i=1:row; phampsq = sum + phantampsq(i,index); end;
                         % sum up phantampsq at CNTRFREQ
phamp = phampsq/row;         % ave amp sq'd voltage of phantom at CNTRFREQ
[estimate] = attnprocess(longate,longdepth,inc,fathick,hz);
ri = estimate./phamp;
[m,n] = size(ri);
 % ri is a matrix of ratios of the amp sq'd
% voltages of the unknown data to the phantom.  There is 1:1 corres between
% elements of the estimate matrix and those of ri.
  for q = 1:m
    for u = 1:n
     if ri(q,u) == 0.0000, ri(q,u) = .0001;, end    % end "if" loop.
    end                          % end u "for" loop.
   end                          % end q "for" loop.
% This for/if loop sets any zeros to 1 for the log( ) to work.

  logri = log(ri);
% logri = ln[rb(freq,z)] - 4*[delta(atten)]*Z
% logri is a 1:1 of natural log(ri) [element by element].

[r,c] = size(longdepth);
zl = longdepth(1);
zr = longdepth(c);
y = zr - zl;
```

```
x = zl:(y/n):(zr - 0.0000001);  % need 1 column less than zr in index
% x is an index vector.
alphasum = 0;
delalphasum = 0;

  for j = 1:m
    p = polyfit(x,logri(j,:),1);
     % This creates a one degree polynomial fit to each row of the RI matrix.
    f1 = polyval(p,x(1));
    f2 = polyval(p,x(size(x,2)));
    slope = (f2 - f1)/y;

% Evaluates the poly at the 1st and last pts to determine the slope
% Slope = -4*delta(attn)

    deltalphaestimate(1,j) = slope/(-4);
    alphaestimate(1,j) = phalpha + deltalphaestimate(1,j);
    delalphasum = delalphasum + deltalphaestimate(1,j);
    alphasum = alphasum + alphaestimate(1,j);
   end                % end j "for" loop.

 deltalpha = delalphasum/m;
 alpha = alphasum/m;

 end                % end program
```

```
% ATTNPROCESS.M
% function [Estimators] = attnprocess(gatedmatrix,depth,increment,fathick,hz)
% Estimators is a matrix of the amplitude squared estimators.
% Each row of Estimators is from a separate gated depth section.
% gatedmatrix is the range gated data matrix, range gated into a 1 mm
% section of the data centered at a depth, Z
% depth is a row vector of analysis depths.  increment is the number of
% columns per meter.  fathick is a row vector containing the fat thickness
% value for each a-line.  hz is the hide thickness value.


function[Estimators] = attnprocess(gatedmatx,depth,increm,fathick,hz)


global Z CNTRFREQ SPEED1 SPEED2 ;
% Fixed variables for this calculation:
tau = 4e-6;              % tau = duration of the window
b = 2*pi/tau;
speed3 = 1813;          % speed of sound in the hide (m/sec)
zl = depth(1);
% zl is the lower (left side) limit of the ROI
% ROI is 1.5 cm wide
 [m,n] = size(gatedmatx);
xx = zeros(1,n);
Ampsq = zeros(1,m);


for r = 1:m,
 vreal = xx;
 vimag = xx;
 BH = xx;
 imfiltvolt = xx;
 refiltvolt = xx;
 imagsq = xx;
 realsq = xx;
 fz = fathick(r);

  for k = 1:n
   d = zl + (1/increm)*(k-1);
   t = (2*(d-fz-hz)/SPEED1) + (2*fz/SPEED2) + (2*hz/speed3);
   vreal(k) = gatedmatx(r,k).*cos(2*pi*CNTRFREQ*t);
   vimag(k) = gatedmatx(r,k).*sin(2*pi*CNTRFREQ*t);
   BH(k) = 0.42323 - 0.49755*cos(b*t) + 0.07922*cos(2*b*t);
  end                    % end k "for" loop.
```

```
        imfiltvolt = conv(vimag,BH);
        refiltvolt = conv(vreal,BH);
        imagsq = imfiltvolt .* conj(imfiltvolt);
        realsq = refiltvolt .* conj(refiltvolt);
        Estimators(r,:) = imagsq + realsq;    % 1 row per A-line.
      end                           % end row "for" loop.

      end                           % end program
```

```
% PROCESS.M
% function [ampsqRatio] = process(gatedmatrix,increment,fathick,hz,phantampsq)
% Ampsqvolt is the ave  of the amp squared voltage signal from the range gated
% input voltage (gatedmatrix) signal. Ampsqvolt is an ave value of the amplitude
% sq values for depth Z .
% gatedmatrix is the range gated data matrix where the first column of
% each row is the medium depth for the gated data. Columns is the number of
% columns of the original ungated data matrix. hz is the ave hide thickness.
% increment is the # of columns per meter
% fathick is a row vector containing the fat thickness value for each A-line.
% hz is the hide thickness value.
% phantampsq is the amplitude squared voltage from the phantom

function[ampsqRatio] = process(gatedmatx,increm,fathick,hz,phantampsq)

global Z CNTRFREQ SPEED1 SPEED2;
% Fixed variables for this calculation:
tau = 4e-6;             % tau = duration of the window
b = 2*pi/tau;
speed3 = 1813;          % speed of sound in the hide (m/sec)
 zl = (Z - .0005);
% zl is the lower (left side) limit of the ROI
% ROI is 1.0 mm wide centered at the data pt corresponding to Z

[m,deltzi] = size(gatedmatx);
 xx = zeros(1,deltzi);
 Ampsq = zeros(1,m);
for r = 1:m,
  vreal = xx;
  vimag = xx;
  BH = xx;
  imfiltvolt = xx;
  refiltvolt = xx;
  imagsq = xx;
  realsq = xx;
fz = fathick(r);

  for k = 1:deltzi,
    d = zl + (1/increm)*(k-1);
    t = (2*(d-fz-hz)/SPEED1) + (2*fz/SPEED2) + (2*hz/speed3);
    vreal(k) = gatedmatx(r,k).*cos(2*pi*CNTRFREQ*t);
    vimag(k) = gatedmatx(r,k).*sin(2*pi*CNTRFREQ*t);
```

```
    BH(k) = 0.42323 - 0.49755*cos(b*t) + 0.07922*cos(2*b*t);
end                         % end k "for" loop.


imfiltvolt = conv(vimag,BH);
refiltvolt = conv(vreal,BH);
imagsq = imfiltvolt .* conj(imfiltvolt);
realsq = refiltvolt .* conj(refiltvolt);
Estimators(r,:) = imagsq + realsq;
estcol = size(Estimators,2);


Add = 0;
 for j = 1:estcol
   Add = Add + Estimators(r,j);
 end                        % end j "for" loop.


 Ampsq(1,r) =  Add/estcol;
end                         % end row "for" loop.


Ampsum = 0;
for q = 1:m, Ampsum = Ampsum + Ampsq(1,q);, end
                            % sums up all A-lines at given depth & freq
Ampsqvolt = Ampsum/m;               % ave = sum / # A-lines


ampsqRatio = Ampsqvolt/phantampsq;    % divides ave by phantom ave for
                            %         same depth & freq


end                         % end program
```

```
% BSCOEF.M
% function ratioBSC =
%          bscoef(deltalpha,ampsqRatio,phantalpha,fat_alpha,fathick,hidealpha,hz)
% bsccoef.m calculates the backscatter coefficients ratio.
% ratioBSC is a vector of the averaged backscatter coefficients ratios for each row
% in the range gated data matrix.
% deltalpha is a matrix of the difference between the unknown attenuation
% coefficient and the phantom's.
% ampsqRatio is an array of the ave values of the ratio of the amp sq'd voltages of
% unknown to phantom.        phantalpha is the phantom attn coef (Np/m)
% fat_alpha is the attn coef of the fat tissue (Np/m)
% fathick is a row vector containing the fat thickness value for each A-line.
% hidealpha is the attn coef (Np/m) of the anml hide. hz is the ave hide thickness.
% hz is the hide thickness value.

function ratioBSC =
            bscoef(deltalpha,ampsqRatio,phalpha,fatalpha,fathick,hdalpha,hz)

 global Z ;
k = size(ampsqRatio,2);
 sum = 0.000;

 for j = 1:k
   fz = fathick(j);
   attnknown = exp(4*(fatalpha*fz + hdalpha*hz - phalpha*(fz+hz)));
   attnROI = exp(4*(deltalpha*(Z-fz-hz)));
   rb = ampsqRatio(1,j)*(attnknown)*(attnROI);        % rb = ratio estimates
   sum = sum + rb;
 end                        % end of j "for" loop.

 ratioBSC = sum/k;
% This is the Backscatter coef for the depth Z ave'd over the ROI.

 end                        % end program.
```

APPENDIX D

BACKSCATTER ATTENUATION RESULTS

The data table in Appendix D is a listing of the attenuation results for each of the 108 animals studied.

HIDE File #	ON Anml #	SCAN ATTN .7MHz	in dB/cm .8MHz	at .9MHz	Analysis 1.0MHz	Frequency 1.1MHz	1.2MHz	Slope dB/cm /MHz
NXA36M	21	1.544	0.995	0.7783	0.623	0.4776	0.3782	-2.153
NXA36M	22	0.0758	0.2955	0.4954	0.8146	0.8177	0.8894	1.701
NXA36M	23	2.053	1.908	1.913	1.952	1.984	2.045	0.065
NXA36M	24	1.381	1.5	1.433	1.599	1.72	1.706	0.7
NXA36M	25	1.551	1.666	1.643	1.779	1.974	2.111	1.103
NXA36M	26	0.8265	0.9367	1.07	1.122	1.24	1.378	1.063
NXA36M	27	0.8965	0.9699	1.319	1.32	1.501	1.452	1.249
NXA36M	28	2.171	2.122	2.18	2.241	2.402	2.413	0.603
NXA36M	29	0.9674	0.6988	0.5623	0.2865	0.1656	0.2311	-1.588
NXA36M	30	0.09939	0.05524	0.3039	0.4726	0.4685	0.4596	0.917
NXA36M	31	0.3024	0.08908	0.1963	0.2982	0.2858	0.383	0.313
NXA36M	32	1.097	1.381	1.461	1.688	1.691	1.744	1.255
NXA36M	33	0.7358	0.3476	0.0911	0.06925	0.2156	0.2106	-0.87
NXA36M	34	0.5838	0.3223	0.1239	0.04248	0.1506	0.1678	-0.765
NXA36M	35	0.8803	0.4276	0.2926	0.03351	0.1594	0.1161	-1.396
NXA36M	36	0.6617	0.2878	0.07696	0.1345	0.2442	0.4406	-0.337
NXA36M	37	0.5019	0.2702	0.01128	0.2081	0.3218	0.3222	-0.156
NXA36M	38	1.194	0.9975	0.6351	0.5566	0.4881	0.311	-1.72
NXA36M	39	0.2297	0.4934	0.7085	0.8765	1.051	1.076	1.735
NXA36M	40	0.7972	0.4695	0.1663	0.1419	0.1496	0.3769	-0.882
NXA36M	41	0.5942	0.3372	0.03675	0.1592	0.1586	0.195	-0.688
NXA36M	42	1.05	0.5647	0.3431	0.2307	0.08536	0.01184	-1.926
NXA36M	43	1.062	0.6161	0.3402	0.2319	0.1258	0.02207	-1.937
NXA36M	44	1.333	1.49	1.594	1.734	1.831	1.9	1.142
NXA36M	45	0.7505	0.5446	0.2023	0.0655	0.03379	0.05482	-1.471
NXA36M	46	1.501	1.747	1.986	2.135	2.092	2.249	1.407

NXA36M	47	0.84	0.4407	0.01649	0.06695	0.2919	0.2646	-0.935
NXA36M	48	0.03061	0.09109	0.2222	0.4268	0.5049	0.609	1.239
NXA36M	49	1.811	1.747	1.863	1.983	1.992	2.13	0.7
NXA36M	50	0.9687	1.185	1.386	1.408	1.524	1.429	0.954
NXA36M	51	0.5102	0.2437	0.05442	0.1188	0.2008	0.2444	-0.398
NXA36M	52	3.272	3.132	3.106	3.163	3.171	3.333	0.137
NXA36M	53	1.63	1.722	1.749	1.848	1.899	1.951	0.639
NXA36M	54	1.143	0.8506	0.5978	0.5093	0.4506	0.2897	-1.587
NXA36M	55	0.4674	0.6428	0.8767	0.961	1.039	1.097	1.263
NXA36M	56	0.1641	0.3853	0.4796	0.6093	0.7003	0.792	1.204
NXA36M	57	1.189	0.799	0.5425	0.4982	0.4859	0.3282	-1.511
NXA36M	58	0.8377	0.5688	0.2271	0.1446	0.05677	0.02373	-1.625
NXA36M	59	2.487	2.421	2.444	2.587	2.667	2.753	0.632
NXA36M	60	1.19	0.8502	0.4339	0.3246	0.2049	0.07485	-2.177
NXA36M	61	0.5818	0.8171	0.9513	1.021	1.261	1.265	1.376
NXA36M	62	1.134	0.8242	0.565	0.341	0.1629	0.1056	-2.1
NXA36M	63	0.2446	0.04432	0.1923	0.3625	0.3763	0.4445	0.619
NXA36M	64	0.7111	0.2924	0.223	0.1434	0.1701	0.1185	-0.974
NXA36M	65	0.5516	0.6595	0.7809	0.8219	0.9051	1.006	0.871
NXA36M	66	0.02208	0.2428	0.4472	0.6027	0.7372	0.7889	1.564
NXA36M	67	3.178	3.013	3.046	3.02	3.213	3.347	0.405
NXA36M	68	1.065	1.206	1.326	1.502	1.364	1.345	0.586
NXA36M	69	2.733	2.765	2.655	2.775	2.855	2.964	0.441
NXA36M	70	.	.	.	.	.	.	.
NXA36M	71	0.03377	0.3087	0.321	0.5839	0.6745	0.7227	1.373
NXA36M	72	2.407	2.217	2.188	2.209	2.296	2.463	0.154
NXA36M	73	0.4713	0.1368	0.05991	0.2862	0.3462	0.4946	0.277
NXA36M	74	0.7305	0.3015	0.01172	0.1852	0.3241	0.4285	-0.362
NXA36M	75	1.475	1.132	0.8497	0.6897	0.4554	0.3724	-2.201
NXA36M	76	2.61	2.602	2.631	2.747	2.836	2.947	0.715
NXA36M	77	1.683	1.746	1.889	1.919	2.123	2.137	0.98
NXA36M	78	1.197	0.8991	0.604	0.3287	0.1497	0.1329	-2.241
NXA36M	79	2.248	2.225	2.216	2.345	2.306	2.433	0.371
NXA36M	80	0.7823	0.6467	0.2029	0.1683	0.07302	0.0468	-1.552
NXA36M	81	0.7779	1.033	1.233	1.395	1.506	1.709	1.782
NXA36M	82	2.134	2.066	2.061	2.144	2.277	2.379	0.555
NXA36M	83	1.457	1.719	1.679	1.798	1.846	1.849	0.703
NXA36M	84	1.584	1.234	0.9498	0.6871	0.6363	0.4973	-2.14
NXA36M	85	2.653	2.495	2.586	2.559	2.628	2.726	0.211
NXA36M	86	1.963	1.863	1.781	1.825	2	2.075	0.29
NXA36M	87	1.124	0.7758	0.4317	0.3849	0.261	0.2262	-1.737
NXA36M	88	0.3985	0.2373	0.1488	0.3027	0.3445	0.4833	0.257
NXA36M	89	2.793	2.689	2.606	2.76	2.82	2.935	0.359
NXA36M	90	2.847	2.739	2.739	2.79	2.854	2.924	0.223
NXA36M	91	2.485	2.472	2.464	2.58	2.701	2.767	0.632
NXA36M	92	1.292	1.31	1.343	1.449	1.573	1.67	0.796
NXA36M	93	1.655	1.298	1.052	0.8354	0.7343	0.6326	-2.006
NXA36M	94	1.172	1.306	1.37	1.436	1.604	1.618	0.911
NXA36M	95	2.211	2.197	2.219	2.289	2.435	2.518	0.663
NXA36M	96	1.241	1.322	1.328	1.526	1.573	1.674	0.89
NXA36M	97	0.344	0.5952	0.839	1.08	1.156	1.259	1.857
NXA36M	98	2.244	2.149	2.253	2.21	2.396	2.45	0.494
NXA36M	99	0.4718	0.2566	0.0913	0.1138	0.1337	0.2278	-0.447
NXA36M	100	2.527	2.462	2.504	2.496	2.582	2.708	0.359

NXA36M	101	0.8736	1.022	1.088	1.217	1.359	1.436	1.129
NXA36M	102	0.9693	0.4884	0.3001	0.02898	0.1123	0.01109	-1.769
NXA36M	103	0.5679	0.6305	0.9093	0.9798	1.064	1.297	1.433
NXA36M	104	0.1178	0.1576	0.401	0.484	0.6217	0.6966	1.248
NXA36M	105	0.5801	0.1251	0.03635	0.1648	0.4046	0.3072	-0.114
NXA36M	106	0.3551	0.0617	0.2117	0.3862	0.4718	0.5384	0.663
NXA36M	107	0.8222	0.9082	0.9653	1.114	1.271	1.294	1.027
NXA36M	108	1.102	0.7932	0.5636	0.3634	0.3527	0.2287	-1.682
NXA36M	109	1.449	1.516	1.503	1.67	1.649	1.797	0.659
NXA36M	110	2.954	3.036	2.903	2.952	3.099	3.102	0.279
NXA36M	111	1.868	1.673	1.737	1.534	1.896	1.838	0.09
NXA36M	112	0.722	0.8986	1.048	1.067	1.179	1.312	1.089
NXA36M	113	1.678	1.746	1.882	1.983	2.167	2.211	1.151
NXA36M	114	0.9408	1.035	1.207	1.376	1.539	1.625	1.458
NXA36M	115	1.422	1.428	1.595	1.648	1.722	1.873	0.911
NXA36M	116	1.761	1.828	1.78	1.88	2.004	2.076	0.629
NXA36M	117	1.245	0.8784	0.5402	0.38	0.318	0.2389	-1.963
NXA36M	118	1.3	1.102	0.7176	0.5036	0.3545	0.1289	-2.375
NXA36M	119	1.421	1.127	0.7674	0.7188	0.4727	0.4169	-2.009
NXA36M	120	0.3211	0.05317	0.1315	0.3132	0.4893	0.5436	0.744
NXA36M	121	1.456	1.204	0.8136	0.4739	0.4197	0.3208	-2.391
NXA36M	122	1.068	0.8928	0.5152	0.3633	0.255	0.1168	-1.949
NXA36M	123	0.7935	0.5985	0.3309	0.2247	0.1453	0.00725	-1.542
NXA36M	124	1.064	0.7799	0.6095	0.3615	0.2698	0.2851	-1.621
NXA36M	125	1.422	1.173	0.8535	0.7582	0.5773	0.4855	-1.876
NXA36M	126	2.126	2.035	1.928	2.044	2.113	2.242	0.266
NXA36M	127	0.6281	0.8493	0.9421	0.9738	1.115	1.247	1.121
NXA36M	128	0.9947	0.8778	0.5834	0.3717	0.3855	0.2971	-1.479

HIDE	**OFF**	**SCAN ATTN** in dB/cm at Analysis Frequency						**Slope**
File #	Anml #	.7MHz	.8MHz	.9MHz	1.0MHz	1.1MHz	1.2MHz	dB/cm MHz
FXA36M	21	1.647	1.598	1.695	1.861	1.885	1.998	0.795
FXA36M	22	1.678	1.25	0.9634	0.6987	0.5744	0.3705	-2.523
FXA36M	23	2.895	2.912	3.096	3.101	3.23	3.263	0.8
FXA36M	24	0.9648	1.134	1.348	1.457	1.573	1.704	1.463
FXA36M	25	1.619	1.702	1.776	2.056	2.146	2.105	1.155
FXA36M	26	2.66	2.495	2.364	2.349	2.456	2.532	-0.221
FXA36M	27	1.497	1.131	0.7858	0.5616	0.4817	0.293	-2.341
FXA36M	28	1.225	1.02	0.6443	0.3982	0.3478	0.1914	-2.123
FXA36M	29	0.09034	0.2397	0.4317	0.5639	0.8157	0.9045	1.695
FXA36M	30	0.7222	0.4678	0.2917	0.07657	0.04032	0.1334	-1.269
FXA36M	31	0.1422	0.3239	0.3348	0.5705	0.6603	0.6661	1.104
FXA36M	32	0.8509	0.8737	0.9548	1.126	1.072	1.286	0.84
FXA36M	33	0.2253	0.0024	0.1351	0.2328	0.4513	0.5143	0.826
FXA36M	34	2.481	2.473	2.514	2.568	2.649	2.704	0.485
FXA36M	35	2.579	2.552	2.722	2.883	2.94	3.041	1.039
FXA36M	36	0.8356	0.5331	0.1784	0.0226	0.08817	0.2196	-1.306
FXA36M	37	0.9393	0.5709	0.3528	0.08924	0.0317	0.09186	-1.748
FXA36M	38	1.308	1.44	1.593	1.709	1.852	1.867	1.185
FXA36M	39	1.559	1.398	0.978	0.7284	0.6707	0.6138	-2.045
FXA36M	40	0.7074	0.3328	0.136	0.08289	0.1621	0.3249	-0.708
FXA36M	41	0.2773	0.02236	0.2482	0.2744	0.316	0.4153	0.456

FXA36M	42	0.7674	0.8655	0.954	1.137	1.22	1.265	1.067
FXA36M	43	0.9664	1.115	1.166	1.37	1.397	1.454	0.997
FXA36M	44	1.753	1.563	1.138	0.9361	0.829	0.7537	-2.114
FXA36M	45	0.1796	0.5474	0.7618	0.8681	1.038	1.21	1.923
FXA36M	46	1.405	1.049	0.7526	0.4366	0.2237	0.1578	-2.579
FXA36M	47	1.988	1.975	1.973	2.085	2.127	2.184	0.442
FXA36M	48	0.9525	0.6812	0.3424	0.2673	0.0865	0.00412	-1.886
FXA36M	49	1.176	0.8577	0.5599	0.3733	0.2593	0.1521	-2.029
FXA36M	50	1.282	0.9142	0.5516	0.4479	0.2931	0.2144	-2.087
FXA36M	51	0.609	0.1274	0.1634	0.4177	0.565	0.5848	0.413
FXA36M	52	0.8967	1.213	1.305	1.657	1.607	1.721	1.616
FXA36M	53	1.549	1.348	1.062	0.9065	0.8007	0.6402	-1.812
FXA36M	54	0.3273	0.1512	0.1446	0.2065	0.3023	0.4823	0.369
FXA36M	55	1.908	1.967	2.113	2.13	2.25	2.395	0.943
FXA36M	56	1.43	1.158	0.7881	0.5775	0.4528	0.1999	-2.422
FXA36M	57	0.8285	1.046	1.151	1.281	1.462	1.553	1.429
FXA36M	58	0.877	1.016	1.116	1.254	1.302	1.47	1.132
FXA36M	59	2.924	2.815	2.787	2.864	2.961	3.043	0.317
FXA36M	60	0.8112	1.063	1.203	1.533	1.542	1.614	1.652
FXA36M	61	3.161	3.05	3.084	3.106	3.172	3.264	0.258
FXA36M	62	0.8588	0.9948	1.064	1.092	1.196	1.291	0.798
FXA36M	63	1.664	1.386	1.105	0.9939	0.8373	0.7134	-1.86
FXA36M	64	0.3367	0.03058	0.04289	0.1571	0.3767	0.4193	0.447
FXA36M	65	3.247	3.214	3.204	3.176	3.252	3.455	0.322
FXA36M	66	3.742	3.718	3.779	3.886	3.946	4.055	0.673
FXA36M	67	0.6435	0.3357	0.2022	0.05484	0.1464	0.22	-0.809
FXA36M	68	0.6613	0.4868	0.4296	0.2316	0.1604	0.07817	-1.169
FXA36M	69	0.07235	0.4115	0.6819	0.7466	0.95	1.128	1.988
FXA36M	70	2.152	2.076	2.022	2.187	2.282	2.394	0.569
FXA36M	71	1.395	1.292	1.186	0.956	0.9009	0.7404	-1.336
FXA36M	72	2.37	2.492	2.523	2.53	2.685	2.838	0.836
FXA36M	73	0.2816	0.02068	0.1317	0.259	0.3475	0.4965	0.624
FXA36M	74	2.446	2.431	2.38	2.535	2.61	2.677	0.528
FXA36M	75	0.2554	0.4335	0.5196	0.6974	0.7523	0.9771	1.355
FXA36M	76	0.9246	1.186	1.25	1.498	1.68	1.779	1.715
FXA36M	77	2.952	2.991	2.961	2.968	3.217	3.176	0.516
FXA36M	78	0.1538	0.2173	0.2869	0.3465	0.5359	0.6545	1.005
FXA36M	79	1.222	1.007	0.7624	0.5101	0.442	0.2751	-1.909
FXA36M	80	1.05	0.6974	0.4298	0.2563	0.1006	0.00977	-2.047
FXA36M	81	0.7195	0.3172	0.1914	0.1022	0.1132	0.2389	-0.887
FXA36M	82	1.634	1.336	1.14	0.8266	0.7941	0.6529	-1.956
FXA36M	83	1.741	1.495	1.08	0.8548	0.8572	0.7015	-2.096
FXA36M	84	0.09364	0.255	0.5223	0.543	0.6204	0.7695	1.285
FXA36M	85	1.434	1.232	1.047	0.6855	0.5635	0.3768	-2.187
FXA36M	86	1.592	1.304	1.035	0.9462	0.8714	0.821	-1.498
FXA36M	87	0.5717	0.6089	0.7318	0.8657	0.9692	1.097	1.098
FXA36M	88	0.9874	0.7811	0.4435	0.3608	0.09796	0.02801	-1.98
FXA36M	89	0.9763	0.6826	0.4972	0.3874	0.1324	0.1075	-1.744
FXA36M	90	2.562	2.592	2.726	2.952	3.07	3.138	1.297
FXA36M	91	0.9395	0.6582	0.3834	0.2726	0.1621	0.00944	-1.786
FXA36M	92	1.462	1.188	0.8551	0.6155	0.5861	0.5074	-1.948
FXA36M	93	0.1544	0.2341	0.2406	0.3465	0.3859	0.5954	0.79
FXA36M	94	1.687	1.386	1.12	0.9348	0.851	0.6909	-1.934
FXA36M	95	0.772	0.4912	0.3142	0.2015	0.1295	0.05411	-1.368

File #	Anml #	.7MHz	.8MHz	.9MHz	1.0MHz	1.1MHz	1.2MHz	Slope
FXA36M	96	1.916	1.611	1.448	1.181	1.148	0.9279	-1.885
FXA36M	97	3.248	3.159	3.096	3.151	3.275	3.29	0.175
FXA36M	98	1.163	1.125	0.9502	0.7941	0.7554	0.6812	-1.05
FXA36M	99	2.908	2.855	2.789	2.876	2.92	2.944	0.132
FXA36M	100	1.111	0.8791	0.5609	0.3745	0.2514	0.1711	-1.934
FXA36M	101	1.382	1.409	1.421	1.542	1.623	1.701	0.674
FXA36M	102	0.1366	0.1063	0.2453	0.4314	0.5062	0.598	1.055
FXA36M	103	1.457	1.079	0.821	0.6551	0.6116	0.4819	-1.841
FXA36M	104	2.643	2.566	2.48	2.546	2.562	2.725	0.133
FXA36M	105	3.015	2.919	2.779	2.894	3.006	3.009	0.099
FXA36M	106	2.164	2.036	1.966	2.102	2.198	2.25	0.301
FXA36M	107	0.9751	1.125	1.172	1.239	1.312	1.496	0.924
FXA36M	108	0.6962	0.7139	0.8267	0.9322	1.019	1.17	0.969
FXA36M	109	1.582	1.313	1.171	1.015	0.9217	0.7891	-1.513
FXA36M	110	0.9569	0.6843	0.467	0.4462	0.2341	0.1993	-1.474
FXA36M	111	0.9516	0.7569	0.499	0.2566	0.1619	0.03988	-1.882
FXA36M	112	0.3492	0.5886	0.7584	0.736	0.9893	1.204	1.558
FXA36M	113	2.535	2.54	2.598	2.538	2.707	2.855	0.583
FXA36M	114	3.183	3.006	2.989	3.04	3.169	3.203	0.183
FXA36M	115	1.504	1.204	0.955	0.7327	0.4251	0.4716	-2.206
FXA36M	116	0.9671	0.6547	0.4619	0.3105	0.1343	0.1865	-1.604
FXA36M	117	0.5048	0.6235	0.704	0.8461	0.8929	1.021	1.009
FXA36M	118	0.1085	0.1438	0.3192	0.4493	0.5402	0.6842	1.199
FXA36M	119	0.169	0.00246	0.1442	0.3587	0.4688	0.5234	0.967
FXA36M	120	0.4483	0.423	0.6569	0.6973	0.7098	0.8883	0.886
FXA36M	121	1.555	1.463	1.478	1.56	1.625	1.748	0.438
FXA36M	122	1.484	1.527	1.606	1.661	1.822	1.902	0.866
FXA36M	123	0.8593	0.9388	1.068	1.2	1.395	1.443	1.263
FXA36M	124	0.4278	0.7126	0.7822	0.8085	1.048	1.101	1.257
FXA36M	125	1.388	1.466	1.426	1.591	1.61	1.752	0.691
FXA36M	126	1.424	1.187	0.9423	0.8615	0.6802	0.5954	-1.641
FXA36M	127	1.808	1.505	1.308	1.084	1.016	0.8184	-1.897
FXA36M	128	0.3037	0.06213	0.04979	0.2235	0.3039	0.5155	0.559

COLD SCAN

File #	Anml #	ATTN in dB/cm at .7MHz	.8MHz	.9MHz	Analysis 1.0MHz	Frequency 1.1MHz	1.2MHz	Slope dB/cm MHz
CXA36M	21	1.89	1.499	1.268	1.112	0.9558	0.9265	-1.887
CXA36M	22	2.117	1.759	1.529	1.401	1.275	1.19	-1.776
CXA36M	23	2.013	1.798	1.535	1.41	1.213	1.288	-1.573
CXA36M	24	1.762	1.442	1.231	1.039	0.83	0.7263	-2.059
CXA36M	25	1.917	1.483	1.201	1.101	0.9675	0.9676	-1.827
CXA36M	26	1.57	1.399	1.109	1.022	1.007	0.9301	-1.275
CXA36M	27	2.33	1.968	1.787	1.633	1.503	1.479	-1.658
CXA36M	28	2.296	2.045	1.741	1.623	1.487	1.43	-1.749
CXA36M	29	1.82	1.426	1.143	0.9813	0.9191	0.8906	-1.808
CXA36M	30	2.436	2.096	1.876	1.698	1.658	1.591	-1.633
CXA36M	31	2.039	1.749	1.52	1.363	1.236	1.166	-1.732
CXA36M	32	2.126	1.861	1.594	1.429	1.353	1.248	-1.737
CXA36M	33	2.268	1.985	1.8	1.624	1.48	1.427	-1.685
CXA36M	34	2.142	1.852	1.566	1.448	1.336	1.244	-1.759
CXA36M	35	1.91	1.457	1.203	1.057	0.9134	0.907	-1.941
CXA36M	36	2.343	2.016	1.814	1.647	1.512	1.426	-1.79

CXA36M	37	1.894	1.548	1.36	1.231	1.162	1.099	-1.503
CXA36M	38	1.895	1.506	1.265	1.156	1.064	1.025	-1.653
CXA36M	39	1.124	0.8789	0.6548	0.6341	0.549	0.5375	-1.127
CXA36M	40	1.949	1.704	1.557	1.356	1.333	1.261	-1.358
CXA36M	41	1.983	1.706	1.554	1.433	1.319	1.232	-1.439
CXA36M	42	2.016	1.726	1.484	1.394	1.307	1.263	-1.461
CXA36M	43	2.258	2.068	1.858	1.747	1.539	1.409	-1.698
CXA36M	44	2.322	1.989	1.71	1.595	1.505	1.44	-1.708
CXA36M	45	1.993	1.737	1.522	1.419	1.298	1.236	-1.487
CXA36M	46	2.123	1.764	1.417	1.297	1.184	1.155	-1.914
CXA36M	47	2.277	1.788	1.732	1.51	1.457	1.421	-1.57
CXA36M	48	2.313	1.956	1.718	1.563	1.518	1.399	-1.725
CXA36M	49	2.27	1.943	1.763	1.63	1.516	1.385	-1.668
CXA36M	50	2.445	2.127	1.985	1.867	1.733	1.586	-1.599
CXA36M	51	2.202	1.872	1.707	1.562	1.426	1.405	-1.562
CXA36M	52	2.581	2.265	2.055	1.857	1.826	1.739	-1.636
CXA36M	53	2.274	1.996	1.76	1.531	1.514	1.354	-1.793
CXA36M	54	2.49	2.194	1.945	1.775	1.657	1.58	-1.809
CXA36M	55	2.332	2.019	1.778	1.574	1.533	1.539	-1.608
CXA36M	56	2.451	2.185	1.922	1.813	1.611	1.64	-1.682
CXA36M	57	2.478	2.227	2.003	1.799	1.722	1.628	-1.705
CXA36M	58	3.011	2.754	2.478	2.297	2.142	2.027	-1.982
CXA36M	59	2.502	2.151	1.938	1.79	1.639	1.625	-1.734
CXA36M	60	2.764	2.501	2.212	2.091	1.944	1.832	-1.843
CXA36M	61	2.641	2.347	2.156	1.98	1.813	1.803	-1.705
CXA36M	62	2.437	2.089	1.943	1.838	1.726	1.671	-1.435
CXA36M	63	2.74	2.505	2.249	2.129	1.992	1.884	-1.697
CXA36M	64	2.639	2.281	2.093	2.011	1.875	1.765	-1.62
CXA36M	65	2.291	1.967	1.694	1.499	1.455	1.35	-1.839
CXA36M	66	2.01	1.646	1.541	1.332	1.325	1.349	-1.279
CXA36M	67	2.087	1.841	1.606	1.435	1.358	1.362	-1.499
CXA36M	68	2.793	2.449	2.244	2.085	1.908	1.863	-1.838
CXA36M	69	2.321	1.933	1.742	1.536	1.395	1.368	-1.881
CXA36M	70	2.295	1.974	1.741	1.655	1.53	1.49	-1.555
CXA36M	71	2.597	2.223	2.017	1.874	1.713	1.694	-1.768
CXA36M	72	2.394	2.176	1.965	1.794	1.696	1.584	-1.617
CXA36M	73	2.382	2.041	1.878	1.79	1.614	1.53	-1.608
CXA36M	74	2.1	1.806	1.557	1.462	1.276	1.188	-1.784
CXA36M	75	2.836	2.51	2.217	2.087	1.941	1.872	-1.902
CXA36M	76	2.688	2.437	2.113	1.989	1.864	1.81	-1.781
CXA36M	77	2.478	2.108	1.885	1.746	1.624	1.617	-1.685
CXA36M	78	2.578	2.184	1.943	1.794	1.664	1.642	-1.825
CXA36M	79	2.435	2.159	1.931	1.777	1.682	1.59	-1.66
CXA36M	80	2.687	2.406	2.164	2.026	1.899	1.824	-1.707
CXA36M	81	2.288	2.094	1.88	1.693	1.614	1.532	-1.545
CXA36M	82	2.557	2.273	2.063	1.874	1.815	1.726	-1.634
CXA36M	83	2.641	2.324	2.028	1.892	1.762	1.68	-1.893
CXA36M	84	2.25	2.04	1.693	1.61	1.529	1.402	-1.673
CXA36M	85	2.582	2.299	2.075	2.018	1.851	1.784	-1.54
CXA36M	86	2.634	2.348	2.157	1.979	1.843	1.748	-1.749
CXA36M	87	2.872	2.624	2.401	2.304	2.175	2.106	-1.507
CXA36M	88	2.729	2.484	2.28	2.124	1.994	1.878	-1.68
CXA36M	89	2.34	2.077	1.803	1.709	1.668	1.553	-1.502
CXA36M	90	2.523	2.227	2.044	1.856	1.776	1.726	-1.579

CXA36M	91	2.406	2.088	1.972	1.708	1.551	1.547	-1.763
CXA36M	92	2.569	2.285	2.023	1.914	1.801	1.72	-1.659
CXA36M	93	2.57	2.297	2.069	1.939	1.827	1.696	-1.689
CXA36M	94	2.354	2.073	1.757	1.591	1.467	1.397	-1.934
CXA36M	95	2.36	2.044	1.773	1.653	1.491	1.463	-1.79
CXA36M	96	2.627	2.344	2.053	1.813	1.69	1.548	-2.171
CXA36M	97	2.969	2.691	2.519	2.372	2.2	2.136	-1.653
CXA36M	98	2.307	2.031	1.808	1.766	1.636	1.52	-1.475
CXA36M	99	2.849	2.562	2.388	2.26	2.15	2.06	-1.517
CXA36M	100	2.224	1.902	1.653	1.486	1.374	1.341	-1.762
CXA36M	101	2.841	2.5	2.314	2.176	2.047	1.943	-1.711
CXA36M	102	2.157	1.912	1.703	1.559	1.533	1.429	-1.406
CXA36M	103	2.624	2.284	2.072	1.901	1.79	1.737	-1.739
CXA36M	104	2.772	2.524	2.303	2.153	2.061	2.006	-1.534
CXA36M	105	2.582	2.336	2.187	2	1.961	1.882	-1.375
CXA36M	106	2.667	2.403	2.178	2.076	1.957	1.898	-1.51
CXA36M	107	2.603	2.277	2.064	1.949	1.835	1.758	-1.619
CXA36M	108	2.875	2.615	2.341	2.277	2.133	2.041	-1.623
CXA36M	109	2.252	1.986	1.707	1.537	1.493	1.359	-1.747
CXA36M	110	2.404	2.215	1.954	1.867	1.736	1.626	-1.547
CXA36M	111	2.432	2.044	1.814	1.621	1.592	1.428	-1.877
CXA36M	112	2.784	2.529	2.301	2.155	2.031	1.986	-1.609
CXA36M	113	2.692	2.388	2.251	2.124	2.01	1.958	-1.409
CXA36M	114	2.557	2.33	2.135	1.985	1.874	1.851	-1.442
CXA36M	115	2.495	2.221	1.98	1.813	1.699	1.617	-1.749
CXA36M	116	2.641	2.362	2.174	2.056	1.926	1.82	-1.58
CXA36M	117	1.887	1.624	1.546	1.494	1.457	1.493	-0.721
CXA36M	118	1.976	1.788	1.705	1.588	1.594	1.632	-0.691
CXA36M	119	2.624	2.334	2.163	2.06	1.943	1.834	-1.493
CXA36M	120	2.58	2.248	2.006	1.947	1.829	1.767	-1.537
CXA36M	121	2.299	2.065	1.879	1.749	1.713	1.623	-1.305
CXA36M	122	2.544	2.261	2.026	1.917	1.803	1.759	-1.545
CXA36M	123	2.41	2.235	1.954	1.867	1.704	1.666	-1.543
CXA36M	124	2.536	2.208	2.051	1.9	1.817	1.71	-1.558
CXA36M	125	2.671	2.445	2.225	2.169	2.025	1.921	-1.447
CXA36M	126	2.478	2.293	2.043	1.906	1.775	1.752	-1.52
CXA36M	127	2.632	2.407	2.2	2.079	2	1.894	-1.438
CXA36M	128	2.402	2.144	1.985	1.866	1.779	1.7	-1.35

APPENDIX E

BACKSCATTER COEFFICIENT RESULTS

The data table in Appendix E is a listing of the backscatter coefficient ratio results for each of the 108 animals studied.

HIDE	ON	SCAN BSC	Ratio	at	Analysis	Frequency		Slope
File #	Anml	.7MHz	.8MHz	.9MHz	1.0MHz	1.1MHz	1.2MHz	
NXA36M	21	1706800	2652920	2146400	1645680	1348040	1072100	-2168246
NXA36M	22	2715540	2533820	2314090	2903150	1787280	1337620	-2440046
NXA36M	23	360135000	133347000	673692000	392957000	248761000	178193000	-5.90E+09
NXA36M	24	496617000	302098000	138804000	102502000	76396000	48190200	-8.44E+08
NXA36M	25	593720000	357155000	173686000	123089000	107168000	89769300	-9.49E+08
NXA36M	26	360491000	211001000	134099000	80887500	61211800	51784900	-5.85E+08
NXA36M	27	11320200	7762860	10794600	6562120	6407780	3645140	-13335149
NXA36M	28	170072000	85043100	58112700	41436700	39285200	25795200	-2.50E+08
NXA36M	29	2714350	2575550	1916260	1992190	1586270	899560	-3418817
NXA36M	30	2738420	2292960	2536000	2364740	1455790	923851	-3358747
NXA36M	31	5915520	7081090	4786610	3418300	2061020	1660570	-10772363
NXA36M	32	157200000	144100000	89512600	82347300	51430600	38067100	-2.52E+08
NXA36M	33	2920550	3546490	3382880	2774100	2333080	1490210	-3257346
NXA36M	34	13112300	10753500	8145410	5365150	4805570	3294620	-19917843
NXA36M	35	9519720	11211200	7451240	7690440	5912320	3508750	-13060654
NXA36M	36	1435440	1864390	2437690	1675330	1336250	1328400	-823423
NXA36M	37	2405410	2205260	2311560	2089160	1644340	1050030	-2480589
NXA36M	38	2081490	1684630	1974730	1358800	966595	895870	-2485181
NXA36M	39	7002110	7267880	6876960	6040900	5628990	3813130	-6199323
NXA36M	40	1087810	1342150	1599760	2004020	1260070	1393390	481691
NXA36M	41	4477280	4352120	4788460	4330560	2623260	1809680	-5423566
NXA36M	42	1505500	2282540	2008320	1486130	1278970	1046650	-1664900
NXA36M	43	3897650	5297490	5199910	3782720	2917100	2351440	-4654117
NXA36M	44	40949100	33062600	24201000	20124100	15615600	11676800	-57936971
NXA36M	45	6064620	4935960	5419750	4077790	2607270	1960830	-8241994
NXA36M	46	73579300	73961800	75074700	63638300	34923100	31986900	-96147000

NXA36M	47	13844000	14897700	18704700	11508600	10908800	6755410	-15601643
NXA36M	48	13252200	8111830	6002420	5524960	3985620	3201610	-18031154
NXA36M	49	114917000	54409600	43528000	36464200	23381000	21832300	-1.62E+08
NXA36M	50	39670400	37404100	34811200	21638600	17499800	8707340	-65057371
NXA36M	51	6075890	6072410	5214290	4494610	3299750	2310250	-7961674
NXA36M	52	1.85E+10	756028000	3.92E+09	2.48E+09	1.51E+09	1.28E+09	-3.02E+10
NXA36M	53	111411000	79186600	49174000	38276900	27164800	19832400	-1.79E+08
NXA36M	54	3260020	3224660	2991200	2048310	1391610	1232780	-4736640
NXA36M	55	274833000	192413000	155599000	101504000	70969100	50644400	-4.40E+08
NXA36M	56	15770600	14291200	9951210	7772600	5793600	4481790	-24032989
NXA36M	57	6240960	7374180	6772060	4207340	2604710	2303030	-10446509
NXA36M	58	56784500	51463100	56123100	37243400	27222900	18754800	-80499657
NXA36M	59	1.37E+10	601621000	3.22E+09	2.30E+09	1.60E+09	1.19E+09	-2.19E+10
NXA36M	60	197359000	135102000	101810000	62348700	41301400	29156100	-3.32E+08
NXA36M	61	455174000	329307000	208322000	128719000	118089000	77445200	-7.43E+08
NXA36M	62	6541670	6410160	5839910	5248100	4590900	3300730	-6358369
NXA36M	63	6082000	5140180	4820260	4072110	2559560	1894660	-8407631
NXA36M	64	6957100	8695350	5433300	3669230	4291870	2487920	-10662974
NXA36M	65	288138000	167112000	103775000	62018900	44401100	35336900	-4.78E+08
NXA36M	66	55966800	45889100	35044400	26839700	22090600	16587000	-78999771
NXA36M	67	1.40E+10	496909000	3.13E+09	1.73E+09	1.82E+09	1.68E+09	-2.06E+10
NXA36M	68	256661000	167403000	108953000	83986000	39642800	24600200	-4.48E+08
NXA36M	69	170715000	983201000	492828000	336166000	229104000	167866000	-2.89E+09
NXA36M	70	.	.	.	.	.	.	.
NXA36M	71	6867240	8289700	4926140	5238310	3946190	2800390	-9443603
NXA36M	72	688158000	261999000	1.31E+09	750178000	513976000	420486000	-1.12E+10
NXA36M	73	9324060	9919680	8057170	7452950	5159480	4613870	-10981649
NXA36M	74	15431500	17378000	15748200	12929900	10317200	8140750	-17272700
NXA36M	75	3549700	3635050	3395930	2639880	2523570	1898070	-3528183
NXA36M	76	374474000	190502000	1.06E+09	718395000	502903000	384484000	-6.10E+09
NXA36M	77	337685000	191012000	1.30E+09	768209000	693132000	460218000	-5.36E+09
NXA36M	78	6264450	5650810	5252550	5016390	4308730	2901120	-6022586
NXA36M	79	754450000	401378000	228300000	191593000	108396000	97041300	-1.20E+09
NXA36M	80	2315940	1750120	2836970	1801760	1394940	1199640	-2194929
NXA36M	81	118629000	114520000	99841000	83488900	65150400	65305800	-1.23E+08
NXA36M	82	188130000	92622300	55750200	43507700	39647100	33856700	-2.69E+08
NXA36M	83	135318000	141365000	74887000	59108300	40776000	26026300	-2.47E+08
NXA36M	84	561826	666498	694249	723989	493339	435863	-319872
NXA36M	85	180067000	677919000	498721000	281555000	210473000	173408000	-2.79E+09
NXA36M	86	219697000	93353900	43326100	29079300	28506700	22206000	-3.42E+08
NXA36M	87	24074200	23599900	23614100	14623900	11183000	7698200	-36605971
NXA36M	88	8748140	6934290	9385970	7782800	5239310	4606190	-7827960
NXA36M	89	573044000	247310000	1.16E+09	1.07E+09	791673000	704508000	-8.65E+09
NXA36M	90	1.52E+10	662175000	3.52E+09	2.15E+09	1.44E+09	1.03E+09	-2.51E+10
NXA36M	91	197535000	106303000	593783000	466775000	387290000	290758000	-3.02E+09
NXA36M	92	68046700	40262300	25483300	20085000	17112400	14024200	-98560143
NXA36M	93	1769550	1990570	1817490	1648540	1251660	1008390	-1768994
NXA36M	94	80041800	62568300	42435700	29938100	27794400	18461100	-1.21E+08
NXA36M	95	770650000	419634000	258252000	187260000	172863000	138544000	-1.14E+09
NXA36M	96	86983100	59449800	34942000	33303900	23124800	18857700	-1.29E+08
NXA36M	97	366954000	286489000	230072000	202563000	144708000	117824000	-4.85E+08
NXA36M	98	117261000	528501000	400606000	217615000	216737000	159918000	-1.77E+09
NXA36M	99	224009000	156664000	104717000	80980300	51669400	39826900	-3.60E+08
NXA36M	100	186410000	897864000	587212000	348669000	273486000	244277000	-2.92E+09

NXA36M	101	674469000	448849000	268333000	189957000	147836000	109796000	-1.09E+09
NXA36M	102	5271600	7663980	6258120	6423450	5340860	2806370	-5465766
NXA36M	103	63096100	42653900	49241300	35946500	28183300	32634000	-59719171
NXA36M	104	218201000	179494000	145422000	97250300	79487900	62091600	-3.22E+08
NXA36M	105	94174100	100228000	58975800	46093400	42888300	23933400	-1.53E+08
NXA36M	106	93543300	101995000	69584800	54595500	40027900	30493400	-1.47E+08
NXA36M	107	952350000	579329000	345157000	252325000	199651000	133652000	-1.52E+09
NXA36M	108	5901050	5518120	4640460	3948070	2557680	2133640	-8117360
NXA36M	109	207197000	141899000	80172400	75101200	44542800	42608000	-3.20E+08
NXA36M	110	1.56E+10	1.15E+10	4.85E+09	3.41E+09	3.20E+09	2.11E+09	-2.68E+10
NXA36M	111	635662000	229715000	167948000	62282300	104877000	59814000	-9.60E+08
NXA36M	112	387046000	276405000	195775000	118690000	91447200	77517700	-6.23E+08
NXA36M	113	539918000	298561000	1.92E+09	1.28E+09	1.07E+09	774565000	-8.43E+09
NXA36M	114	169260000	995289000	706646000	547367000	467141000	370205000	-2.39E+09
NXA36M	115	233350000	139896000	126413000	89152200	68024200	64079700	-3.14E+08
NXA36M	116	503920000	348795000	182256000	145757000	128576000	102643000	-7.72E+08
NXA36M	117	7698650	8150050	8568060	6833270	4905600	3919170	-8675869
NXA36M	118	3370620	2794270	3499950	3219620	2732670	2859850	-862566
NXA36M	119	1504540	1543910	1898660	1230140	1341950	1006090	-1076186
NXA36M	120	29350900	25913000	20045600	16725400	15124800	11302800	-35978657
NXA36M	121	5073580	4300740	4979780	5575630	3808200	3018940	-3187134
NXA36M	122	10272100	7479800	8406120	6579220	5125090	4462830	-10839251
NXA36M	123	34381300	24579100	20879700	14359900	10338300	8866170	-50519386
NXA36M	124	22491900	19082200	13779500	12351200	9110670	5944520	-32594226
NXA36M	125	9168320	7641000	7627410	5309780	4800520	3885830	-10643291
NXA36M	126	518443000	233986000	105379000	85250400	63810100	56963200	-8.11E+08
NXA36M	127	39962400	36793500	26111600	16840800	14496300	12667600	-60753257
NXA36M	128	8346310	5591100	5540170	4953590	3017480	2397710	-10871554

HIDE	OFF	SCAN BSC	Ratio	at	Analysis	Frequency		Slope
File #	Anml #	.7MHz	.8MHz	.9MHz	1.0MHz	1.1MHz	1.2MHz	
FXA36M	21	148292000	62183500	39255600	32360900	20738800	17917000	-2.24E+08
FXA36M	22	12663	19254	20977	23289	19535	21613	13687
FXA36M	23	268973000	152764000	127457000	74791600	59882800	40542100	-4.21E+08
FXA36M	24	12382600	9341780	7924260	5687100	4370940	3619820	-17418166
FXA36M	25	23526000	15702300	10521800	11385200	8486470	4933760	-32498654
FXA36M	26	288209000	110304000	46482600	26153400	20040100	14907100	-4.74E+08
FXA36M	27	8502	11675	15819	16572	12666	13833	8679
FXA36M	28	10512	10279	16567	19424	13824	13702	8412
FXA36M	29	2055070	2194830	1758400	1345110	1538170	1277180	-1792206
FXA36M	30	59613	62807	54597	58376	40543	45691	-37893
FXA36M	31	1438420	1153190	627199	637942	490826	325843	-2154067
FXA36M	32	5414900	3045600	2037570	1794060	975882	1064690	-8058204
FXA36M	33	913708	780450	563853	401891	423257	325447	-1192813
FXA36M	34	467513000	233670000	136246000	88301600	65997000	49088000	-7.55E+08
FXA36M	35	791261000	371151000	284190000	227419000	154354000	123618000	-1.16E+09
FXA36M	36	151702	160312	201554	168197	138539	128284	-61647
FXA36M	37	163002	200096	174554	186670	154000	117237	-101428
FXA36M	38	40713900	28966200	22466600	17080400	15074400	10212400	-57019743
FXA36M	39	20881	15775	24730	26733	19035	14529	-5708
FXA36M	40	194666	271561	241709	248466	190864	196067	-65237
FXA36M	41	1333980	1249120	1268940	743877	505399	429865	-2079086

FXA36M	42	10201200	6476600	4182080	3760170	2878830	2140180	-14720091
FXA36M	43	31607400	22504600	13060600	12110800	7940150	6002940	-49332986
FXA36M	44	8040	6964	11535	11295	9203	7258	734
FXA36M	45	5079130	5944130	4973610	3484580	3136910	3048520	-5732497
FXA36M	46	23103	30527	35624	46510	49474	37561	40004
FXA36M	47	330967000	158593000	80610000	57902400	38607400	28553700	-5.41E+08
FXA36M	48	160835	159904	197508	131776	128110	102889	-128813
FXA36M	49	12220	16944	22782	23144	20061	17881	10863
FXA36M	50	73058	100173	139510	103216	93838	73503	-15164
FXA36M	51	630917	1061520	1133250	1205940	1079830	744909	199309
FXA36M	52	4946240	5415590	3739600	4677890	2546610	2049630	-6329057
FXA36M	53	11620	10838	13239	11856	9861	10055	-3468
FXA36M	54	2044720	1485520	1501130	935657	710880	720331	-2717525
FXA36M	55	285613000	159817000	112738000	64348400	50832700	45444500	-4.50E+08
FXA36M	56	111836	110564	144743	136418	112526	136771	34925
FXA36M	57	46526600	38831200	25493800	19419000	18550800	15148100	-63945286
FXA36M	58	231390000	166163000	110785000	86988400	59200700	58157800	-3.46E+08
FXA36M	59	401445000	177330000	95280600	66238900	49636800	37157900	-6.38E+08
FXA36M	60	127466000	84163000	49987300	41005700	24663700	17251300	-2.11E+08
FXA36M	61	140230000	611560000	368365000	223348000	154947000	117877000	-2.27E+09
FXA36M	62	40203900	27295500	16349300	9618530	7494960	6117100	-67590397
FXA36M	63	42873	41341	41900	30392	27333	24447	-41619
FXA36M	64	1694730	1704450	1020220	737323	763193	557277	-2512552
FXA36M	65	106376000	548405000	304908000	170645000	123743000	121735000	-1.75E+09
FXA36M	66	743412000	381915000	2.48E+09	1.90E+09	1.36E+09	1.15E+09	-1.13E+10
FXA36M	67	16945	24032	20598	19080	21670	17385	-1830
FXA36M	68	1084490	778567	453391	380263	266595	204087	-1717445
FXA36M	69	5873390	5170870	4243820	2727580	2253070	1878360	-8641369
FXA36M	70	530380000	214870000	95777000	80321000	61961000	53709000	-8.16E+08
FXA36M	71	58989	38539	26243	26093	18362	17884	-76059
FXA36M	72	93431700	65289700	39731400	23874800	19351300	16115300	-1.54E+08
FXA36M	73	1360600	1290650	966381	736658	560164	533169	-1873810
FXA36M	74	495517000	244121000	115056000	92222700	66237300	49402200	-7.96E+08
FXA36M	75	10785100	7842570	4780330	3940390	2725090	3017500	-15722966
FXA36M	76	6628790	5957750	3853780	3586270	3083050	2365790	-8630460
FXA36M	77	886557000	545469000	292279000	174814000	188930000	108310000	-1.45E+09
FXA36M	78	4588170	4981910	2926540	1854950	1749950	1523590	-7454391
FXA36M	79	28194	27459	29919	35198	26321	27470	-501
FXA36M	80	156235	196518	204945	181378	170348	144801	-45499
FXA36M	81	426254	568650	396612	461881	292536	265341	-447897
FXA36M	82	2423	3254	3339	4924	3366	3235	1708
FXA36M	83	23969	23966	37595	37975	22728	21367	-4671
FXA36M	84	3088820	2258410	2267130	1290460	957209	933458	-4473452
FXA36M	85	14802	14142	13236	20990	18110	19517	12353
FXA36M	86	8194	9826	11419	8405	6299	4645	-8955
FXA36M	87	50461900	27488600	18583900	13838300	10535500	9038700	-75063114
FXA36M	88	317769	267475	328083	225623	273293	249005	-122522
FXA36M	89	20445	27184	26955	22229	29127	20335	158
FXA36M	90	89256800	53565400	40246000	37288700	29142400	21276900	-1.19E+08
FXA36M	91	63730	73292	84522	65267	53262	51320	-40399
FXA36M	92	29751	33415	45220	50002	33141	26502	-3510
FXA36M	93	7894450	4674240	2385990	1711670	1157410	1297100	-12631874
FXA36M	94	35739	40806	43668	40144	30473	29958	-18122
FXA36M	95	72960	89419	83294	67673	51767	57720	-58507

FXA36M	96	16657	18758	15090	16856	11151	12667	-11715
FXA36M	97	523532000	227232000	1.08E+09	707911000	579942000	384480000	-8.49E+09
FXA36M	98	50584	30760	27509	24369	16562	12996	-66765
FXA36M	99	378215000	181545000	868705000	593651000	393645000	263963000	-6.32E+09
FXA36M	100	44038	46730	64550	64272	56272	45624	10365
FXA36M	101	106129000	53580100	27379100	19212300	13892600	10822300	-1.73E+08
FXA36M	102	3121740	2729920	1936750	1700540	1268720	1065220	-4257831
FXA36M	103	111703	154992	163698	147134	104776	99981	-64521
FXA36M	104	135106000	643870000	309386000	215109000	140536000	130757000	-2.20E+09
FXA36M	105	387192000	163930000	651588000	475320000	368125000	238276000	-6.33E+09
FXA36M	106	873992000	324776000	143904000	110868000	85307100	63366600	-1.37E+09
FXA36M	107	81994500	53158200	29289200	18449500	13142600	12530600	-1.37E+08
FXA36M	108	14186100	7565930	5159790	3749510	2856530	2662080	-20902451
FXA36M	109	12341	13869	11259	10162	8268	7989	-11332
FXA36M	110	62240	78764	86248	55402	63712	45797	-45204
FXA36M	111	60154	62435	78840	97651	81473	95082	71589
FXA36M	112	11139900	9304610	7045790	3913060	4188370	4416610	-14885114
FXA36M	113	392155000	224367000	145445000	78536500	68620000	59917100	-6.27E+08
FXA36M	114	392803000	148729000	826396000	554208000	464243000	325742000	-6.10E+09
FXA36M	115	69063	81914	87983	93387	133056	77782	57835
FXA36M	116	85706	112319	108396	98901	104013	59984	-46579
FXA36M	117	24699300	16078400	10028900	7990120	5646820	5247860	-37311634
FXA36M	118	4566010	4095170	3166610	2415400	1878410	1802600	-6062440
FXA36M	119	2549210	1960520	1488390	1472550	1224400	945631	-2926313
FXA36M	120	12831300	6196200	5839980	3688370	2361350	2407120	-18793446
FXA36M	121	205454000	82239400	44074700	29889000	21178900	18388900	-3.24E+08
FXA36M	122	136697000	76435300	48414000	31336500	28420900	22706200	-2.09E+08
FXA36M	123	62969200	37822600	26353600	19995400	19093900	14094600	-87690657
FXA36M	124	31494000	27637700	16037900	9408130	9849520	7530180	-51375260
FXA36M	125	204740000	125155000	60209600	51165900	33791100	31942600	-3.28E+08
FXA36M	126	30516	31434	33846	24649	24970	20552	-22403
FXA36M	127	45523	49412	42848	42736	31442	34116	-31732
FXA36M	128	3441230	2968730	1973380	1672150	1270630	1426750	-4419409

COLD		SCAN BSC	Ratio	at	Analysis	Frequency		Slope
File #	Anml #	.7MHz	.8MHz	.9MHz	1.0MHz	1.1MHz	1.2MHz	
CXA36M	21	302726	387643	351166	285140	251255	173526	-320340
CXA36M	22	21072	27216	26019	20348	17122	13745	-20740
CXA36M	23	4353780	3407980	3045160	2189790	1967110	1077500	-6159823
CXA36M	24	11072700	10715300	8684030	7185670	6586810	5195820	-12362351
CXA36M	25	2257140	2888240	2805800	1981020	1596800	1027940	-3098600
CXA36M	26	6201550	4609140	4529680	3131200	2007050	1531720	-9301114
CXA36M	27	2949	4060	3552	3086	2696	1861	-2856
CXA36M	28	3837	4011	5033	4030	3625	2747	-2174
CXA36M	29	326465	432805	458248	388697	279425	195663	-338200
CXA36M	30	543	772	802	784	551	443	-339
CXA36M	31	95308	100334	94512	79722	67119	51937	-94654
CXA36M	32	101654	99382	101327	86610	64627	54213	-101768
CXA36M	33	73324	75772	64451	57012	49812	36872	-76451
CXA36M	34	426622	423916	432462	324498	257496	206077	-488557
CXA36M	35	1053850	1491270	1401720	1099440	913622	591488	-1242010
CXA36M	36	23408	27910	25317	22395	19473	15658	-19138

CXA36M	37	98765	120032	101232	78690	56716	42658	-140864
CXA36M	38	199086	270244	267811	204012	156999	110832	-241373
CXA36M	39	350794	342056	327699	195225	149748	100178	-560708
CXA36M	40	22459	23110	18936	18975	12478	9749	-27260
CXA36M	41	108170	112290	87438	67154	54891	44228	-146340
CXA36M	42	61483	65849	65200	47095	36394	26816	-79944
CXA36M	43	126120	104363	93732	70492	71773	63843	-123541
CXA36M	44	12712	15869	17767	13794	10794	8302	-11784
CXA36M	45	514443	482288	422306	302124	241077	176640	-723666
CXA36M	46	24483	32036	42157	32392	26378	18230	-16573
CXA36M	47	668650	1017210	610109	569606	393715	276927	-1105601
CXA36M	48	25317	32431	31586	26433	17950	15645	-27703
CXA36M	49	1432	1934	1759	1494	1295	1246	-891
CXA36M	50	15742	18776	14467	11107	9522	8916	-18642
CXA36M	51	70315	84152	68751	56750	49062	33283	-86409
CXA36M	52	1283240	1272950	1045770	888346	573356	438063	-1852026
CXA36M	53	6244	7025	7299	7946	5166	5276	-2792
CXA36M	54	108890	113585	108837	91655	73251	56312	-114592
CXA36M	55	1222680	1237540	1103550	964898	637526	400365	-1728648
CXA36M	56	77151	75903	76426	56084	55911	33187	-85754
CXA36M	57	158632	150354	137453	126386	91802	73008	-175670
CXA36M	58	110084	108012	113333	99329	87286	73447	-74104
CXA36M	59	2469010	2584820	2112880	1607850	1313840	859914	-3532414
CXA36M	60	159675000	113691000	854043000	554694000	392297000	278861000	-2.61E+09
CXA36M	61	3011170	2756280	2138020	1715240	1449000	952977	-4181596
CXA36M	62	220655	259541	196725	143335	113352	82462	-337978
CXA36M	63	28627	25779	25358	19185	16431	13934	-30767
CXA36M	64	98383	116793	96723	66815	56517	47686	-132635
CXA36M	65	4281620	4133770	3767720	3170230	2152850	1743680	-5494271
CXA36M	66	434639	516025	353154	329435	208566	130034	-705463
CXA36M	67	1848	1963	2092	1982	1542	995	-1610
CXA36M	68	792586	810541	648789	503906	438205	309381	-1050833
CXA36M	69	342612000	308913000	219506000	167923000	125484000	84423900	-5.41E+08
CXA36M	70	97451	108580	101450	71067	58863	42316	-130060
CXA36M	71	23666	31249	28129	22967	20996	14221	-23756
CXA36M	72	44562500	33309900	25249800	18961300	13444100	10317000	-67746686
CXA36M	73	57730	68391	54176	38034	35827	28540	-74224
CXA36M	74	860859	864484	810185	573966	519559	398518	-1023628
CXA36M	75	162222	174807	179705	136129	114113	85147	-174581
CXA36M	76	15702900	12441000	11552200	8176640	6239730	4483160	-22308020
CXA36M	77	938849	1094010	963243	748024	594833	389782	-1273739
CXA36M	78	634538	757726	675837	530387	430392	294966	-807232
CXA36M	79	3466	3886	3932	3464	2786	2360	-2656
CXA36M	80	5179	5676	5793	4788	4149	3318	-4255
CXA36M	81	96281	79764	71517	64405	47811	37928	-112781
CXA36M	82	982	1178	1184	1185	872	732	-620
CXA36M	83	17367	20780	24004	19349	16188	12529	-12178
CXA36M	84	26555	23574	30745	21464	16089	14452	-26357
CXA36M	85	4109	4580	4512	3022	2946	2304	-4405
CXA36M	86	1791	2021	1814	1674	1487	1255	-1263
CXA36M	87	947692	847103	736380	519273	417817	311595	-1338700
CXA36M	88	16638	16224	14654	12429	10607	9215	-16055
CXA36M	89	2956	3276	3873	2922	2039	1866	-2890
CXA36M	90	19260500	16588000	12152200	9537260	6669400	4693210	-30059197

CXA36M	91	10649	12720	9103	10339	9519	6178	-8777
CXA36M	92	7122	8012	8760	6738	5605	4524	-6353
CXA36M	93	60849	61843	58025	45619	36806	32926	-64896
CXA36M	94	44138	47325	57132	49921	42102	32881	-22618
CXA36M	95	2730	3467	4023	3253	3229	2310	-1023
CXA36M	96	20561	21626	23895	24715	20566	19146	-2696
CXA36M	97	188946	181970	142867	112447	100065	74020	-243076
CXA36M	98	20719	22344	21534	13604	11737	10392	-26109
CXA36M	99	7181980	6552610	4985900	3673030	2789770	2151580	-10786683
CXA36M	100	13106	16547	17618	15936	13319	9455	-8463
CXA36M	101	2778490	2750550	2104110	1575510	1254690	1010900	-3958323
CXA36M	102	244084	223965	196403	157729	103512	86869	-338888
CXA36M	103	26097	33311	31564	28928	24507	18872	-18622
CXA36M	104	1769570	1616420	1440290	1174050	902635	674260	-2252613
CXA36M	105	2767900	2368930	1728480	1442140	958009	726577	-4207348
CXA36M	106	531620	486621	423865	302492	242531	181585	-743948
CXA36M	107	10675000	10259800	8257830	5869460	4466570	3354880	-16105331
CXA36M	108	258305	245212	247988	171049	147485	118337	-305703
CXA36M	109	6439	7184	8612	8098	5717	5512	-2728
CXA36M	110	8777	7940	9065	6724	6055	5428	-7070
CXA36M	111	5841	9689	10584	10975	7549	7923	1252
CXA36M	112	1713050	1518960	1324570	1049300	853786	626556	-2200932
CXA36M	113	19258800	17323400	12044600	8795070	6750890	4943010	-30441717
CXA36M	114	1556730	1334730	1105020	887360	705293	493101	-2121176
CXA36M	115	32409	34905	35788	32367	27380	22618	-21414
CXA36M	116	2994	3430	3161	2572	2346	2130	-2332
CXA36M	117	992609	944262	607670	398872	275496	171471	-1805939
CXA36M	118	385142	318030	210387	161064	98705	59187	-667736
CXA36M	119	19803	21823	18373	13901	11715	10269	-23562
CXA36M	120	127614	145537	139513	93175	76995	58933	-170106
CXA36M	121	268950	244672	205117	159909	106808	84680	-394329
CXA36M	122	289615	290248	270212	201660	162451	117303	-375287
CXA36M	123	1862560	1406490	1374400	950596	832749	591591	-2428535
CXA36M	124	1626870	1639910	1206290	950791	709164	597208	-2341728
CXA36M	125	264391	233986	211391	141014	123435	104483	-343306
CXA36M	126	11846	10073	10531	8761	7746	5457	-11627
CXA36M	127	61581	55163	49149	38065	28950	25000	-77893
CXA36M	128	269247	254148	198126	151091	115674	92753	-384265

APPENDIX F

THROUGH TRANSMISSION ATTENUATION MEASUREMENT RESULTS

Appendix F, section F.1, is a listing of the data obtained from through-transmission measurements of muscle attenuation. Section F.2 is a listing of the through-transmission attenuation values and the backscatter attenuation values that were correlated together for the results shown in Chapter 6.

F.1 Through-Transmission Data

Anml #	Temp (C)	Orient	1 MHz dB/cm	2 MHz	3 MHz	4 MHz	5 MHz	6 MHz	7 MHz	Slope dB/cm MHz
63	4	paral	1.29	3.37	7.21	14.8	20.88	37.36		6.87
	4	perp	1.88	4.68	4.03	3.77	6.46	7.14		0.89
	20	paral	1.03	3.12	3.54	3.83	4.98	5.51		0.81
	20	perp	2.03	2.96	2.4	2.94	4.03	6.73		0.78
	37	paral	4.69	11.98	10.55	11.53	13.01	13.79	13.14	1.12
	37	perp	2.24	1.38	2.26	2.92	3.87	6.43	8.87	1.13
64	4	paral	5.51	11.31	15.69	22.13	22.66	26.16		4.11
	4	perp	4.51	4.46	7.15	10.67	12.54	14.3		2.19
	20	paral	3.64	6.37	10.38	15.2	18.48	22.86		3.92
	20	perp	2.36	3.51	6.32	7.42	8.26	13.86		2.08
	37	paral	5.55	10.39	13.61	17.58	21.18	21.51	22.58	2.89
	37	perp	3.97	5.97	7.28	9.78	11.32	12.11	15.3	1.86
65	4	paral	2.98	3.62	3.91	4.72	6.04	6.87	7.72	0.81
	4	perp	1.53	2.07	2.63	4.7	7.99	8.9	10.79	1.67
	20	paral	1.76	3.33	5.41	6.61	5.52	11.45	9.61	1.42
	20	perp	3.07	3.35	4.61	5.87	8.9	9.18	16.11	1.96
	37	paral	1.56	2.74	3.41	2.19	4.02	3.9	5.4	0.51
	37	perp	1.01	2.19	1.28	2.23	2.39	5.86	8.27	1.08
66	4	paral	2.48	3.73	4.44	7.19	10.28	16.44	22.19	3.32
	4	perp	2.82	4.3	5.89	8.08	11.37	12.55	16.79	2.28
	20	paral	3.22	2.03	2.77	6.66	8.43	14.28	20.27	2.9
	20	perp	0.85	2.2	2.42	2.16	3.73	7.32	13.56	1.78
	37	paral	1.66	1.78	1.83	2.5	2.99	3.56	9.15	0.97
	37	perp	0.97	1.13	0.78	1.9	1.95	3.25	4.25	0.54
67	4	paral	3.89	5.53	10.02	14.98	18.81	22.08	28.13	4.09

	4	perp	3.65	4.97	5.87	8.14	11.1	13.43	14.66	1.97
	20	paral	1.87	2.05	5.05	8.65	13.17	12.54	12.38	2.16
	20	perp	4.63	3.03	5.64	6.81	8.98	11.51	14.95	1.83
	37	paral	3.56	3	4.13	6	7.82	9.62	12.3	1.54
	37	perp	2.48	1.52	2.77	4.26	4.6	7.65	9.4	1.24
68	4	paral	1.02	4.12	5.58	7.63	9.58	12.09	14.79	2.19
	4	perp	0.83	0.57	1.6	3.9	7.28	12.72	15.08	2.6
	20	paral	2.66	3.35	7.78	8.72	11.01	14.3	25.29	3.32
	20	perp	2.75	3.09	4.66	6.33	7.79	8.09	9.77	1.22
	37	paral	4.89	5.38	7.37	10.16	12.33	12.08	16.98	1.95
	37	perp	3.34	3.39	4.03	4.85	5.76	5.95	8.12	0.76
69	4	paral	5.09	8.67	14.33	19.03	24.2	27.7	33.4	4.74
	4	perp	7.72	10.17	12.86	15.2	16.72	14.53	19.81	1.73
	20	paral	3.14	6.21	9.89	14.09	17.46	20.93	27.6	3.94
	20	perp	1.82	1.25	2.29	3.73	4.67	7.17	11.5	1.54
	37	paral	6.21	10.51	14.68	19.48	21.6	23.7	28.59	3.58
	37	perp	1.69	6.13	7.48	4.58	6.91	11.57	14.05	1.7
70	4	paral	3.96	4.12	7.44	10.34	11.89	14.42	17.97	2.39
	4	perp	2.27	2.37	3.05	3.38	4.04	6.74	11.49	1.33
	20	paral	3.41	5.7	8.52	13.27	13.75	15.56	20.31	2.7
	20	perp	2.59	1.59	3.22	5.13	6.18	9.77	15.36	2.06
	37	paral	2.39	7.32	10.67	15.72	18.09	18.11	25.93	3.5
	37	perp	0.66	3.37	3.97	10.15	7.78	8.2	15.03	2.01
73	4	paral	4.93	7.14	9.69	13.38	15.53	21.89	29.36	3.88
	4	perp	1.98	3.34	3.63	6.36	7.52	9.11	12.09	1.65
	20	paral	3.91	4.55	5.91	7.88	9.61	10.57	13.05	1.54
	20	perp	2.4	0.86	1.91	2.98	4.29	6.63	6.61	0.09
	37	paral	7.57	9.44	10.6	13.68	15.35	16.79	21.47	2.19
	37	perp	1.13	1.32	4.51	6.04	5.07	6.86	8.76	1.23
74	4	paral	3.2	4.24	5.53	6.52	7.13	6.59	13.13	1.28
	4	perp	0.59	2.46	2.86	5.5	8.13	9.71	12.91	2.02
	20	paral	2.91	5.26	6.98	10.55	11.99	14.33	20.75	2.74
	20	perp	1.52	1.89	1.6	2.24	5.12	3.96	9.93	1.17
	37	paral	5.88	8.22	10.59	12.81	14.34	16.25	20.88	2.31
	37	perp	1.95	1.58	3.01	5.21	5.27	7.88	8.88	1.27
83	4	paral	1.14	3.82	6.61	9.9	11.93	13.8	18.8	2.79
	4	perp	3.95	4.18	5.11	6.48	7.17	11.72	15.18	1.81
	20	paral	2.37	3.32	4.49	5.48	6.26	9.51	10.39	1.36
	20	perp	1.63	1.86	2.57	2.48	3.27	3.17	4.41	0.41
	37	paral	4.43	6.52	8.77	10.11	11.59	14.09	18.23	2.18
	37	perp	3.16	4.43	5.88	5.39	5.21	7.64	14.14	1.37
84	4	paral	1.62	1.61	4.63	6.99	10.14	10.58	15.2	2.29
	4	perp	1.11	2.93	3.24	4.38	5.45	6.86	7.51	1.04
	20	paral	2.89	2.98	3.06	4.18	4.97	6.54	5.71	0.64
	20	perp	0.49	1.87	2.06	2.29	2.64	3.08	3.65	0.44
	37	paral	1.96	3.25	6.15	7.97	10.31	9.31	12.77	1.74
	37	perp	0.61	1.84	3.1	5.25	3.02	3.38	5.73	0.65
85	4	paral	3.61	3.38	5.48	7.11	9.73	10.84	10.88	1.46
	4	perp	3.01	3.49	4.85	6.24	7.67	8.7	11.18	1.35
	20	paral	3.89	3.01	3.62	5.25	5.49	6.57	10.85	1.07
	20	perp	2.1	5.25	3.3	4.36	5.48	5.87	8.47	0.88
	37	paral								
	37	perp								
86	4	paral	3.8	5.23	7.67	10.74	14.71	17.1	21.25	2.97

	4	perp	1.47	1.81	3.24	4.42	4.7	8.33	10.98	1.53
	20	paral	1.02	3.17	4.29	6.28	8.2	9.2	9.88	1.51
	20	perp	1.59	1.99	3.16	4.24	5.52	9.43	11.92	1.72
	37	paral								
	37	perp								
87	4	paral	1.46	5.87	8.99	12.36	15.76	20.13	23.21	3.59
	4	perp	0.76	3.11	3.84	5.61	7.18	6.56	10.31	1.38
	20	paral	3.48	4.35	6	8.43	9.73	10.89	14.6	1.97
	20	perp	2.76	1.4	1.54	2.43	1.84	3.32	3.53	0.23
	37	paral	3.19	4.52	6.62	7.62	9.42	12.48	12.43	1.65
	37	perp	2.25	3.07	3.28	3.19	5.57	3.25	10.67	0.99
88	4	paral	2.6	5.86	8.51	11.07	12.71	14.21	21.92	2.81
	4	perp	0.81	2.91	3.15	4.59	5.37	4.08	8.56	0.99
	20	paral	2.76	4.21	7.06	9.38	10.69	13.91	16.59	2.3
	20	perp	2.6	2.15	3.05	4.68	5.33	6.52	7.93	0.96
	37	paral	5.16	5.87	8.49	12.26	13.5	13.04	17.56	2.01
	37	perp	3.66	2.4	2.99	4.7	5.57	5.19	8.66	0.82
89	4	paral	3.33	5.85	8.87	10.26	11.15	14.09	16.93	2.12
	4	perp	0.33	3.54	6.24	8.4	9.59	16.27	17.63	2.88
	20	paral	4.19	2.27	3.14	4.99	5.35	16.09	28.65	3.69
	20	perp	1.94	0.23	0.73	1.13	1.52	2.5	5.4	0.56
	37	paral	2.28	9.58	8.86	7.66	9.28	15.95	12.65	1.59
	37	perp	3.57	0.67	2.16	3.34	3.43	4.85	5.99	0.6
90	4	paral	2.05	1.86	2.88	5.26	7.43	8.6	16.97	2.24
	4	perp	4.96	6.8	9.61	14.27	16.86	14.93	22.14	2.65
	20	paral	0.39	2.32	3.74	4.61	5.03	7.06	10.29	1.44
	20	perp	3.47	4.28	5.53	7.35	6.85	7.9	3.39	0.29
	37	paral	3.52	6.27	7.58	8.58	12.87	14.51	13.41	1.83
	37	perp	2.72	1.9	2.81	3.98	4.21	5.98	4.89	0.57
99	4	paral	3.56	9.46	14.89	20.94	24.09	27.52	21.06	3.5
	4	perp	2.24	6.87	9.72	12.69	14.15	18.23	19.71	2.84
	20	paral	3.2	6.9	12.38	16.49	17.94	21.07	20.68	3.08
	20	perp	1.93	2.43	1.84	2.89	4.83	5.26		0.83
	37	paral	6.39	10.93	11.94	12.19	11.91	13.84	31.24	2.86
	37	perp	1.84	0.53	3.59	2.99	5.48	6.57	5.89	0.93
100	4	paral	0.96	5.34	5.08	6.81	10.03	9.23	18.38	2.32
	4	perp	0.62	3.55	2.91	4.1	5.94	5.28	12.94	1.54
	20	paral	2.66	4.18	7.8	12.08	14.87	18.82	14.6	2.57
	20	perp	1.27	1.19	1.33	2.03	3.17	4.21	2.5	0.41
	37	paral								
	37	perp	0.59	2.72	2.44	2.47	4.32	5.04	6.21	0.83
101	4	paral	1.97	7.76	14.58	22.37	26.44	26.26		4.42
	4	perp	3.03	8.24	9.19	11.99	13.9	11.73		1.37
	20	paral	2.88	4.78	7.77	11.15	13.59	14.33	21.43	2.78
	20	perp	2.67	3.46	3.61	5.02	6.85	9.78	13.98	1.78
	37	paral	6.12	7.77	10.02	13.44	16.21	17.8	21.28	2.56
	37	perp	5.37	8.96	9.97	11.59	13.2	15.85	15.3	1.67
102	4	paral	3.47	6.03	12.32	16.98	14.03	15.09	17.66	2.23
	4	perp	0.63	5.57	9.99	13.26	9.4	9.15	9.33	1.66
	20	paral	0.6	2.3	3.41	5.82	9.77	19.7	21.9	3.75
	20	perp	1.65	2.38	3.35	4.15	4.03	2.95	5.84	0.51
	37	paral	1.33	6.17	5.79	6.53	8.35	10.67	16.61	2.05
	37	perp	3.37	2.71	2.92	4.02	5.2	7.74	8.53	0.99
105	4	paral	4.05	3.95	5.32	12.87	17.5	19.2	21.85	3.43

	4	perp	2.34	3.65	3.96	6.04	8.95	12.45	15.23	2.81
	20	paral	3.79	6.33	7.43	9.51	13.4	16.29	20.47	2.71
	20	perp	2.06	3.39	5.05	6.59	6.9	9.06	11.06	1.43
	37	paral	4.18	6.85	7.02	8.9	9.5	10.45	14.19	1.42
	37	perp	5.97	8.76	10.06	12.88	13.03	13.62	15.75	1.5
106	4	paral	3.35	5.23	6.65	8.86	17.24	18.45	23.56	3.49
	4	perp	3.67	6.42	4.65	7.34	12.34	14.84	17.93	2.39
	20	paral	1.89	4.45	6.84	10.75	14.76	17.89	27.19	3.95
	20	perp	4.61	467	6.23	8.78	10.41	12.08	15.73	1.68
	37	paral	5.45	7.4	8.9	14.15	15.72	16.2		2.1
	37	perp	1.66	2.48	2.2	2.81	4.22	2.43		0.32
107	4	paral	4.23	8.06	13.15	18.98	22.3	22.2	22.89	3.35
	4	perp	2.25	4.87	6.46	8.58	9.64	10.74	14.21	1.81
	20	paral	10.03	8.37	9.23	12.09	15.04	16.87	18.42	1.71
	20	perp	6.61	7.82	8.8	9.22	9.68	10.64	11.73	0.75
	37	paral								
	37	perp								
108	4	paral	0.82	3.29	4.93	6.91	8.61	10.06	8.42	1.43
	4	perp	1.08	4.33	6.49	9.09	11.33	13.24	11.08	1.87
	20	paral	3.46	3.87	5.01	7.61	10.17	11.42	12.71	1.71
	20	perp	5.27	4.23	4.24	4.5	5.82	7.22	7.73	0.53
	37	paral								
	37	perp								
109	4	paral	3.07	2.14	4.38	7.54	9.41	6.44	9.75	1.2
	4	perp	2.37	2.43	3.91	5.87	8.01	10.55	8.69	1.4
	20	paral	0.86	2	1.97	2.4	4.89	4.5	10.95	1.36
	20	perp	1.23	2.4	2.77	3.62	5.24	7.5	8.14	1.19
	37	paral	1.74	1.95	4.28	5.79	6.79	7.7	9.43	1.32
	37	perp	1.82	2.37	2.99	4.06	5.15	6.28	8.17	1.03
110	4	paral	2.42	2.55	3.85	5.77	7.39	8.36	9.24	1.27
	4	perp	4.55	3.43	5.44	9.13	8.17	7.71	13.72	1.38
	20	paral	3.25	2.18	3.13	4.12	6	8.93	9.62	1.26
	20	perp	1.23	1.46	1.89	2.28	2.54	3.5	6.47	0.73
	37	paral	1.62	3.07	3.72	5.08	5.82	7.13	10.57	1.32
	37	perp	1.93	2.99	4.25	5.71	7.2	8.33	10.43	1.39
111	4	paral	1.71	3.41	4.86	6.72	9.87	12.03	13.51	2.05
	4	perp	1.67	2.22	2.27	1.94	4.25	7.91	7.33	1.08
	20	paral	0.71 ·	4.76	4.64	5.34	9.46	5.96	10.44	1.3
	20	perp	0.77	1.27	1.44	1.36	1.91	4.63	4.91	0.7
	37	paral	0.36	2.66	2.77	3.71	3.72	5.3	3.46	0.55
	37	perp	0.36	1.13	1.15	2.29	4.13	8.41	3.05	0.91
112	4	paral	0.23	4.14	7.2	11.21	14.59	17.69	22.17	2.05
	4	perp	2.74	5.91	8.07	10.27	11.96	8.8	16.78	1.08
	20	paral	1.48	4.69	6.32	9.1	13.21	16.23	21.3	1.3
	20	perp	0.2	0.41	0.99	1.3	1.8	1.69	1.58	0.7
	37	paral	2.3	7.98	12.65	13.2	13.35	11.07	18.5	0.55
	37	perp								
113	4	paral	9.54	7.14	12.83	20.29	23.39	28.26	29.8	4.05
	4	perp	0.56	3.21	3.92	5.57	6.7	9.45	10.35	1.59
	20	paral	8.87	9	9.98	10.66	9.57	15.66	18.85	1.53
	20	perp	9.69	7.2	7.23	8	8.95	8.47	14.32	0.64
	37	paral	2.94	5.8	8.68	9.51	12.74	9.22	16.29	1.81
	37	perp	0.53	2.92	4.88	9.57	17.65	12.5	14.19	2.6
114	4	paral	1.65	6.54	10.48	13.48	14.91	17.27	22.53	3.16

	4	perp	0.9	3.26	3.56	4.24	4.2	8.89	13.77	1.8
	20	paral	5.54	7.77	8.64	10.12	12.52	10.73	19.15	1.8
	20	perp	1.64	4.37	4.95	6.08	8.79	9.19	12.41	1.63
	37	paral	2.19	3.68	5.71	6.8	6.72	11.34	12.19	1.65
	37	perp	2.48	5.62	6.65	6.22	11.71	11.97	13.95	1.86
115	4	paral	2.96	4.61	5.66	7.55	9.93	13.07	16.65	2.23
	4	perp	2.92	2.54	3.03	3.16	3.78	3.64	4.77	0.03
	20	paral	1.94	4.11	5.28	6.49	8.02	7.85	13.27	1.57
	20	perp								
	37	paral	8.41	6.58	7.72	9.38	9.36	12.45	12.38	0.9
	37	perp	7.9	5.99	6.51	7.26	7.94	8.2	8.61	0.28
116	4	paral	3.55	3.39	4.82	7.86	11.82	14.41	18.2	2.6
	4	perp	1.52	1.7	2.57	3.26	3.21	4.24	5.01	0.57
	20	paral	3.43	4.07	4.71	6.3	8.62	10.8	16.31	2
	20	perp								
	37	paral	6.2	6.04	7.39	9.42	11.22	13.04	14.63	1.54
	37	perp	3.78	3.46	4.21	4.65	4.95	5.14	6.46	0.43
117	4	paral	3.06	5.57	8.54	11.55	14.66	17.18	20.72	2.94
	4	perp	3.28	3.11	4.84	6.34	7.97	10.5	12.83	1.66
	20	paral	3.79	3.5	4.58	6.92	9.73	10.95	13.05	1.7
	20	perp	3.39	3.11	3.19	4.63	6.54	8.18	8.5	1.02
	37	paral	3.31	3.79	4.85	6.49	8.33	9.34	12.16	1.46
	37	perp	4.6	4.19	5.35	6.83	8.31	9.6	11.43	1.22
118	4	paral	3.73	4.9	6.97	8.65	10.69	12.7	15.5	1.95
	4	perp	2.92	3.87	5.1	6.26	7.7	9.46	10.59	1.31
	20	paral	4.3	4.31	5.1	6.82	8.76	9.9	11.39	1.28
	20	perp	4.45	4.5	3.78	4.68	5.92	6.87	6.82	0.5
	37	paral	4.76	5.74	7.78	10.45	10.5	11.49	13.31	1.42
	37	perp	4.31	4.74	4.71	4.21	4.45	5.86	8.06	0.47
119	4	paral	2.42	2.75	4.24	6.21	8.01	9.41	12.58	1.69
	4	perp	0.3	1.87	1.94	2.32	3.31	4.86	5.54	0.82
	20	paral	2.39	2.77	3.29	3.84	4.88	6.64	6.55	0.77
	20	perp	0.9	1.11	2.07	2.4	2.73	3.83	5.74	0.73
	37	paral	2.27	2.73	3.23	4.53	5.71	6.08	7.88	0.92
	37	perp	1.9	2.53	2.65	2.5	3.41	3.84	4.91	0.44
120	4	paral	3.15	4.97	10.13	13.33	16.1	18.15		3.18
	4	perp	4.72	3.98	8.75	11.82	13.34	12.75	14.9	1.53
	20	paral	1.29	2.29	2.95	3.34	4.18	5.19	7.09	0.87
	20	perp	1.26	1.43	1.15	4.28	8.33	8.56	6.44	1.32
	37	paral	2.97	5.4	7.05	9.46	11.22	11.22	10.24	1.34
	37	perp	1.22	1.69	3.56	5.1	6.49	8.65	9.92	1.53
121	4	paral	1.26	0.43	1.15	4.29	8.33	8.56	6.44	1.39
	4	perp	0.55	3.01	4.09	6.23	9.91	9.1	11.29	1.79
	20	paral	0.33	1.69	2.67	4.39	5.99	8.11	10.76	1.64
	20	perp	0.9	1.73	2.05	2.76	3.83	5.42	6.49	0.92
	37	paral	2.08	1.14	6.02	8.61	11.37	11.64	16.07	2.44
	37	perp	1.3	3.06	4.42	6.12	5.78	6.9	10.25	1.28
122	4	paral								
	4	perp	2.87	2.41	3.47	4.83	5.05	7.63	7.09	0.81
	20	paral	0.59	1.21	0.76	0.43	1.07	2.1	4.62	0.5
	20	perp	0.95	1.59	2.02	2.68	2.87	4.4	5.74	0.74
	37	paral								
	37	perp	4.04	4.4	6.45	8.33	8.91	8.61	14.19	1.47

F.2 Comparison Data

Thru Anm l#	Trans Temp	Meas Orient	(TTM) 1 MHz dB/cm	Slope dB/cm MHz	Hide on 1 MHz	Slope	Hide off 1 MHz	Slope	Cold 1 MHz	Slope
63	4	Paral	1.29	6.87					2.129	-1.697
	4	Perp	1.88	0.89					2.129	-1.697
	20	Paral	1.03	0.81			0.99	-1.86		
	20	Perp	2.03	0.78			0.99	-1.86		
	37	Paral	4.69	1.12	0.363	0.619	0.99	-1.86		
	37	Perp	2.24	1.13	0.363	0.619	0.99	-1.86		
64	4	Paral	5.51	4.11					2.011	-1.62
	4	Perp	4.51	2.19					2.011	-1.62
	20	Paral	3.64	3.92			0.16	0.447		
	20	Perp	2.36	2.08			0.16	0.447		
	37	Paral	5.55	2.89	0.143	-0.97	0.16	0.447		
	37	Perp	3.97	1.86	0.143	-0.97	0.16	0.447		
65	4	Paral	2.98	0.81					1.499	-1.839
	4	Perp	1.53	1.67					1.499	-1.839
	20	Paral	1.76	1.42			3.18	0.322		
	20	Perp	3.07	1.96			3.18	0.322		
	37	Paral	1.56	0.51	0.822	0.871	3.18	0.322		
	37	Perp	1.01	1.08	0.822	0.871	3.18	0.322		
66	4	Paral	2.48	3.32					1.332	-1.279
	4	Perp	2.82	2.28					1.332	-1.279
	20	Paral	3.22	2.9			3.89	0.673		
	20	Perp	0.85	1.78			3.89	0.673		
	37	Paral	1.66	0.97	0.603	1.564	3.89	0.673		
	37	Perp	0.97	0.54	0.603	1.564	3.89	0.673		
67	4	Paral	3.89	4.09					1.435	-1.499
	4	Perp	3.65	1.97					1.435	-1.499
	20	Paral	1.87	2.16			0.05	-0.81		
	20	Perp	4.63	1.83			0.05	-0.81		
	37	Paral	3.56	1.54	3.02	0.405	0.05	-0.81		
	37	Perp	2.48	1.24	3.02	0.405	0.05	-0.81		
68	4	Paral	1.02	2.19					2.085	-1.838
	4	Perp	0.83	2.6					2.085	-1.838
	20	Paral	2.66	3.32			0.23	-1.17		
	20	Perp	2.75	1.22			0.23	-1.17		
	37	Paral	4.89	1.95	1.502	0.586	0.23	-1.17		
	37	Perp	3.34	0.76	1.502	0.586	0.23	-1.17		
69	4	Paral	5.09	4.74					1.536	-1.881
	4	Perp	7.72	1.73					1.536	-1.881
	20	Paral	3.14	3.94			0.75	1.988		
	20	Perp	1.82	1.54			0.75	1.988		
	37	Paral	6.21	3.58	2.775	0.441	0.75	1.988		
	37	Perp	1.69	1.7	2.775	0.441	0.75	1.988		
70	4	Paral	3.96	2.39					1.655	-1.555
	4	Perp	2.27	1.33					1.655	-1.555

	20	Paral	3.41	2.7			2.19	0.569		
	20	Perp	2.59	2.06			2.19	0.569		
	37	Paral	2.39	3.5			2.19	0.569		
	37	Perp	0.66	2.01			2.19	0.569		
73	4	Paral	4.93	3.88					1.79	-1.608
	4	Perp	1.98	1.65					1.79	-1.608
	20	Paral	3.91	1.54			0.26	0.624		
	20	Perp	2.4	0.09			0.26	0.624		
	37	Paral	7.57	2.19	0.286	0.277	0.26	0.624		
	37	Perp	1.13	1.23	0.286	0.277	0.26	0.624		
74	4	Paral	3.2	1.28					1.462	-1.784
	4	Perp	0.59	2.02					1.462	-1.784
	20	Paral	2.91	2.74			2.54	0.528		
	20	Perp	1.52	1.17			2.54	0.528		
	37	Paral	5.88	2.31	0.185	-0.36	2.54	0.528		
	37	Perp	1.95	1.27	0.185	-0.36	2.54	0.528		
83	4	Paral	1.14	2.79					1.892	-1.893
	4	Perp	3.95	1.81					1.892	-1.893
	20	Paral	2.37	1.36			0.85	-2.1		
	20	Perp	1.63	0.41			0.85	-2.1		
	37	Paral	4.43	2.18	1.798	0.703	0.85	-2.1		
	37	Perp	3.16	1.37	1.798	0.703	0.85	-2.1		
84	4	Paral	1.62	2.29					1.61	-1.673
	4	Perp	1.11	1.04					1.61	-1.673
	20	Paral	2.89	0.64			0.54	1.285		
	20	Perp	0.49	0.44			0.54	1.285		
	37	Paral	1.96	1.74	0.687	-2.14	0.54	1.285		
	37	Perp	0.61	0.65	0.687	-2.14	0.54	1.285		
85	4	Paral	3.61	1.46					2.018	-1.54
	4	Perp	3.01	1.35					2.018	-1.54
	20	Paral	3.89	1.07			0.69	-2.19		
	20	Perp	2.1	0.88			0.69	-2.19		
	37	Paral			2.559	0.211	0.69	-2.19		
	37	Perp			2.559	0.211	0.69	-2.19		
86	4	Paral	3.8	2.97					1.979	-1.749
	4	Perp	1.47	1.53					1.979	-1.749
	20	Paral	1.02	1.51			1.825	0.29		
	20	Perp	1.59	1.72			1.825	0.29		
	37	Paral								
	37	Perp								
87	4	Paral	1.46	3.59					2.304	-1.507
	4	Perp	0.76	1.38					2.304	-1.507
	20	Paral	3.48	1.97			0.87	1.098		
	20	Perp	2.76	0.23			0.87	1.098		
	37	Paral	3.19	1.65	0.385	-1.74	0.87	1.098		
	37	Perp	2.25	0.99	0.385	-1.74	0.87	1.098		
88	4	Paral	2.6	2.81					2.124	-1.68
	4	Perp	0.81	0.99					2.124	-1.68
	20	Paral	2.76	2.3			0.36	-1.98		
	20	Perp	2.6	0.96			0.36	-1.98		
	37	Paral	5.16	2.01	0.303	0.257	0.36	-1.98		
	37	Perp	3.66	0.82	0.303	0.257	0.36	-1.98		
89	4	Paral	3.33	2.12					1.709	-1.502
	4	Perp	0.33	2.88					1.709	-1.502

	20	Paral	4.19	3.69			0.39	-1.74		
	20	Perp	1.94	0.56			0.39	-1.74		
	37	Paral	2.28	1.59	2.76	0.359	0.39	-1.74		
	37	Perp	3.57	0.6	2.76	0.359	0.39	-1.74		
90	4	Paral	2.05	2.24					1.856	-1.579
	4	Perp	4.96	2.65					1.856	-1.579
	20	Paral	0.39	1.44			2.95	1.297		
	20	Perp	3.47	0.29			2.95	1.297		
	37	Paral	3.52	1.83	2.79	0.223	2.95	1.297		
	37	Perp	2.72	0.57	2.79	0.223	2.95	1.297		
99	4	Paral	3.56	3.5					2.26	-1.517
	4	Perp	2.24	2.84					2.26	-1.517
	20	Paral	3.2	3.08			2.88	0.132		
	20	Perp	1.93	0.83			2.88	0.132		
	37	Paral	6.39	2.86	0.114	-0.45	2.88	0.132		
	37	Perp	1.84	0.93	0.114	-0.45	2.88	0.132		
100	4	Paral	0.96	2.32					1.486	-1.762
	4	Perp	0.62	1.54					1.486	-1.762
	20	Paral	2.66	2.57			0.37	-1.93		
	20	Perp	1.27	0.41			0.37	-1.93		
	37	Paral								
	37	Perp	0.59	0.83	2.496	0.359	0.37	-1.93		
101	4	Paral	1.97	4.42					2.176	-1.711
	4	Perp	3.03	1.37					2.176	-1.711
	20	Paral	2.88	2.78			1.54	0.674		
	20	Perp	2.67	1.78			1.54	0.674		
	37	Paral	6.12	2.56	1.217	1.129	1.54	0.674		
	37	Perp	5.37	1.67	1.217	1.129	1.54	0.674		
102	4	Paral	3.47	2.23					1.559	-1.406
	4	Perp	0.63	1.66					1.559	-1.406
	20	Paral	0.6	3.75			0.43	1.055		
	20	Perp	1.65	0.51			0.43	1.055		
	37	Paral	1.33	2.05	0.029	-1.77	0.43	1.055		
	37	Perp	3.37	0.99	0.029	-1.77	0.43	1.055		
105	4	Paral	4.05	3.43					2	-1.375
	4	Perp	2.34	2.81					2	-1.375
	20	Paral	3.79	2.71			2.89	0.099		
	20	Perp	2.06	1.43			2.89	0.099		
	37	Paral	4.18	1.42	0.165	-0.11	2.89	0.099		
	37	Perp	5.97	1.5	0.165	-0.11	2.89	0.099		
106	4	Paral	3.35	3.49					2.076	-1.51
	4	Perp	3.67	2.39					2.076	-1.51
	20	Paral	1.89	3.95			2.1	0.301		
	20	Perp	4.61	1.68			2.1	0.301		
	37	Paral	5.45	2.1	0.386	0.663	2.1	0.301		
	37	Perp	1.66	0.32	0.386	0.663	2.1	0.301		
107	4	Paral	4.23	3.35					1.949	-1.619
	4	Perp	2.25	1.81					1.949	-1.619
	20	Paral	10.03	1.71			1.24	0.924		
	20	Perp	6.61	0.75			1.24	0.924		
	37	Paral								
	37	Perp								
108	4	Paral	0.82	1.43					2.277	-1.623
	4	Perp	1.08	1.87					2.277	-1.623

ID	Temp	Orient.								
	20	Paral	3.46	1.71			0.93	0.969		
	20	Perp	5.27	0.53			0.93	0.969		
	37	Paral			0.363	-1.68	0.93	0.969		
	37	Perp			0.363	-1.68	0.93	0.969		
109	4	Paral	3.07	1.2					1.537	-1.747
	4	Perp	2.37	1.4					1.537	-1.747
	20	Paral	0.86	1.36			1.02	-1.51		
	20	Perp	1.23	1.19			1.02	-1.51		
	37	Paral	1.74	1.32	1.67	0.659	1.02	-1.51		
	37	Perp	1.82	1.03	1.67	0.659	1.02	-1.51		
110	4	Paral	2.42	1.27					1.867	-1.547
	4	Perp	4.55	1.38					1.867	-1.547
	20	Paral	3.25	1.26			0.45	-1.47		
	20	Perp	1.23	0.73			0.45	-1.47		
	37	Paral	1.62	1.32	2.952	0.279	0.45	-1.47		
	37	Perp	1.93	1.39	2.952	0.279	0.45	-1.47		
111	4	Paral	1.71	2.05					1.621	-1.877
	4	Perp	1.67	1.08					1.621	-1.877
	20	Paral	0.71	1.3			0.26	-1.88		
	20	Perp	0.77	0.7			0.26	-1.88		
	37	Paral	0.36	0.55	1.534	0.09	0.26	-1.88		
	37	Perp	0.36	0.91	1.534	0.09	0.26	-1.88		
112	4	Paral	0.23	2.05					2.155	-1.609
	4	Perp	2.74	1.08					2.155	-1.609
	20	Paral	1.48	1.3			0.74	1.558		
	20	Perp	0.2	0.7			0.74	1.558		
	37	Paral	2.3	0.55	1.067	1.089	0.74	1.558		
	37	Perp								
113	4	Paral	9.54	4.05					2.124	-1.409
	4	Perp	0.56	1.59					2.124	-1.409
	20	Paral	8.87	1.53			2.54	0.583		
	20	Perp	9.69	0.64			2.54	0.583		
	37	Paral	2.94	1.81	1.983	1.151	2.54	0.583		
	37	Perp	0.53	2.6	1.983	1.151	2.54	0.583		
114	4	Paral	1.65	3.16					1.985	-1.442
	4	Perp	0.9	1.8					1.985	-1.442
	20	Paral	5.54	1.8			3.04	0.183		
	20	Perp	1.64	1.63			3.04	0.183		
	37	Paral	2.19	1.65	1.376	1.458	3.04	0.183		
	37	Perp	2.48	1.86	1.376	1.458	3.04	0.183		
115	4	Paral	2.96	2.23					1.813	-1.749
	4	Perp	2.92	0.03					1.813	-1.749
	20	Paral	1.94	1.57			0.73	-2.21		
	20	Perp								
	37	Paral	8.41	0.9	1.648	0.911	0.73	-2.21		
	37	Perp	7.9	0.28	1.648	0.911	0.73	-2.21		
116	4	Paral	3.55	2.6					2.056	-1.58
	4	Perp	1.52	0.57					2.056	-1.58
	20	Paral	3.43	2			0.31	-1.6		
	20	Perp								
	37	Paral	6.2	1.54	1.88	0.629	0.31	-1.6		
	37	Perp	3.78	0.43	1.88	0.629	0.31	-1.6		
117	4	Paral	3.06	2.94					1.494	-0.721
	4	Perp	3.28	1.66					1.494	-0.721

	20	Paral	3.79	1.7			0.85	1.009		
	20	Perp	3.39	1.02			0.85	1.009		
	37	Paral	3.31	1.46	0.38	-1.96	0.85	1.009		
	37	Perp	4.6	1.22	0.38	-1.96	0.85	1.009		
118	4	Paral	3.73	1.95					1.588	-0.691
	4	Perp	2.92	1.31					1.588	-0.691
	20	Paral	4.3	1.28			0.45	1.199		
	20	Perp	4.45	0.5			0.45	1.199		
	37	Paral	4.76	1.42	0.504	-2.38	0.45	1.199		
	37	Perp	4.31	0.47	0.504	-2.38	0.45	1.199		
119	4	Paral	2.42	1.69					2.06	-1.493
	4	Perp	0.3	0.82					2.06	-1.493
	20	Paral	2.39	0.77			0.36	0.967		
	20	Perp	0.9	0.73			0.36	0.967		
	37	Paral	2.27	0.92	0.719	-2.01	0.36	0.967		
	37	Perp	1.9	0.44	0.719	-2.01	0.36	0.967		
120	4	Paral	3.15	3.18					1.947	-1.537
	4	Perp	4.72	1.53					1.947	-1.537
	20	Paral	1.29	0.87			0.7	0.886		
	20	Perp	1.26	1.32			0.7	0.886		
	37	Paral	2.97	1.34	0.313	0.744	0.7	0.886		
	37	Perp	1.22	1.53	0.313	0.744	0.7	0.886		
121	4	Paral	1.26	1.39					1.749	-1.305
	4	Perp	0.55	1.79					1.749	-1.305
	20	Paral	0.33	1.64			1.56	0.438		
	20	Perp	0.9	0.92			1.56	0.438		
	37	Paral	2.08	2.44	0.474	-2.39	1.56	0.438		
	37	Perp	1.3	1.28	0.474	-2.39	1.56	0.438		
122	4	Paral								
	4	Perp	2.87	0.81					1.917	-1.545
	20	Paral	0.59	0.5			1.66	0.866		
	20	Perp	0.95	0.74			1.66	0.866		
	37	Paral								
	37	Perp	4.04	1.47	0.363	-1.95	1.66	0.866		

REFERENCES

[1] I. A. Hien, J. A. Novakofski, and W. D. O'Brien Jr., "Ultrasound Data Acquisition System Design for Collecting High Quality RF Data from Beef Carcasses in the Slaughterhouse Environment," *Proc. IEEE Ultrasonics Symposium*, Tucson, AZ, 1992.

[2] J. Nicolas, "A New Method for the Analysis of the Frequency Dependence of the Backscattering Coefficient in Tissue-Like Media," *Acoustical Imaging*, vol. 14, pp. 761-764, 1985.

[3] E.L. Madsen, M.F. Insana, and J.A. Zagzebski, "Method of Data Reduction for Accurate Determination of Acoustic Backscatter Coefficients," *Journal of the Acoustic Society of America*, vol. 76, pp. 913 - 923, Sept 1984.

[4] J. F. Greenleaf, Tissue Characterization with Ultrasound, Volume I. Boca Raton, FL: CRC Press, 1986.

[5] L.X. Yao, J.A Zagzebski, and E.L. Madsen, "Backscatter Coefficient Measurements Using a Reference Phantom to Extract Depth-Dependent Instrumentation Factors," *Ultrasonic Imaging*, vol. 12, pp. 58 - 70, 1990.

[6] J.A. Zagzebski, Z.F. Lu, and L.X. Yao, "Quantitative Ultrasound Imaging: In Vivo Results in Normal Liver," *Ultrasonic Imaging*, vol. 15, no. 4, Oct 1993.

[7] L. X. Yao, Reference Phantom Method For Acoustic Backscatter Coefficient and Attenuation Coefficient Measurements. Ph.D. dissertation, University of Wisconsin at Madison, 1990.

[8] E.J. Boote, J.A. Zagzebski, E.L. Madsen, and T.J. Hall, "Instrument Independent Acoustic Backscatter Coefficient Imaging," *Ultrasonic Imagining*, vol. 10, pp. 121 - 138, 1988.

[9] C. A. Balanis, Advanced Engineering Electromagnetics. New York: Wiley, 1989.

[10] R. C. Chivers, "The Scattering of Ultrasound by Human Tissues - Some Theoretical Models," *Ultrasound Med. & Bio.*, vol. 3, pp. 1-13, 1977.

[11] Murray R. Spiegel, Schaum's Outline of Theory and Problems of Statistics. New York: McGraw-Hill, 1994.

[12] Microsoft Excel Function Reference Guide, Microsoft Corporation, Redmond, Washington, 1992.

[13] Matlab User's Guide, The Math Works, Inc., Natick, Massachusetts, 1992.

[14] H. B. Hedrick, J. C. Miller, G. B. Thompson and R. R. Freitag, "Factors Affecting Longissimus Dorsi Area and Fat Thickness of Beef and Relation Between These Measurements and Retail Yield," *Journal of Animal Science*, vol. 24, no. 2, pp. 333-337, May 1965.

[15] Personal correspondance with Nadine Barrie Smith, MSEE.

[16] Matlab Reference Guide, The Math Works, Inc., Natick, Massachusetts, 1992.

[17] Personal correspondance with Dr. Jan Novakofski, Ph.D.